FINAL REPORT

ON

THE DEVELOPMENT OF CONTOURED INTERLOCKING TAPE WOUND TITANIUM ROCKET MOTOR CASES

Contract DA-30-069-ORD-3101

May 15, 1962

CURTISS-WRIGHT CORPORATION

WOOD-RIDGE, NEW JERSEY

Wright Aeronautical Serial Report No. MP.00-249

FINAL REPORT

ON

THE DEVELOPMENT OF CONTOURED INTERLOCKING TAPE WOUND TITANIUM ROCKET MOTOR CASES

Submitted in Partial Fulfillment of U. S. Army Ordnance Materials Research Office Contract DA-30-069-ORD-3101

Director of Engineering

Wright Aeronautical Serial Report No. MP.00-249

Copy No. 52 of 160 Copies

Date of Report: May 15, 1962

FINAL REPORT

ON

THE DEVELOPMENT OF CONTOURED INTERLOCKING TAPE WOUND TITANIUM ROCKET MOTOR CASES

Submitted in Partial Fulfillment of U. S. Army
Ordnance Materials Research Office Contract DA-30-069-ORD-3101

Curtiss-Wright Corporation
Wright Aeronautical Division
Wood-Ridge, New Jersey

Wright Aeronautical Serial Report No. MP.00-249

Compiled by:

Asst. Mgr. of Metallurgy

W. Taylor

Project Engineer

Project Engineer - Stress

Approved by:

Manager of Metallurgy

TABLE OF CONTENTS

1.0 INTRODUCTION

The development of pressure vessels for use in solid fuel motor cases had reached a state in 1960 wherein further progress was restricted by the lack of suitable high strength materials and limitations in methods of fabrication. Though the potentially high strength-to-weight ratio of fiber reinforced cases was recognized, the use of metallic cases offered certain advantages peculiar to metals alone. The application of metal wire or tape reinforcement in pressure vessels dates back at least a century. High tensile steel wire has been used as the banding material on certain rifles and guns, as well as on other hollow bodies. With the possible exception of one recent investigation, no attempt has been made to utilize the transverse strength of wire or tape to support the axial stress in cylindrical pressure vessels. Previously vessels had been reinforced with wound profile strip which was shrunk onto the vessel (while the strip was simultaneously quenched to high strength), putting the cylindrical portion of the vessel into compression. Though the tape was contoured and interlocked, it does not appear to support any of the axial load. The Curtiss-Wright proposed method provided a means whereby the transverse strength of severely cold reduced tape was utilized. The method simultaneously facilitated application of ultra high strength materials which might otherwise be difficult or impossible to use.

The interlocking Titanium concept was an outgrowth of relatively recent work carried out by the Wright Aeronautical Division of the Curtiss-Wright Corporation on the development of the high strength Titanium alloy B120VCA. In sheet form, this alloy is heat treatable to a yield strength of 180,000 psi, with a strength-to-weight ratio higher than that of the best ferrous materials used in rocket motor casings. Unfortunately, this alloy is difficult to weld and even a successful weld cannot be heat treated to maximum strength because the aging response of base material and weldment differ considerably. It was observed that this alloy, similar to most precipitation hardened alloys, benefits considerably as a result of severe cold work prior to aging. In this manner, the strength of B120VCA was increased to 300,000 psi, a strength which if fully utilized in a pressure vessel would result in a strength-to-density ratio of about 1.7×10^6.

The objective of the subject contract consisted of developing the fabrication, tooling, and metallurgical procedures for the fabrication of sub-scale pressure vessels utilizing the interlocking tape wrapped method of construction for attaining high strength-to-density ratios.

1.0 INTRODUCTION (Continued)

The Curtiss-Wright Corporation wishes to acknowledge financial support of the U. S. Army through the Ordnance Materials Research Office. The assistance of Mr. I. Kahn of that office, as well as of Mr. C. H. Martin of the U. S. Army Rocket and Guided Missile Agency, is gratefully acknowledged.

2.0 SUMMARY

2.1 Phase I

During the Phase I contract, the Wright Aeronautical Division of Curtiss-Wright Corporation pursued the work program aimed at demonstrating [the feasibility of fabricating interlocked Titanium wound pressure vessels from the material and experimental manufacturing was studied standpoint utilizing an original design concept. The program was directed toward the fabrication of 6" diameter hydrotest vessels.

The original design consisted of three layers of spirally wound contoured Titanium tape which interlocked ~~(Figure 1)~~. The tape was wound on end adapters into which pistons could be inserted so that the cylinder could be pressurized ~~(Figure 2)~~. The three layer structure consisted of an I-beam shaped tape separating two layers of channel shaped tape. The interlock was obtained by inserting the butted legs of the adjacent winds of the channel shaped tape into the I-beam shaped tape with an interference fit. The wires maintained the interlock through designing the tangent of the angle on the wires to be less than the coefficient of friction for B120VCA Titanium.]

The stresses present in a cylindrical pressure vessel are two times as great in the hoop direction as they are in the axial direction. By using the interlocking tape concept, a portion of the material stressed in the axial direction is eliminated so that the remaining material is stressed to the same degree as the material in the hoop direction. This type of design predicts cylindrical vessels with efficiencies approaching that of spherical methods of construction.

The design includes an end adapter which was successively stepped for the three (3) layers of tape and provides for pinning or staking of each wire to the adapter to prevent unwinding (Figure 3). In addition, a coating was provided for the internal surface so that the vessel could be pressurized without seapage into the windings. The projected weight savings of the cylindrical portion as compared to a solid wall steel vessel of 200,000 psi uniaxial yield strength, was 50% (Figure 4).

The original wire design was fabricated from round wire through the use of a Turks Head mill (Figure 5). Satisfactory shapes of both the channel and I-beam were fabricated in 100 ft. lengths. The external tape dimensions were obtained by micrometer measurements. However, the internal dimensions required destructive analysis. This limited the internal inspections to the start and finish of each 100 ft. length. The internal dimensions were obtained by sectioning the wire and projecting it at 50 magnifications (Figure 6).

2.1 Phase I (Continued)

The heat treatments for both the channel and I-beam tapes were optimized to produce a minimum 250,000 psi yield strength (Figure 7, 8, and 9). In addition, the mechanical property in both the smooth and notched condition was established for temperatures as low as -320°F (Figure 10). The coefficient of friction of B120VCA Titanium was established experimentally as between .270 and .348.

Twisting and bowing of the tapes after the final Turks Heading operation was found to cause difficulty during subsequent wrapping. This difficulty was eliminated through the use of specially designed spools onto which the tape was wrapped and subsequently vacuum heat treated. Materials for the vessel liner were evaluated, and a vinyl coating was selected as being the optimum from the standpoint of adherence, resistance to cracking or flaking, and adequate ductility with low modulus

The fabrication equipment for the sub-scale vessels was accomplished through the conversion of a lathe (Figure 11). The wrapping apparatus consisted of a collapsible mandrel (Figure 12) onto which the three layers of tape are wound. The interlocking of the wires during assembly was accomplished by three equally spaced pneumatically loaded rollers capable of applying a radial force of 2500 lbs. on the tape (Figure 13) The helix of the wrap was obtained through the use of gage blocks and sine bar devices mounted at the end of the mandrel shaft. A spring loaded guide pushed the tape axially at the point of tangency with the mandrel to insure that adjacent wraps were butted.

Two 6" diameter pressure vessels were fabricated using the tape, tooling, and fabrication method developed in Phase I (Figure 14). The wrapping of the first vessel revealed that the maximum radial force of 2500 lbs. was sufficient to plastically deform the tape. The second layer was removed and, using new tape, rewound under a radial force of 1350 lbs. which was found to be satisfactory. The third layer of tape was applied using a force of approximately 1300 lbs. The vessel was successfully wrapped in all areas except the adapter to mandrel transition, where a step occurred. After extraction of the collapsible mandrel, the profile of the tape showed a saw tooth effect indicating the interlock had been partially disengaged as a result of the removal of the mandrel.

The second vessel was wrapped in a similar manner as the first vessel with minor corrections to the tooling and modifications to the radially applied assembly loading. After completion of the wrapping, the collapsible arbor was removed with little difficulty. The vessel diameter was approximately 0.020" smaller at the center than at the adapter ends.

2.1 Phase I (Continued)

The outer diameter remained smooth but the inner surface was slightly saw toothed in a manner similar to vessel No. 1.

The vessel was assembled with pistons and pressurized. The vessel leaked at 30 psi as a result of a separation of the tape at the cylinder-to-adapter interface. This area was repaired with the use of an inner and outer molded shell in order to re-hydrotest. The second hydrotest resulted in separation of the tape in the cylindrical section remote from the end adapters. From the examination of the vessel, it was concluded that the interlock was insufficient to prevent the tapes from disengaging during hydrotesting.

2.2 Phase II

Analysis of the failed vessels from Phase I indicated that additional surface contact was required between the I-beam and channels to insure interlock. The redesign consisted of increasing the height of the I-beam and channel legs to twice their original value (Figure 15). In addition to the redesign, several other areas of investigation appeared to be required. These other areas to be investigated included a continuous method for the inspection of the wire to insure uniform quality. Alternate designs were also considered to insure the interlock of the tapes. The effect of these alternate designs on the structure strength and weight were to be investigated through the use of structural and interference rigs. Since the design concept is based on the coefficient of friction of Titanium. which establishes the angles on the tape legs, further work on the effect of surface finish, surface contamination, and load on coefficient of friction was performed. Theoretical analyses were also run to establish the effect of the curvature of the wire over the 6 inch mandrel on the dimensions of the wire.

The inspection procedures investigated in Phase I were reviewed with respect to the most feasible methods of continuously inspecting the wires. The air gage method or optical comparator method appeared to be the most practical. The optical comparator method was developed through the use of a special light source and special tooling to provide a continuous inspection method at 62½ maghifications with the use of comparator charts (Figure 16). The process resulted in excellent results for the internal dimensions of the tape and in combination with the micrometer method developed in Phase I, provided the required continuous inspection method for the tapes.

Numerous alternate designs were investigated for increasing the reliability of the interlock of the tape construction. These designs included welding, brazing, adhesives, explosive forming, soft metal

2.2 Phase II (Continued)

shims, and present design with increased tolerance and decreased angles (Figure 17). The decreased angles on the tape legs and the use of a shim between the channels appeared to be the most feasible, and these alternates were included in a 10 times size interference rig evaluation.

As previously noted, the results of the analysis of the sub-scale vessels indicated that additional interlock was necessary between the layers of tape. It was also felt that the disengagement of the wires could have been attributed to a lower coefficient of friction than established during Phase I. Rig testing of actual tapes with various surface finishes and degrees of surface contamination under varying loads was performed during Phase II. These tests showed that increasing loads decreased the coefficient of friction and that small amounts of surface contamination reduced the coefficient of friction below the required value based on the original design (Figure 18). It was also established that, when the coefficient of friction was greater than the desired magnitude (that established during Phase I), the wires actually welded together. The results of this analysis were incorporated into the interference rig by the use of vapor blasting to prepare the surfaces and through the decreased angle test. It should be noted that a lower coefficient of friction reduces the angle on the tape legs and makes the tolerances more critical and smaller.

The interference rig consisted of two, 10 times size channels and half of an I-beam. Interference could be varied through the use of bolts and load cell washers in the I-beam portion of the rig (Figure 19). The rig utilized the original 12° angle on the legs and the redesigned twice height legs. The test showed that interlocking was not accomplished until the mating surfaces picked up and galled. Even though the contact surfaces were increased by the redesign, the failures were similar to those experienced during the testing of the vessels in Phase I.

The analysis of the failed rig indicated that the coefficient of friction between Titanium and Titanium was less than the design values of .3 to .5 assumed and experimentally determined. Since the required coefficient of friction must be greater than .213 which is the tangent of the 12° angle, it was felt that surface contamination such as oxidation, slight misalignment, or a decrease in the coefficient of friction due to an increase in load were the factors affecting the performance of the rig.

Other programs were undertaken in conjunction with the redesigned wire. These programs included methods of fabrication, the ductility of Titanium tape and the Titanium sheet metal which would be used in the

2.2 Phase II (Continued)

10 times size rigs, and the effect of the wrapping on a 6" diameter on the dimensions of the wires.

Attempts to fabricate the increased height leg channel and I-beam wires by the process developed during Phase I proved unsuccessful. The inside surfaces of the legs were incompletely filled due to insufficient material (Figure 20). Various modifications to the roller design were attempted but proved unsuccessful due to the pulling down of material at the internal surfaces during the rolling operation. The solution appeared to be to form the legs during early rolling passes to a height greater than the finished dimension, and then in the final pass collect the metal in order to fill the leg cavity. This method was attempted but proved unsatisfactory due to excessive loads on the tongue of the rollers. Hard rollers failed by shearing of the corners of the roll tongues, and the softer rollers failed by flowing of the material in the same area.

Alternate methods of fabrication were investigated. These methods included the Turks Heading operation for performing the shape and obtaining the final dimension through die drawing. Other methods investigated included alternate methods of rolling, drawing, machining, and chemical milling.

The use of dies proved unsuccessful due to insufficient die life because of the lack of a suitable lubricant for the B120VCA material. The chemical milling and machining procedures would not produce the required tolerances. An experimental rolling of the redesigned wires proved successful in that the experiments showed that the required dimensions and tolerances could be obtained. Fixed priced orders were placed for quantities of tape sufficient to fabricate sub-scale vessels. However, these orders were terminated due to insufficient time to complete by the end of the contract and the results of the rig tests which indicated further redesign.

Metallurgical investigations were undertaken to establish the ductility of the Titanium material in both the tape and sheet metal forms for both the heat treated and annealed condition (Figure 21). This testing was required in order to establish the feasibility of increasing the tolerances for the interference fit of the channel and I-beam tapes and to establish whether the interference rig would have sufficient ductility. Samples of cold rolled rectangular tape and sheet material were fabricated with machined simulated wire shapes. The dimensions were equal to the actual wires and to 10 times size, simulating the interference rig. The results of these tests show that the material has adequate ductility for the fabrication of vessels and the evaluation of the interference and effect of interlocking in

2.2 Phase II (Continued)

the 10 time size rig. Additional tests were run in both the smooth and the notched condition to establish the strength and notch sensitivity of the material.

Two significant results were obtained from the material tests. The notched to smooth ratio of one was obtained at approximately 170,000 psi tensile strength (Figure 22). At strengths greater than this, the material became notch sensitive to a degree directly proportional to the increase in the ultimate tensile strength. Vacuum annealing was used on one series of smooth tensile specimens fabricated from the cold worked wire. The maximum room temperature strength was obtained with an air anneal at 700°F (Figure 23). As the annealing pressure was decreased to a vacuum of 10^{-6} Torr, the ultimate tensile strength decreased. The results indicated that the strengthening of the cold work tape was due to absorbed interstitial gases such as oxygen, nitrogen, or hydrogen. The anneal at low pressures, outgasses the material thereby eliminating the strengthening effect of the interstitials. As the result of material testing, it was evident that the full strength of the cold worked B120VCA Titanium could not be used in the tape wrapped construction due to notch sensitivity which would cause premature failure due to the stress raising effect of the small internal radii.

The effect of the wrapping curvature on the dimensions of the wire during assembly of sub-scale vessels and during inspection were theoretically analyzed. The changes in the dimensions of the tapes were found to be significant for 6 inch diameter curvatures (Table 1). The wire shape used for sub-scale vessels was changed to compensate for the distortion. However, in diameters greater than 12 inches, such as contemplated for full size hardware, the distortion is insignificant and compensation need not be made.

The ten times size structural rigs were fabricated from B120VCA Titanium plate. These rigs were designed to establish the effect of the various designs and alternate designs on the assembly and performance (Figure 24). The rigs were instrumented with both strain gages and photostress plastic. The analyses of the rigs with the minimum interference of .012" and with 12° angles showed that the stress concentration of the internal radii of the I-beam exceeded the tensile strength of the fully heat treated material (Table 2 and Figure 25). In the annealed condition, the contact stresses were sufficiently high to plastically deform the material during assembly and reduce the interference so that failure occurred due to bending upon application of the tensile load (Figure 26). The failure during assembly of the fully heat treated rig was due to the flexure of the I-beam during the assembly of the first set of channels. This flexure

2.2 Phase II (Continued)

has to be overcome in the assembly of the second set of channels, which resulted in a greater than normal load during the assembly of the rig. This adverse condition was compensated for by assembling the four channel pieces simultaneously. This procedure resulted in a satisfactory assembly of the fully heat treated specimens. The test results on the structural rig showed that the fully heat treated material rig failed at an axial load of 16,200 pounds and that the annealed material rig failed at 30,000 pounds axial load. The heat treated rig failed through the I-beam while the annealed rig failed by flexure of the channel and disengagement. The analyses of the strain gage and photostress measurements taken during testing revealed that in both cases the rig experienced flexure of the channels shortly after application of load. This flexure indicated that the precompression of the channels and the tension in the I-beam was not of the magnitude originally calculated or sufficient to eliminate flexure of the channel legs. The hardened material failed due to the increase in the stress at the internal radii of the I-beam while the soft rig failed due to the precompression yielding of the contact surfaces.

A 9° angle rig failed during assembly due to non-uniform loading. A 12° angle rig with .040" interference failed at approximately the same load for the same reason.

The analysis of the rig results indicated that the cause for the premature failures was the increased stresses from non-uniform precompression and stress concentrations. To substantiate this, a 9° rig with .012" interference was reworked to relieve the outer corners of the butted surfaces of the channel so that only the inner portion below the gage points made contact. This rework would produce a maximum condition of non-uniform stress during tensile testing. The rig confirmed the assumption and failure occurred at 7,600 pounds which was approximately one-half the value obtained on the rig that had not been relieved and one-fourth value of the other rig which had not been relieved and fabricated from the annealed material.

Two additional rigs were assembled, utilizing brass shims between the butted faces of the channels. One of the rigs was 9° and the other was 12°, and both the rigs were of .012" interference. The intent of the brass shim was to uniformly distribute the stresses in the area of compression. The stress calculations based on the photoelastic analyses of the previous tests and the photoelastic analysis on the assembled rig indicated that the failure load would be approximately 20,000 pounds. Both rigs failed at 21,000 pounds, confirming the stress analysis which had been modified for non-uniform load distribution at the areas of precompression.

2.2 Phase II (Continued)

The results of these rig tests were used to redesign the tape wrapped structure to compensate for the non-uniform precompression and for the notch sensitivity of the B120VCA Titanium. The redesign resulted in a weight increase and a loss in efficiency of the structure (Figure 27).

Fabrication of this design is not contemplated since the weight reduction for the 250,000 psi Titanium tape construction is 9.4% when compared to a monolithic design using the new maraging steel 18% nickel.

3.0 CONCLUSIONS

1. The feasibility of fabricating sub-scale pressure vessels by the tape wrap method was demonstrated on a converted lathe.

2. The fabrication of the I-beam and channel shaped tapes was accomplished on the original design by the Turks Heading method, and the feasibility of producing the tapes redesigned for increased contact surface was demonstrated by rolling.

3. The structural testing of the increased contact surface design, and alternate designs showed that the tape wrap concept was feasible and that the structure required modification to compensate for non-uniform precompression stress distribution, and for the inherently lower strength of B120VCA in the presence of stress concentrations.

4. A compensated redesign using 250,000 psi Titanium tape was made which would result in a structure having a weight 9.4% lighter as compared to a monolithic case fabricated from the newly developed 300,000 psi maraging steels.

5. The coefficient of friction of B120VCA Titanium which is the controlling design parameter of the Tape Wrap concept is significantly effected by surface finish, load, and slight amounts of contamination.

   (a) Increasing the surface roughness by vapor blasting results in cold welding and increased coefficients.

   (b) Increasing the load decreases the coefficient for Titanium.

   (c) Contamination reduced the coefficient to a value below that required by the design.

6. The strength of the B120VCA Titanium is greatly effected by cold work, notches, and absorbed gases.

   (a) Cold working can increase the tensile strength of Titanium from 180,000 psi to greater than 250,000 psi.

   (b) At the high strength levels, stress concentrations (K_T) of 5 and 10 can reduce the strength to 170,000 psi.

3.0 CONCLUSIONS (Continued)

6. (c) The absorbed gases in the Titanium are a significant factor in the strength and ductility obtained with cold worked material.

4.0 DISCUSSION

4.1 Alternate Designs

4.1.1 Redesign of Shapes for Deeper Groove

The vessels fabricated during Phase I revealed that the interlock between the tapes was not sufficient to withstand the loads imposed during disassembly of the wrapping mandrel or during pressurization. The disengagement of the tapes was evidenced by a stepped irregular surface on both the inside and the outside of the vessels. The analysis as to the cause of the disengagement concluded that one or a combination of the following were contributory:

1. Low coefficient of friction between contact surfaces.
2. Distortion of the cross-section due to bending to the radius of the mandrel.
3. Insufficient pressure or tension during wrapping.
4. Deviation of the cross-section dimensions from specified tolerances.

4.1.1.1 Design

The original wire design was modified to increase the height of the legs to ensure that sufficient contact existed between the layers of the tape. The modification consisted of an increase in the height of the legs in combination with compensating the thickness of the I-beam web in order to result in the least increase in weight for the same structure thickness. The modification provided for increased internal radii and also resulted in a larger entrance gap during assembly precluding interference before engagement. The comparison of the new design to the old design is shown in Figure 28.

4.1.1.2 Dimensional Change During Wrapping and Inspection

During the fabrication of the sub-scale vessels, the wire is formed over a 6" mandrel. This curvature results in distortion of the tapes which effects the angles and dimensions. In addition, the inspection method developed during Phase II uses an optical comparator and measures the wire cross-section by passing a beam of light tangent to the wire while it is bent to a diameter of 6". In order to use this instrument effectively, a theoretical change in the wire cross-section as a function of the radius must be established. This dimensional change would be used to compensate the observed measurements of the tape shapes. Two variations of the wire cross-

4.1.1.2 Dimensional Change During Wrapping and Inspection (Continued)

section were considered; one for the Phase I I-beam and channel and the other for the deeper flanged Phase II design.

4.1.1.2.1 Method of Analysis

The analysis was divided into two parts; the change in section due to Poisson's ratio and the change due to strain energy. The Poisson's ratio analysis accounts for the changes in the wire cross-section due to tensile and compressive bending stresses transmitted to the cross-section by Poisson's effect. The total strain for any fiber in the cross-section is given by:

$$\Delta = \frac{\mu Y_o \ell}{R_o}$$

in which

Δ = total strain (in.)

μ = Poisson's ratio

Y_o = distance from neutral axis to the fiber (in.)

ℓ = original length of the fiber (in.)

and R_o = radius of curvature of the neutral axis

In the strain energy analysis, the flanges of the channel or I-beam tapes are assumed to rotate through the angle, β, such that at any radius, R, the total strain energy in the wire is a minimum. The assumptions made in the analysis were:

1. The flanges of the wire cross-section are considered as rings subjected to uniform twisting moment about the z- axis (Figure 29). In addition, the rotated flanges are subjected to bending along the length of the wire due to curvature (Figure 30).

2. The web acts as a beam of unit width subjected to end moments due to the rotation of the flanges (Figure 29). In addition, the web is also subjected to bending along the length of the wire (Figure 30).

For minimum strain energy, the following equation relating β, b, h, d, t, and R (defined as shown in Figure 28) is obtained:

4.1.1.2.1 Method of Analysis (Continued)

$$\left(\frac{1}{2\beta^2} - \frac{1}{\beta}\right) = A + B\left(\frac{3\pi t^3 R^6}{hb^3 d} + \frac{BR^5}{d} + 8R^3\right) \tag{2}$$

in which

$$A = \frac{8h^4}{9d^3 t}\left(4\pi K^3 - K + K^{-1}\right)$$

$$K = \frac{b}{h}$$

and

$$B = 88.977\,\frac{t^2}{d^4}$$

4.1.1.2.2 Results of the Analysis

The family of curves in Figure 31 shows the variation of the strains Δb, and Δd for both the shallow (Phase I design) and deep wires (Phase II design) with respect to the bend radius of the wire. In all cases, the strains in the deep channel and "I" sections are greater than those in the similar wires with shallow flanges. The curves are asymptotic to the X- and Y- axis because the displacement (Δ) is inversely proportional to the radius (R).

The family of curves in Figure 32 shows the rotation, β, of the flanges as a function of the bend radius, (R). At any constant radius the rotations of the flanges vary directly as the depths of the flanges, resulting in greater rotation for sections with greater depth. Also, the rotation of the flanges varies inversely as the "stiffness" of the web. Figure 33 shows the variation of Δd due to strain energy as a function of the radius. The variation of total strain (Δ) due to Poisson's ratio and strain energy are plotted against the radius in Figures 34, 35, 36, and 37.

Table 1 shows the change in the dimensions for the 6" sub-scale vessel fabricated from both tape designs. It can be seen that with the Phase I design the change in dimensions was significant, however, it should not have effected the performance of the interlock to the extent of disengagement at 50 psi. For larger vessels these distortions of dimensions are insignificant and can be neglected.

4.1.1.2.3 Redundant Forces and Moments in a Helical Coil

Since several designs were to be evaluated by structural testing of simple uniaxial specimens, it was necessary to develop an IBM program to design the actual wire shape to be used in biaxially loaded tape wound pressure vessels. This was necessary since it was anticipated that several designs of tape would result from the structural testing

4.1.1.2.3 Redundant Forces and Moments in a Helical Coil (Continued)

and the availability of an IBM program would eliminate the necessity of solving a series of simultaneous equations for each of the proposed designs to establish the dimensions for the biaxial state of stress.

In order to evaluate the axial, bending and torsional stresses in the wire when wound helically to any desired radius, an investigation was made to determine theoretically the redundant forces and moments in a helical coil of one turn subjected to uniformly distributed loads, consisting of radial load (p), axial load (w) and circumferential shear flow (q).

The method of the elastic center was used for the solution of this highly redundant structure. The redundants were applied at the elastic center of the helical coil which coincides with the centerline of the coil. The displacements at the elastic center were obtained using the Castigliano's theorem of the Differential Coefficient of the Internal Work which states, "If the internal work of a frame structure is expressed as a function of the external forces, the resulting expression is such that its partial differential coefficients give the relative displacements of their points of application". The general equation is as follows:

$$\theta_Q = \delta_Q = \int M_r\left(\frac{\partial M_r}{\partial Q}\right)\frac{ds}{EI_r} + \int M_x\left(\frac{\partial M_x}{\partial Q}\right)\frac{ds}{EI_x} + \int M_t\left(\frac{\partial M_t}{\partial Q}\right)\frac{ds}{JG} \quad \text{- - - - - - - (3)}$$

in which, Q = the direction of the displacements or, in other words, the direction of the redundants.

M = the moment due to the redundants and the externally applied loads.

and subscripts r, x, t refer to radial, axial, and tangential directions, respectively.

The integration was performed for one turn between the limits of zero to 2π.

Knowing the displacements (rotations and deflections) due to unit redundant forces and the externally applied loads, a system of simultaneous equations are set up incorporating the unknown redundant moments and forces. Solution of these moments and forces will determine the stresses in the wire (Table 3).

4.1.1.2.4 Derivation of Formulas

This section outlines the detailed derivation of formulas for the solution of the redundant moments and forces in a helical coil of one turn due to radial and axial loads and circumferential shear flow. Fig. 38 shows a free body diagram of the coil with the loads and redundants. All moment redundants are shown in vectors.

Nomenclature

X_o, Y_o, Z_o - Redundant forces at the elastic center in the X, Y, Z directions, respectively

M_{x_o}, M_{y_o}, M_{z_o} - Redundant moments at the elastic center in the X, Y, Z directions, respectively

q - shear flow (lbs. per in.)

p - uniform distributed radial load (lbs. per in.)

w - uniform distributed axial load (lbs. per in.)

λ_o - pitch of helical coil

ψ - helix angle

α - angle in plane normal to coil axis

R - radius of coil

M_{α_t}, M_{α_x}, M_{α_r} - moments at α- location in t, x, r directions, respectively

τ - uniform distributed torque along circumference (in.-lbs. per in.)

θ_{xx}, θ_{yy}, θ_{zz} - angular rotations at the elastic center about the x, y, z axis, respectively, due to unit redundants in x, y, z direction, respectively.

δ_{xx}, δ_{yy}, δ_{zz} - linear displacements at the elastic center about the x, y, z axis, respectively, due to unit redundants in x, y, z direction, respectively.

θ_{xy}, θ_{xz}, θ_{yz} - angular rotations at the elastic center about x, x, y axis, respectively, due to unit redundants in y, z, z directions, respectively.

δ_{xy}, δ_{xz}, δ_{yz} - linear displacements at the elastic center about x, x, y axis, respectively, due to unit redundants in y, z, z directions, respectively.

$\theta_{x_o}, \theta_{y_o}, \theta_{z_o}$ - angular rotations at the elastic center about x, y, z axis, respectively, due to applied loads.

$\delta_{x_o}, \delta_{y_o}, \delta_{z_o}$ - linear displacements at the elastic center about x, y, z axis, respectively, due to applied loads.

I_x, I_r, J - moments of inertia about axial, radial and tangential axis, respectively (in.^{4})

E, G - moduli of elasticity and rigidity, respectively

K - constant

Assumptions

The following assumptions were made in the analysis:

a) Angular rotations about x, y, z axis, respectively, at elastic center are zero, i.e., $\theta_{x_o} = \theta_{y_o} = \theta_{z_o} = 0$

b) Linear displacements in x, y, z directions, respectively, at elastic center are zero; i.e., $\delta_{x_o} = \delta_{y_o} = \delta_{z_o} = 0$

c) The redundant forces and moments are in the plane which includes the starting point of the helix coil for one turn; i.e., $\alpha = 0$.

d) Uniform distributed radial pressure, shear flow, axial load, and circumferential torque.

e) Wire of unit width and uniform cross section.

The following are the moments at α, R due to the redundants applied at the elastic center of the helical coil. (Figs. 39 and 40)

$$M_{\alpha_t} = +M_{y_o}\cos\alpha - M_{z_o}\sin\alpha + X_oR - (Z_o\cos\alpha + Y_o\sin\alpha)\,R\alpha\tan\psi \quad (4)$$

$$M_{\alpha_r} = +M_{z_o}\cos\alpha + M_{y_o}\sin\alpha + (Y_o\cos\alpha - Z_o\sin\alpha)\,R\alpha\tan\psi \quad (5)$$

$$M_{\alpha_x} = +M_{x_o} + Z_oR\sin\alpha - Y_oR\cos\alpha \quad (6)$$

The moments at α, R due to the applied loads are given below (Figs. 41-43):

$$M_{\alpha_t} = pR^2\frac{\tan\psi}{\cos\psi}(\alpha\sin\alpha + \cos\alpha - 1) + qR^2\tan\psi(\alpha\cos\alpha - 2\sin\alpha + \alpha)$$
$$+wR^2\left\{\tan^2\psi(\sin\alpha - \alpha\cos\alpha) + \alpha - \sin\alpha\right\} + \tau R\sin\alpha \quad (7)$$

$$M_{\alpha_r} = pR^2\frac{\tan\psi}{\cos\psi}(\sin\alpha - \alpha\cos\alpha) - qR^2\tan\psi(\alpha\sin\alpha)$$
$$-wR^2\left\{\tan^2\psi(\alpha\sin\alpha + \cos\alpha - 1) + 1 - \cos\alpha\right\}$$
$$-\tau R(1 - \cos\alpha) \quad (8)$$

$$M_{\alpha_x} = -p\frac{R^2}{\cos\psi}(1 - \cos\alpha) + qR^2 (\alpha - \sin\alpha)$$
$$+wR^2 \tan \psi(\alpha - \sin\alpha) + \tau R \alpha \tan \psi \quad (9)$$

The rotational and translational displacements at the elastic center for unit redundant moments and forces are:

$$\theta_{xx} = 2\pi R K_4 \quad (10)$$

$$\theta_{yy} = \pi R (K_2 + K_3) \quad (11)$$

$$\theta_{zz} = \pi R (K_2 + K_3) \quad (12)$$

$$\theta_{xy} = \theta_{xz} = \theta_{yx} = \theta_{zx} = 0 \quad (13)$$

$$\theta_{yz} = \theta_{zy} = 0 \quad (14)$$

$$\delta_{xx} = 2\pi R^3 K_2 \quad (15)$$

$$\delta_{yy} = \pi R^3 \left\{ K_4 + \tan^2\psi (K_5 K_2 + K_6 K_3)\right\} \quad (16)$$

$$\delta_{zz} = \pi R^3 \left\{ K_4 + \tan^2\psi (K_6 K_2 + K_5 K_3)\right\} \quad (17)$$

$$\delta_{xy} = \delta_{yx} = 2\pi R^3 K_2 \tan\psi \quad (18)$$

$$\delta_{xz} = \delta_{zx} = 0 \quad (19)$$

$$\delta_{yz} = \delta_{zy} = \pi^2 R^3 \tan^2\psi (K_3 - K_2) \quad (20)$$

In which

$$K_2 = \frac{1}{JG}, \quad K_3 = \frac{1}{EI_y}, \quad K_4 = \frac{1}{EI_x}, \quad K_5 = \frac{8\pi^2}{6} - \tfrac{1}{2}, \quad K_6 = \frac{8\pi^2}{6} + \tfrac{1}{2}$$

The rotational and translational displacements at the elastic center due to the applied loads are:

$$\theta_{x_0} = -2\pi\frac{R^3}{\cos\psi} K_4 p + 2\pi^2 R^3 K_4 q + 2\pi^2 R^3 K_4 w \tan\psi$$
$$+2\pi^2 R^2 K_4 \tau \tan\psi \quad (21)$$

$$\theta_{y_0} = +\pi \frac{R^3}{2} \frac{\tan\psi}{\cos\psi} (K_2+3k_3)p + \pi^2 R^3 \tan\psi (K_2 - K_3) q$$
$$+ \pi^2 R^3 \tan^2\psi (K_2 - K_3) w \quad (22)$$

$$\theta_{z_0} = -\pi^2 R^3 \frac{\tan\psi}{\cos\psi}(K_2+K_3)p + \pi \frac{R^3}{2} \tan\psi (9K_2+K_3)q + \frac{\pi R^2}{2}$$
$$-\tan^2\psi (3K_2+K_3) + 8 w + \pi R (K_2+K_3 \tau \quad (23)$$

$$\delta_{x_o} = -4\pi R^4 \frac{\tan\psi}{\cos\psi} K_2 p + 2\pi^2 R^4 \tan\psi K_2 q + 2\pi^2 R^4 K_2 w \tag{24}$$

$$\delta_{y_o} = \frac{-\pi R^4}{\cos\psi} (K_4+K_7 \tan^2\psi (K_2+K_3) p + \pi^2 R^4 \tan^2\psi (7K_2+K_3) q$$
$$-\pi^2 R^4 \tan\psi (2K_2 \tan^2\psi (2K_2 \tan^2\psi - (5K_2+K_3))w$$
$$-\pi^2 R^3 \tan\psi (K_2-K_3)\tau \tag{25}$$

$$\delta_{z_o} = -2\pi 2K_3 R^4 \frac{\tan^2\psi}{\cos\psi} p + \pi R^4 (\tan^2\psi (K_3K_5-K_2K_8)-3K_4) q$$
$$+ \frac{\pi R^4}{2} \tan\psi (2K_7 \tan^2\psi - 9)K_2 + (2K_7 \tan^2\psi - 3)K_3 - 6K_4) w \tag{26}$$
$$+ \frac{R^3}{2} \tan (2K_2-3K_3-4K_4)\tau$$

In which

$$K_7 = \frac{8\pi^2}{6} + 1 \qquad K_8 = \frac{8\pi^2}{6} + 11/2$$

The general load-deflection equations for determining the redundant forces and moments at the elastic center of the helical coil with external loads of radial distributed load p, circumferential shear flow q, axial distributed load w, and circumferential torque τ are:

$$\theta_{xx} M_{x_o} + \theta_{xy} M_{y_o} + \theta_{xz} M_{z_o} + \theta_{x_o} = 0 \tag{16}$$

$$\theta_{yx} M_{x_o} + \theta_{yy} M_{y_o} + \theta_{yz} M_{z_o} + \theta_{y_o} = 0 \tag{17}$$

$$\theta_{zx} M_{x_o} + \theta_{zy} M_{y_o} + \theta_{zz} M_{z_o} + \theta_{z_o} = 0 \tag{18}$$

$$\delta_{xx} X_o + \delta_{xy} Y_o + \delta_{xz} Z_o + \delta_{x_o} = 0 \tag{19}$$

$$\delta_{yx} X_o + \delta_{yy} Y_o + \delta_{yz} Z_o + \delta_{y_o} = 0 \tag{20}$$

$$\delta_{zx} X_o + \delta_{zy} Y_o + \delta_{zz} Z_o + \delta_{z_o} = 0 \tag{21}$$

When the redundant forces and moments are determined at the elastic center, the stresses anywhere along the coil can be determined using equilibrium equations. When the deflections at the elastic center are not zero, then the load deflection equations are not set equal to zero but to the known deflection.

4.1.2 Alternate Methods of Interlocking

The present method of interlocking between layers is the interference fit between the I-beam wire and the adjacent legs of the channel wire. This interference fit places the adjacent legs of the channel wire in precompression which prevents bending in the channel web. The wires remain in place by maintaining the tangent of the angle of the contact surfaces of the I-beam and channel less than the coefficient of friction for the materials being mated.

The theoretical analysis of the frictional method of maintaining interlock performed during Phase I showed this approach to be feasible. During Phase II it was deemed desirable to investigate alternate methods of joining the legs of the tapes together in an attempt to reduce the tolerance requirements or to further reduce the weight of the structure. Various methods other than making use of the friction between the layers of tape were studied (Figure 17).

4.1.2.1 Metal Inserts

There are two areas in the wire construction where an extrudable metal insert could be included to either increase the coefficient of friction or reduce the tolerance requirements in the fabrication of the wire. The first of these areas is between the channel and the I-beam legs at the contact surfaces, and the second area is between the adjacent legs of the channel wire. The first method was determined to be unsatisfactory since during pressurization the loads on the insert would increase resulting in additional extrusion. This would result in reducing the precompression in the channel legs, thereby allowing bending to occur in the channel which increases the stress. In addition, when the pressure is released the layers would be loose, which could result in unwrapping.

The second method was to insert the soft metal shim between the butted legs of the channel. With the use of a shim in the first layer of channel the application of the I-beam over the channel legs would result in extrusion of the soft metal shim. A tangential force would have to be applied to the winding adjacent to the engaged channel tape in order to butt it to prevent interference during application of the next winding of the I-beam. This would also continually reduce the helix causing an increase in diameter resulting in a tapered vessel. Another approach to eliminating this build-up of tolerance would be to wrap all layers at the same time. This would be a very difficult fabrication technique. The use of the insert did look promising for applying the second layer of channel (the outer layer), and for this reason the method was included in the structural testing of the ten times size structural rig.

4.1.2.2 Adhesive Bonding

The adhesives appeared to have the same disadvantages as the soft metal inserts between the channel and I-beam mating surfaces. The relatively low elastic modulus of adhesives would relieve the pre-compression load in the channels and I-beam legs which would result in excessive bending and failure of the channel flanges. If the design were modified to reduce or eliminate the legs and increase the contact surfaces in the axial direction, the adhesives did show promise. The optimum design using this method would be layers of strip with spaces in between the winds. The major problem of this method of fabrication would be in the attachment to the adapters.

4.1.2.3 Brazing

Various braze materials for B120VCA titanium were investigated. All of the braze alloys which would have adequate strength required brazing temperature well in excess of 750°F which is the aging temperature of the B120VCA titanium wire for obtaining high strength. Any temperature in excess of this aging temperature results in over-aging and loss in strength or recrystallization which will anneal the material.

4.1.2.4 Welding

Two methods of welding were investigated; namely, high frequency resistance welding, and ultrasonic welding.

The high frequency resistance welding would be used to weld the channel legs together as they are assembled onto the mandrel. The method appeared promising from the structural standpoint; however, the welding of B120VCA titanium has not progressed to the point where consistent crack free welds can be produced. In addition, this type of welding has created a problem of delayed cracking due to strain aging. For these reasons it was decided that high frequency resistance welding would not be reliable until a new welding procedure had been developed.

The ultrasonic method of welding appeared to be satisfactory for this alloy of titanium because it did not require the excessive heat to fuse the metal. Investigation of ultrasonically welding the butted faces of the channels showed that steel sheet as thick as .040" had been welded by ultrasonic methods. To date this method has not been applied to beta titanium alloys. The development of an ultrasonic welding procedure for the B120VCA titanium material was beyond the scope of this contract. It was decided to hold this method of fabrication as an alternate in the anticipation of the expected advancements in the area of ultrasonic welding.

4.1.2.5 Differential Heating and Cooling

Differential heating of the I-beam and channel was considered as a method of assembly to replace the present hydraulic loading during the wrapping operation. This method would reduce the tolerance requirements of the wires, but could increase the preloads to the point of plastically deforming the material. The procedure required heating the I-beam when wrapping over the first layer of channel and then cooling the third layer (channel) when wrapping it over the second layer (I-beam) which would still have to be at the preheat temperature. The method of tooling for this procedure could not be resolved. It was apparent that all three layers have to be wrapped simultaneously.

4.1.2.6 Explosive Forming

Explosive forming was investigated as a method of increasing the tolerances on the wire and applying the preload in the legs of the channel and I-beam through the use of explosives. The three layers would be wrapped loose and then explosively formed against an O.D. mandrel. There were several problems which made this method impractical. When the collapsible mandrel would be removed from the loosely wrapped assembly the layers would twist out of shape and disengage. The basic principle of obtaining the high strength lightweight structure was to provide voids between the I-beam winds. These voids could not be filled in order to prevent the web of the inner layer of channel from deforming into the void during the explosive forming operation. Filling the void with a fluid during the explosive forming process would result in a lack of preload being obtained on the inner layer.

4.2 Inspection Techniques

During Phase I of the contract, various methods of inspection for the wire shapes were investigated. These included measurement by means of a comparator, projection by means of a metallograph, micrometer measurement of the external dimensions, measurement of a calcium sulphate molding and use of toolmakers microscopes and air gages. The method that was most successful was the metallographic method. This was accomplished by copper plating (non-adhering) the tape to a thickness of approximately 0.005". The tape was then placed in a special metallographic clamp, polished and photographed at 50 magnifications. The photographs were then measured. This method presented two problems. The first problem was that it was very difficult to cut and polish the tape without some distortion or rounding of the edges on the inside surfaces. More important, however, was the problem that every time the tape was to be measured it had to be cut. This meant that only the beginning and the end of the tape could be

4.2 Inspection Techniques (Continued)

inspected and that the deviation throughout the length of the fabricated tape was unknown for the internal dimension.

The objective of Phase II was to obtain a continuous method of inspection for the newly designed tape shape. Twelve vendors were contacted which included the inspection areas of comparators, air gages, blade edge microscopes, and electrical methods. Two sources or methods of inspecting continuously were located.

An inspection with the use of air gages appeared to be satisfactory; however, considerable skill would be required to operate the equipment and to make any minor changes. In addition, a completely new set of tooling would be required for any design changes. The air gage method was also found to be inadequate for measuring the angles.

The second method for continuous inspection was optical, using a comparator and a special lighting source. The lighting source consisted of a mercury arc lamp with filters and a polarizing device to provide parallel light beams

The tooling for continuously inspecting the tape consists of a mandrel with a groove to guide the wire. The mandrel is 6" in diameter and includes adjusting devices to align the wire so that the light can strike the wire normal to the profile.

The inspection device includes a lens system for $62\frac{1}{2}$ magnification with glass comparator charts giving minimum and maximum dimensions and angles. The external dimensions of the wires are checked by micrometer or electrical measuring devices.

The optical method selected has the advantage of being easily adapted to any design changes by the procurement of a new comparator chart. Figure 16 shows the comparator with the mercury arc lamp housing, the power supply, and the comparator chart installed on the viewing screen. The comparator chart for the redesigned wire is shown in Figure 44.

4.3 Fabrication of the Redesigned Deeper Groove Tape

4.3.1 Turks Heading

Various methods of fabrication of wire were investigated during Phase I. The Turks Heading method was selected as being the most feasible for fabricating the two different tape shapes. The investigation and experimentation included establishing the size of the starting wire, the spring-back of titanium, the number of passes

4.3.1 Turks Heading (Continued)

through the Turks Head, and the design of the breakdown rollers. Through the use of this process, wire was produced in sufficient quantities to fabricate the sub-scale vessels.

During Phase II, various experiments were performed with the Turks Head mill in an attempt to fabricate the new design tape to blueprint tolerances. The Turks Head rolls were redesigned, based on the rolling procedure developed during Phase I, to produce the deeper groove tape design. The initial attempts to roll these forms revealed that the inner corners of the legs did not fill, and that this condition was more prevalent in the channel shape than in the I-beam shape. Successive examinations of the wire during the various stages of the rolling, revealed that pulling down of the material during each successive pass was responsible for the insufficient filling of the internal shape (Figure 20). This pulling down of the metal reduces the amount of material in the leg area so that there is insufficient material remaining prior to the final pass to form the finished shape.

In an attempt to overcome this condition, a series of tests were run in which the deep groove channel rollers were used to collect material in the leg areas followed by using the old design shorter leg rolls for the final pass. The results of this experiment show that by collecting the metal prior to the final pass, the legs could be filled. This procedure is shown in the second and third sketch of Figure 20.

Another approach to collecting the material prior to the final pass is also shown in Figure 20. This method would leave material on the outside of the leg so that during the final pass the legs would bend or flow into the existing voids from where the material had been pulled down during previous passes. Investigation of this method revealed that the stiffness of the material is such that the flow would not result in filling the void but go into increasing the length of the tape.

Rolling experiments designed to produce deep groove tape revealed that increasing the height of the tongue on the rolls resulted in flowing of the edges of the tongue. It was apparent that the strength of the roll material in this unsupported condition was insufficient to form the newly designed tape. An additional set of rolls were fabricated and heat treated to a higher strength level. Initial attempts to fabricate wire using these rolls were performed on aluminum wire which has a lower strength than titanium in order to prove the fabrication sequence without damaging the rolls. This series of experiments showed that by collecting the material in the leg area prior to the final pass, the required shape and dimensions could be produced. However, the aluminum did not offer sufficient resistance

4.3.1 Turks Heading (Continued)

to the rolling operation and the center of the groove wandered with respect to the side dimensions. The experiments were repeated with the use of annealed steel. The principle of the rolling operations were again confirmed. The center groove again was not within blueprint tolerance with respect to the side dimensions; however, it was improved with respect to the experience with the aluminum material. It was felt that this condition could be corrected with additional tooling and rolling equipment since the major objective of filling the corners of the shapes had been demonstrated.

Based on the aluminum and steel rolling experiments the starting size of the rectangular titanium wire for fabricating the I-beam shape was increased in order to fill the corners. On the second pass the tongue of the top and bottom rollers sheared off. It was established that the heavy load on the roller tongue exceeded the tensile strength of the increased hardness rollers. This condition was not prevalent with the old design of wire shape because the tongue of the roller was only .009" instead of the .018" for the redesign. This increased height of the roller tongue reduced the side support. When the rollers were heat treated to the strength of the original rolls, the material flowed, rounding the edges of the tongue. With the increased hardness rollers, the tensile strength of the material was exceeded and the corners of the tongue sheared off. Due to these problems of excessive loads on the rollers during the fabrication of titanium tape, it was felt that the rolling procedure would have to be modified to provide several breakdown passes with shapes that are substantially different from the final design in order to reduce the loads on the roller.

Various vendors were contacted to establish a source to fabricate the newly designed tape. Two vendors were selected to perform experimental fabrication to establish the feasibility of producing the wire to the required shape and within the required tolerances. The approaches used were die drawing and rolling. In addition, the feasibility of machining the shape and chemically milling the shape were also investigated under separate programs.

4.3.2 Die Drawing, Machining, and Chemical Milling

The initial attempts to die draw the shape were performed on dies fabricated during Phase I to the original design dimensions. These dies were used to establish the amount of die wear, type of lubrication, and the die dimensions vs. tape dimension. The results of these investigations were negative in that an adequate lubricant could not be found that would prevent pick-up on the carbide dies. Various liquid lubricants, including moly-disulfide, graphite, and various solid lubricants such as silver, copper, and colloidal suspensions were used.

4.3.2 Die Drawing, Machining, and Chemical Milling (Continued)

The die life was found to be very poor and satisfactory lubricants could not be found to prevent the dies from galling.

Another series of experiments were performed using the rolling process up to the final reduction. The final reduction would be accomplished through the use of a die to establish the necessary dimensions and tolerances. The experimental rolling portion of this investigation concluded that it was necessary to anneal the wire between passes. The amount of cold work possible after the last pass could not be predicted and further experiments would be required to establish the degree of remaining cold work in the wire after final sizing by die drawing. This degree of cold work was important since it would control the maximum ultimate tensile strength of the wire. The die drawing portion proved unsatisfactory even with the preformed shape being rolled in, due to lack of die life from galling between the titanium and the dies. Extensive experimental work with various lubricants was also performed but did not result in a satisfactory solution to the problem.

Several other methods of fabricating the wire were also investigated. The first was chemical milling. The approach was to roll the titanium wire into a rectangular shape and then mask all of the wire except for a strip along the top and bottom. The chemical etchant would then be allowed to remove enough material to form the groove within .004" of the finished size. The proper amount of excess material would be left on the shoulders to provide the required prerolling shape to allow for equal area reduction in the shoulders and in the groove during the final pass on the Turks Head mill. With this method, only one pass would be required after the groove was etched in. The results of this investigation showed that a proprietary chemical milling etchant was available for the all-Beta alloy. However, extensive development problems and costs were anticipated in the masking and obtaining of the required tolerances on these relatively small shapes. In addition, there would be very little cold work in the wire due to the one reduction pass on the Turks Head which would again result in very low tensile strength in the final wire.

Machining of cold rolled rectangular titanium wire was also investigated. A sample of the channel shape was fabricated by milling. The material was found to machine satisfactorily without any noticeable tool wear, after machining a 24 foot length of wire. It was, however, established that the continuous milling method could not hold the required $\pm$ .0004" tolerance. It was concluded that a final grinding operation to establish the required dimensions would be required. The requirement for 100 foot continuous lengths of tape for the subscale vessels and up to 10,000 foot continuous lengths for full size vessels would not be feasible by this method.

4.3.3 Rolling

The development program to fabricate the tape shapes by rolling included experiments using existing rolls which simulated the tape shapes. These experiments showed that the feasibility of fabricating the wire by this method was practical and that the required tolerances could be obtained through the use of approximately three reductions. The vendor was willing to proceed with the fabrication of wire on a fixed price basis; however, the order was not placed due to insufficient time remaining on the present contract to complete the order, and the results of the structural rigs testing which dictated a further redesign.

4.4 Material Properties

4.4.1 Tensile Properties of Wire and Sheet

During Phase I of the program, low temperature tensile tests were performed to establish the notch sensitivity characteristics at temperatures varying from room temperature to minus 320°F (Figure 10). The material used was .090" heat treated sheet material. The notched-to-unnotched tensile strength ratio ranged from .76 at room temperature to .34 at minus 320°F. Since the notch sensitivity characteristics are important to the tape wrap design, it was decided to continue the investigation using actual wire specimens at various strength levels and at various stress concentrations.

The tests performed were run at room temperature with specimens which simulated the actual wire. It can be seen in Figure 22 that the notch ratio decreases appreciably as the ultimate tensile strength increases. The smooth ultimate tensile strength is equal to the notched ultimate tensile strength at approximately 170,000 psi, which is considerably lower than the strength of the fully cold worked and aged tape. The specimens which produced the maximum ultimate tensile strength were taken from finished rolled and aged channel tape and they produced the lowest notched ultimate tensile strength. The specimens which produced the lowest ultimate tensile strength were obtained from rectangular tape which was only about 5% cold worked and they resulted in the highest notched ultimate tensile strength. It is significant to note that the results showed the same trend whether the notch concentration factor (K_t) used was five or ten. The specimens with the notch concentration factor (K_t) of 10 had a root radius of .002".

During the studies to establish the notch sensitivity at various length levels, it was necessary to heat treat the specimens in vacuum. As a result of the heat treatments, it was noticed that the strength varied with the degree of vacuum used during the heat treat operation.

4.4.1 Tensile Properties of Wire and Sheet (Continued)

A subsequent series of tests were performed keeping all the variables constant except the degree of vacuum. The specimens were taken from cold worked tape and heat treated at 700°F in air and vacuum ranging from 3×10^{-2} TORR to 10^{-6} TORR. It can be seen from Figure 23 that the ultimate tensile strength decreases as the vacuum increases. Based on the data, it was concluded that the increase in ultimate tensile strength was partially due to the absorbed gases such as hydrogen, nitrogen, and oxygen. It was also apparent that the reduction in tensile strength was accompanied by an increase in ductility which is common to a precipitation strengthening mechanism. From these results, it was concluded that the Titanium outgassed as a result of the vacuum aging which presented a variable which would require control to obtain the optimum combination of strength and toughness during fabrication of tape.

4.4.2 Coefficient of Friction

The coefficient of static friction was initially established during Phase I; however, subsequent testing of rigs and actual tapes indicated that additional tests were required to insure that the design assumptions were correct. The determination of the effect of variables such as surface finish, load, oxidation and cold work was required to insure that the design would perform satisfactorily.

A new friction rig was designed to establish the effect of these variables (Figures 45 and 46). The rig consists of a top and bottom clamp with grooves cut at right angles to each other. The short specimens which are 2" long are inserted in the grooves. Two additional wire specimens 8" long are inserted at right angles to the two specimens retained in the groove. The rig is assembled with the use of two bolts and load indicating washers which are inserted under the bolt heads to record the total clamping load on the specimens. The load was applied with a tensile machine through the 8" long specimens. The static coefficient of friction load was obtained by the load drop indicator on the tensile machine.

The friction specimens were fabricated by cold rolling .123" diameter B120 Titanium wire into a rectangular shape which measured .083" by .140" The rectangular wires were than heat treated in a vacuum for 25 hours at 750°F. The surface treatments for the wires included vapor blasting, acid etching, and as-rolled surface to ascertain the effect of the surface finish upon the coefficient of friction. The wires were then installed in the rig and pulled in opposite directions to establish the load to initiate slippage. The clamping force was varied to determine the effect of the load on the coefficient of friction. The results of these tests are shown in Figure 18 for both heat

4.4.2 Coefficient of Friction (Continued)

treated and non-heat treated wire.

4.4.2.1 Effect of Load

The results of the friction tests show a consistent trend toward decrease in coefficient of friction as the clamping load increases. This decrease is felt to be due to the fact that at the higher clamping loads, the effect of surface finish is reduced by crushing of the asperities. At the low clamping loads, two sliding members will tend to pick up at the asperities. It is significant to note that the majority of the test points showed a coefficient of friction greater than .213, which is the tangent of the design angle of 12°. As previously noted, the design interlock of these wires will only be effective when the coefficient is greater than the tangent of the angle of the interference fit.

4.4.2.2 Effect of Contamination

To establish the effect of surface oxidation and contamination on the coefficient of friction, several of the specimens were heat treated in a manner to provide slight surface oxidation to the specimens. These specimens were tested and the comparative results can be seen in Figure 18. When the long specimens were contaminated and run in combination with shorter specimens which had not been contaminated, the coefficient of friction dropped to .205. When all four specimens were contaminated the coefficient of friction dropped to .113. From these results it was apparent that any slight contamination, even to a degree that is not apparent on the surface of the material, could reduce the coefficient of friction to a value below the tangent of the interference angle. These results explain the inability to interlock apparently clean specimens.

4.4.2.3 Friction Welding

The analysis of the test results showed that there were two distinct curves for the heat treated wire, both having approximately the same slope. The one curve was for specimens that were found welded together upon disassembly of the rig (Figure 47). When the wires slide evenly without welding together, they fall on the lower curve. The cold welded specimens had extensive pick-up and galling, while the oxidized specimens slipped evenly and showed no pick up or galling. Further, the results showed that the specimens that were vapor blasted and etched to produce a clean rough surface resulted in a higher coefficient of friction, because in every case but one the specimens welded together. In all three cases, where the non-heat treated wires were used, the specimens welded together and produced a high

4.4.2.3 Friction Welding (Continued)

coefficient of friction as compared to the wires that were heat treated and did not weld together.

It can be concluded from these results that with the existing design, the interlock should be achieved if the interference angle is held to the desired tolerances, and that necessary precautions are taken to avoid any oxidation or contamination during the heat treat, vapor blasting, and wrapping of the vessel.

4.5 Structural Testing of the Designs

4.5.1 Interference Rig

An interference rig was designed and fabricated to evaluate the effect of variances in interference. The purpose of the tests were to determine the parameters which effect the stresses in the tape. Schematically shown in Figure 48 is a free body diagram of the channel subjected to the loads resulting from the interference fit. It may be seen from the schematic that the interference fit tends to clamp the channel flanges and prevent rotation during axial loading (pressurization). The design of the rig used to evaluate these stresses is shown in Figure 49. A cutaway view of the rig with the load cell washers installed is shown in Figure 19.

The channel sections of the rig were fabricated from B120VCA titanium plate to ten times the size of the actual cross-sectional dimensions of the wire. The clamping plates which simulate the I-beam were also fabricated from B120VCA. The plates are bolted together to produce the interference fit under varying load with the channel section. The hoop restraint which is present in an actual vessel was simulated by transverse clamping which could be varied to simulate the internal pressure effects. A small load cell washer was installed under each of the bolt heads which clamped the rig together. The washers permitted the reading of the clamping loads directly instead of depending on a calculated conversion on equivalent torque.

The instrumentation of the channel sections consisted of strain gages in the areas where bending would occur. The effect of varying the longitudinal clamping loads or the transverse clamping load would be evidenced by the strain gage readings as to the effect of these various loads on the restraint of the bending of the channel. If the longitudinal clamping load was insufficient, the two specimens would separate and bending would occur. This would simulate the interference fit between layers. The load cell washers were also monitored continuously during the test to detect any physical shifting of the specimens which would manifest itself as an increase or decrease in

4.5.1 Interference Rig (Continued)

the values indicated by the load cells.

The initial test on the rig was run with a 2,360 lb. longitudinal clamping load (simulating interference) and 81 lbs. transverse clamping load (simulating hoop restraint).

The load on the simulated channels was slowly increased to 2,000 lbs. At this point, it was observed that the transverse clamping load on each of the bolts had increased from 81 lbs. to 290 lbs. This increase indicated that the specimens were not interlocked and were riding out as a result of the application of axial load. To confirm the lack of interlock, the transverse bolts were removed and the clamping load was applied. This experiment again resulted in riding out of the channel specimens. The channel specimens were again installed and clamped in place while a 200 lb. load was applied to the clamping bolt. Upon removal of the transverse clamp the specimens again were observed to ride out. The test was repeated with a 2500 lb. transverse clamping load and upon release the specimens again rode out.

After repeating the above test several times, the contact surfaces showed signs of pick-up and galling, and the specimens no longer rode out. The specimens were inspected to insure that the radii of the specimens had not interfered and that the specimens were sliding only on flat surfaces.

Since it was impossible to get the specimens to friction lock until the total surfaces became galled, the tests indicated that the coefficient of static friction of these Titanium parts must be less than the assumed design values. The measured angles of the specimens were 12°. Since the design analysis showed that the interlock should be effective when the tangent of the angle is less than the coefficient of friction, and the tangent of the 12° angle is .213, this indicates that the coefficient of friction must have been less than this value. Visual examination of the pieces showed no evidence of contamination.

The analysis of the results of the interference rig testing in combination with the results of the effect of surface finish and contamination on the coefficient of friction indicated that slight surface contamination in combination with annealed smooth surface material were responsible for the lack of interlock on the rigs. Due to the damaged condition of the contact surfaces, i.e., galling, no reworks could be performed to increase the coefficient of friction.

4.5.2 Structural Rig

One of the basic considerations in the design of the tape wrap motor case is the effect of the interference fit on the strength of the tape interlock, prior to and after the application of the axial load. The maximum interference is determined by the allowable elongation of the material, whereas the minimum is determined by the design.

When a tensile load is applied to a tape interlock assembled with a predetermined press-fit, the transfer of load across the joint from the channel web to the adjacent web has been assumed to be accomplished by the relief of precompression at the butted faces of the channel legs. If a sufficiently large compression exists in the butted channel legs, there will not be a bending moment at the intersection of the legs and web. A ten-times size model was designed to experimentally prove the above basic concept, and to evaluate the effects of alternate designs and several interference fits on the strength of the interlock. The design of the test rig is shown in Figure 50.

4.5.2.1 Pre-stress and Pre-strain

When the channel and the I-beam wires are loaded in the elastic region, a direct relationship between the strains in the channel legs and the I-beam web can be established by using the compatibility of the original gage-point width of the combined channel legs and the gage-point separation of the I-beam legs. The resulting equations are:

$$\sigma_I = \frac{2A_{ch}\,(l_{ch} - l_I)\,E}{2l_I A_{ch} + l_{ch} A_I} \qquad (22)$$

and

$$\sigma_{ch} = \frac{A_I\,(l_{ch} - l_I)\,E}{2l_I A_{ch} + l_{ch} A_I} \qquad (23)$$

σ = tensile stresses in the web (psi)

E = Young's modulus of elasticity (15×10^6 psi for Ti.)

and subscripts ch and I refer to the channel and I-beam, respectively.

The relationship between the interference fit and the pre-strain in the I-beam web is given in Figure 51, for titanium with a 0.2% yield strength of 180,000 psi and 250,000 psi. Based on the 180,000 psi yield strength, the theoretical strain in the I-beam web having interference fits of 0.012 in. and 0.080 in. are, respectively, 1.5%

4.5.2.1 Pre-stress and Pre-strain (Continued)

and 15.5%.

4.5.2.2 Behavior of Tape Lock Under Load

When tensile load is applied to the interlock, the precompression in the channel legs is gradually relieved so as to maintain the equilibrium of the channel. If the interlock fails, one of the following conditions must occur:

1. The applied loads have stressed the channel web beyond the yield strength of the material.

2. The applied loads have completely relieved the precompression at the back of the channel legs so as to cause bending of the channel at the intersection of the web and the leg, thus disengaging the joint or failing the channel.

3. After the relief of the precompression, the applied load introduces a very high tensile stress in the I-beam web due to the "wedge" effect, which together with the stress-raising effect of the fillet radius, ruptures the web section of the I-beam.

4. The combined pre-strain and the additional strain induced in the I-beam web as the result of the axial load exceeds the elongation of the material.

5. The frictional forces resisting the disengagement of the channels from the I-beam have been inadequate to hold the assembly together.

When the assembly acts under idealized conditions and fails by yielding in the channel web under simple tension, the test rig will have a theoretical maximum load capacity as shown in Figures 52.

4.5.2.3 Structural Rig - (IS 28719) Test Procedure

The structure rig is a ten times size rig which was designed to evaluate the maximum allowable interference fit and alternate designs. The blueprint of this rig can be seen in Figure 50. The details that simulate the I-beam and channel shapes were rough machined from B120VCA titanium plate, heat treated to 180,000 psi yield strength and then final machined. Both 9° and 12° interface angles were fabricated to ascertain which would be the best angle to use in the finished wire. Figure 24 is a photograph of the rig, loosely assembled, and Figure 53 is an exploded view of the titanium parts.

4.5.2.3 Structural Rig - (LS 28719) Test Procedure (Continued)

The details were stress coated to evaluate the distribution of stresses during assembly of the pieces. In determining the magnitude and distribution of stresses by the photo-stress technique, the end faces of the I-beam and channels were coated with a plastic sheet. As the load was applied to assemble the rig, the stresses developed in the details produced a corresponding stress pattern in the plastic which was visible when viewed through a polarized screen. The stress patterns showed up as color fringes, and by knowing the type and thickness of the plastic used, the magnitude of the stresses was computed by counting the number of fringes.

4.5.2.3.1 Rig No. 1

The first rig that was tested had 12° interface angles and an interference fit of .012" which corresponds to .0012" interference fit in the actual wire size.

Figure 54 shows the method of assembly. Step 1 of the assembly was accomplished successfully at a load (P) of 13,750 lbs. Figure 55 is a photograph of the assembled rig showing the photo-stress pattern. Figure 56 illustrates the stress conditions in the I-beam as determined from photo-stress evaluation following Step 1 of the assembly. The displacement of the neutral axis as evidenced by the stress evaluation shows considerable bending of the I-beam during this step of the assembly.

During Step 2 of the assembly, the I-beam failed at a load (P) of 11,000 lbs. Figures 25 and 57 are photos of the failure. Stress conditions at the time of failure were not obtained.

Due to the brittle nature of the I-beam failure, it was decided to anneal a geometrically similar test rig and repeat the assembly.

4.5.3.2 Rig No. 2

The channels and I-beam were annealed in an argon atmosphere at 1425°F for one hour The hardness was reduced from Rockwell "C" 45 to Rockwell "C" 32.

This rig was successfully assembled as shown in Figure 58. All four channels were pressed in simultaneously to eliminate the excessive bending of the I-beam during two step assembly in an attempt to force the I-beam to elongate evenly. Following the assembly, strain gages were installed to measure any bending of the channels that might occur during the test. If either the precompression of the channel legs is relieved or the coefficient of friction is less than the

4.5.3.2 Rig No. 2 (Continued)

tangent of the interface angle, the channels will back out and the strain gages will show bending. The rig was loaded in tension in 5000 lb. increments to 30,000 lbs. when the interlock failed due to bending of the channels which caused one channel leg to disengage as shown in Figure 26. Examination of the strain gage data taken during the test (Figure 59) indicated that bending of the channels started at very low loads and continued until failure of the interlock. Upon inspection of the rig after failure, it was discovered that the interface angle surfaces had distorted during assembly. With the annealed titanium, the material flowed when the two surfaces came in contact instead of sliding on one another. This indicated that as the channels were forced into the I-beam, the interface angle surfaces experienced surface deformation instead of elongating the I-beam. This resulted in very little precompression between the channel legs and the channels started to ride out as soon as the tensile load was introduced to the rig.

It was concluded that the lowering of the tensile strength to improve the ductility and notch sensitivity, resulted in lowering the compressive yield strength below the design requirement. The improvement in ductility and notch sensitivity cannot be obtained by fully annealing, and additional tests of rigs in this condition were discontinued.

4.5.2.3.3 Rig No. 3

Rig No. 3, a duplicate of Rig No. 1, was instrumented with both photostress plastic and strain gages. This rig was successfully assembled by again pressing in all four channels simultaneously with a load of 24,000 lbs. The photo-stress pattern at the completion of assembly is shown in Figure 60. Figure 61 indicates the approximate magnitude of the stresses in the I-beam and channels after assembly. The compressive stress between the channels was calculated as 44,000 psi. It can be seen in Figure 61, that the photo-stress does now show any stress pattern in the channels. This is due to the fact that the plastic is cut back slightly at the edge to be sure there is no contact of plastic during assembly. Figure 61 does show 120,000 psi stress in the corners of the I-beam after the details were pressed together. These stress values indicate that there is high stress concentrations in the radii, and that the I-beam does not elongate uniformly as was assumed for the original stress analysis. When the tensile load was applied to the assembly, the I-beam broke at 16,200 lbs., which was far below the expected value. Figure 62 shows the strain gage data and again there is evidence of bending in both channels. The failure of the I-beam was identical to Rig No. 1, which can be seen in Figures 25 and 57.

4.5.2.3.4 Rig No. 4

Test Rig No. 4 consisted of a 9° interface angle with a .012" interference fit. All four channels were pressed in simultaneously and the I-beam broke at a load (P) of 40,000 lbs. The photo-stress showed at least 150,000 psi at all four radii of the I-beam.

4.5.2.3.5 Rig No. 5

Test Rig No. 5 had a 12° interface angle with a .040" interference fit. All four elements were again pressed in simultaneously and the I-beam broke at a load (P) of 37,000 lbs. The photo-stress pattern was almost identical to Rig No. 4, showing approximately 150,000 psi stress at the radii of the I-beam.

4.5.2.3.6 Rig No. 6

In an attempt to determine the effect of non-uniform precompression, Rig No. 6 consisted of a reworked 9° interface angle with .012" interference fit. The rework consisted of relieving the end face surfaces of the channels that butt together. This means that as the channels are forced into the I-beam, only .093" at the tips of the legs of the normal .340" surface is touching. This rework can be seen in Figure 63. The three layers were pressed together with a load (P) of 45,000 lbs. The tensile load was applied to the rig and the I-beam broke at 7600 lbs. The strain gage data is shown in Figure 64, and it again shows evidence of bending before failure. It was confirmed that the relief on the ends of the channel, which simulated non-uniform compression, put a moment on the I-beam and caused premature failure.

4.5.2.3.7 Rig No. 7

Test Rig No. 7 utilized a 9° interface angle and .012" interference fit with a .040" brass shim. The brass shim was installed to equalize the precompression load between the channel legs. The rig was assembled with a load (P) of 45,000 lbs. The rig was then installed into the tensile machine and pulled. At 21,000 lbs, two of the channel legs broke. The strain gage data can be seen in Figure 65 and the failure photo is Figure 66.

4.5.2.3.8 Rig No. 8

Test Rig No. 8 was similar to Rig No. 7 except it had 12° interface angle and a .012" interference fit with a .040" brass shim. The rig was assembled with a load (P) of 37,000 lbs. and failed at the exact same tensile load of 21,000 lbs. The strain gage data can be seen in Figure 67.

4.5.2.4 Analysis of Test Rig Results

Table 2 shows a summary of the rig tests. The results in Table 2 indicate that the tensile loads at the time of the failure of the rigs fall far short of the theoretical full capacity of the rig as given in Figure 52. For the heat treated specimens (180,000 psi yield), only 25% of the rig capacity was obtained. At best, a 50% capacity was obtained with the annealed material (130,000 psi yield) in Rig No. 2. These tests reveal, therefore, the importance of the following effects on the actual strength of the rigs:

(1) The magnitude and the distribution of the precompressive stresses at the butted channel legs prior to and after the application of the axial load.

(2) The ductility and strength of the material.

4.5.2.4.1 Precompressive Stresses

One of the factors that caused the decrease in the capacity of the test rigs is the inability of the rig to achieve the theoretical precompression based on a predetermined interference fit. From equations (22) and (23), for an interference fit of 0.012 in., the computed tensile stress in the I-beam and the precompression in the butted channels are 195,000 psi and 127,000 psi, respectively. A photo stress study of Test Rig No. 3 indicated corresponding stresses of 90,000 psi and 44,000 psi. The loss in the precompression is due in part to the distortion of the channel and I-beam interface during assembly and to the insufficient depth and rigidity of the mating flanges.

The free-body diagram of a channel under an assumed uniform precompression is shown in Figure 68 (a). When there is no load ($P_1 = 0$), P_2 is equal to P. As P_1 is gradually increased, the precompression (P_2) is relieved such that at the back of the channel, the total load becomes $P_2 - P_1$. Under this loading condition, the basic equilibrium condition does not change, or $(P_2 - P_1) + P_1 = P$.

The relief of the precompression consists of two parts, a uniform stress reduction ($\frac{P_1}{A}$) and a triangular flexural stress reduction ($\frac{M}{S} = \frac{6P_1d_1}{Wt^2}$. Figure 68 (b) shows graphically the stress distributions. When $\frac{P_1}{A} + \frac{M}{S}$ at point <u>a</u> (Figure 68) in the channel is equal to the precompression stresses $\frac{P_2}{A}$, the butted channel begins to lose pre-

4.5.2.4.1 Precompression Stresses (Continued)

compression and point a of the two channels tends to separate (Figure 72c). At this stage, the channels may be assumed to bear against each other at point b, causing a "wedging" effect and introducing a relatively large load P' on the I-beam.

Based on the method described, Test Rig No. 3 was stress analyzed. The precompression at the back of the channels is taken as 44,000 psi per photo stress analysis. The results are as follows:

For separation at point (a);	P_1'	= 5,260 lbs.
	P	= 21,000 lbs.
For wedging action;	P_1'	= 2,800 lbs.
	P'	= 5,250 lbs.

When the rig failed at 2 (P_1 + P_1') = 16,120 lbs., the tensile force in the I-beam = 2 (P + P') or = 52,500 lbs. The tensile strength of the I-beam is equal to 180,000 psi x 0.465 in.^{2} = 83,500 lbs. Since the tensile force in the test rig is less than the allowable tensile strength, the failure of the I-beam at the intersection of the web and the leg is due, in part, to the stress-raising effect of the sharp fillet radius at the intersection. A detailed discussion of this effect will be presented in the next section.

Test Rig No. 6 was reworked to provide the maximum non-uniform stress distribution at the butted channel by relieving a portion of the contact surface The detrimental effect of this non-uniform stress condition was confirmed by the rig, as evidenced by the failure at 7,200 pounds axial load. Test Rigs Nos. 7 and 8 included brass shims between the butted channel faces to more uniformly distribute the load and to evaluate the alternate design, mentioned previously, which uses a soft metal insert.

The failure of Test Rigs Nos. 7 and 8 at the intersection of the web and leg may be explained as follows: The 0.040" brass shim, which is relatively soft as compared to the heat treated titanium causes a decrease in precompression so that the wedging effect shown in Figure 68 (c) took place shortly after the applied load was increased. As the point (b) in the channel is displaced outward, a large bending moment is introduced at the web section of the channel. This moment is increased further due to stress-raising of the fillet radius. Since the channel web thickness (0.155 in.) is only half of the I-beam web thickness, and since the bending stress varies inversely as the square of the thickness, the channel web failed in flexure. It must be noted that had the material been more ductile, the high bending

4.5.2.4.1 Precompression Stresses (Continued)

stress would be redistributed by yielding, and a much higher axial load would have been achieved prior to failure, such as occurred with Rig No. 2, which was annealed.

The outward displacement of point (b) in the channel, as previously described, was visually observed during the test.

4.5.2.4.2 Ductility of Material

As previously described, the failure of the I-beam in Test Rig No. 3 was attributed to, in part by, the stress-raising effect of the radius. In order for the rig to fail, the stress concentration factor (SCF) should be equal or greater than $\frac{83,500}{52,500} = 1.6$. Figure 69 shows a theoretical SCF vs. fillet radius curve for a T-head which is similar to the I-beam used in the rig. For a fillet radius of 0.015 - 0.020 in. as used in the rig (Figure 70), the theoretical SCF ranges from 5.5 to 6.6. It is, therefore, very likely that the actual SCF in the I-beam was greater than the 1.6 required to fail the member. This belief is further reinforced by the fact that for a similar rig (Test Rig No. 2) with annealed material having a strength in the I-beam approximately 72% of that of the heat treated Rig No. 3, the tensile load was 30,000 lbs. which is greater than the 16,200 lbs. obtained in Test Rig No. 3.

From Figure 73, the theoretical SCF may be reduced from 5.5 to 3.0, if the fillet radius is increased from 0.015 in. to approximately 0 050 in. It is also of interest to note that the effect of increasing the $\frac{M}{d}$ ratio from 1.27 to 3.0 will not reduce the SCF appreciably Therefore, the cross-section of the I-beam web in the present design appears adequate.

The failure of the Test Rig No. 4 during assembly, using a 0.040 in. interference fit, is due to the lack of the ductility of the material to relieve the stress concentration. As indicated in Figure 51, a 0.040 interference fit would require a material having an allowable strain of 6.7%. Obviously, for the present rigs, the heat treated Titanium material has a ductility much less than this value; however, the annealed material, which has the ductility, does not have sufficient compressive strength to withstand the assembly loads. Based on this, the maximum usable strength of the material would be between the two strength levels.

4.5.2.4.3 Conclusions from Rig Tests

The following conclusions may be drawn from the experimental results of the test rigs:

(1) The introduction of a brass shim between the channels reduces the precompression and does not eliminate the high bending stress in the web section of the channel.

(2) The efficiency of the tape-lock using the principle of interference fit is dependent largely on the ductility of the material.

(3) The precompression at the butted faces of the channels in the present design, using a 0.012" interference fit, is not sufficiently large to relieve the theoretical maximum tensile force. The remedies for this deficiency are (a) increasing the interference fit and (b) increasing the depth and rigidity of the channel flanges. Case (a) will require an increase in the ductility of the material and case (b) will increase the weight of the overall design.

(4) The low ductility of the fully heat treated material introduces high stress concentrations at the fillet radii of the I-beam and channels causing failures of the members both during assembly (0.040" interference fit) and under increasing load. Increase in ductility of material is required. Otherwise, the thickness of the I-shank and fillet radii of the I-beam and the channel should be increased.

Assuming that the ductility of the heat treated titanium cannot be satisfactorily increased without resulting in compressive yielding, a proposed wire design that will meet the above requirements and increase the capacity of the unit is shown in Figure 27. A comparison of weights between the titanium tape-wrapped motor using this revised design and the monolithic motor using high-strength steels such as the Ladish D6 and 18% nickel is shown in Figure 71. The weight savings for the 250,000 psi Ti motor casings are 26% and 9.4%, respectively, over the D6 and 18% Ni designs. However, for 180,000 psi titanium material, there is no weight advantage in the tape-wrapped motor design. Redesigning for the use of high strength steel materials would make the fabrication problem even more difficult as a result of smaller size tape and closer tolerances due to the higher modulus of elasticity.

TYPICAL WIRE CONFIGURATION

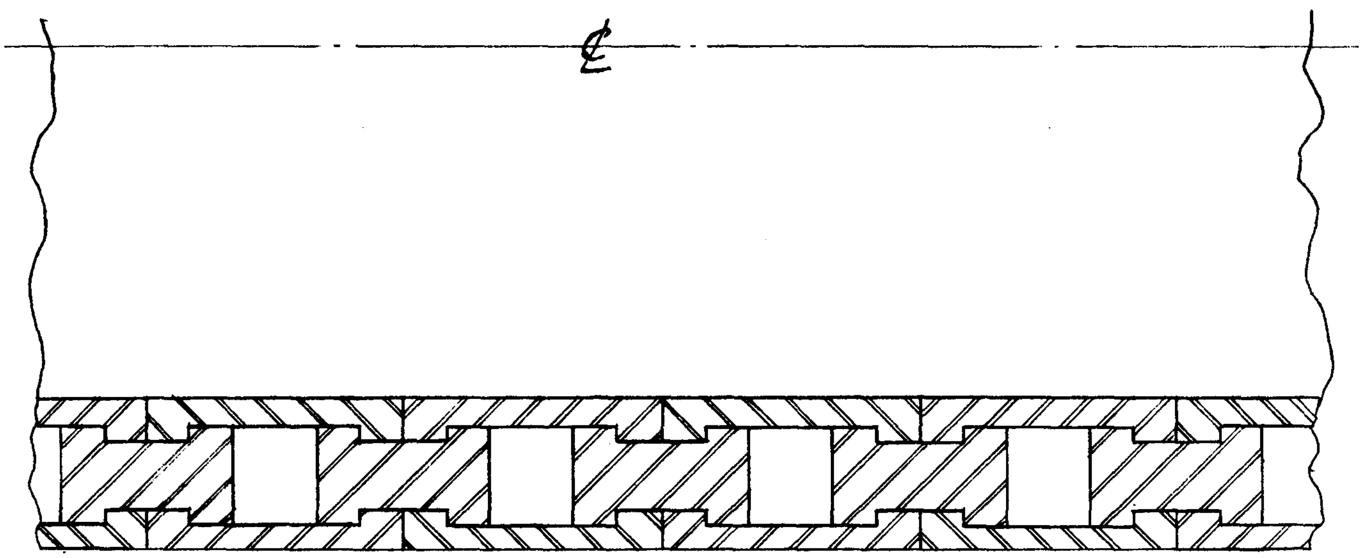

FIGURE 1

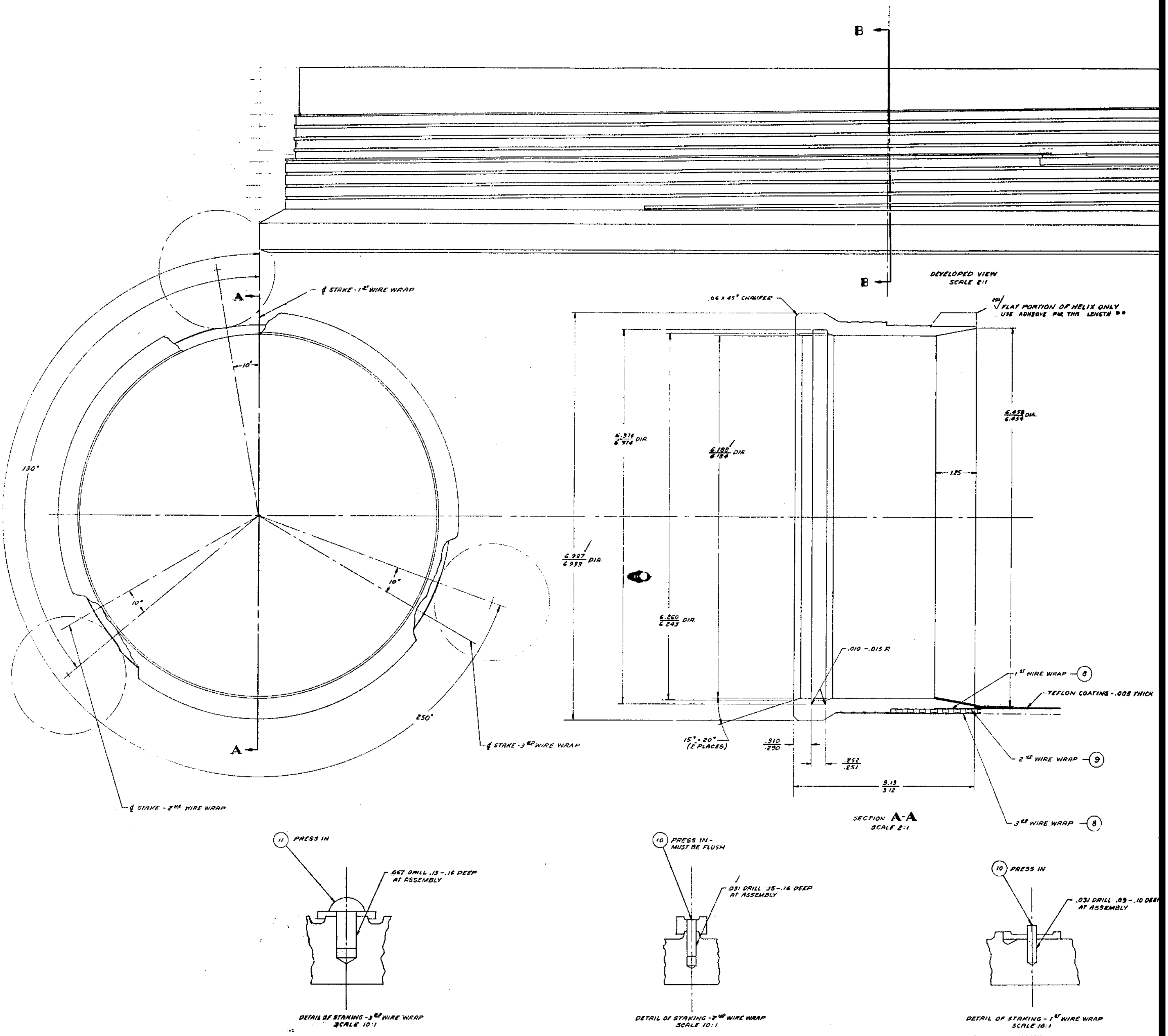

B
B
A
A
℄ STAKE - 1ST WIRE WRAP
10°
130°
10°
10°
250°
℄ STAKE - 3RD WIRE WRAP
℄ STAKE - 2ND WIRE WRAP
DEVELOPED VIEW
SCALE 2:1
.06 X 45° CHAMFER
FLAT PORTION OF HELIX ONLY
USE ADHESIVE FOR THA LENGTH
6.976 / 6.974 DIA.
6.186 / 6.184 DIA.
6.458 / 6.454 DIA.
1.25
6.937 / 6.933 DIA.
6.260 / 6.245 DIA.
.010 -.015 R
1ST WIRE WRAP (8)
TEFLON COATING - .005 THICK
15° - 20° (2 PLACES)
.310 / .290
.252 / .251
3.13 / 3.12
2ND WIRE WRAP (9)
SECTION A-A
SCALE 2:1
3RD WIRE WRAP (8)
(11) PRESS IN
.067 DRILL .15 - .16 DEEP AT ASSEMBLY
DETAIL OF STAKING - 3RD WIRE WRAP
SCALE 10:1
(10) PRESS IN - MUST BE FLUSH
.031 DRILL .15 - .16 DEEP AT ASSEMBLY
DETAIL OF STAKING - 2ND WIRE WRAP
SCALE 10:1
(10) PRESS IN
.031 DRILL .09 - .10 DEEP AT ASSEMBLY
DETAIL OF STAKING - 1ST WIRE WRAP
SCALE 10:1

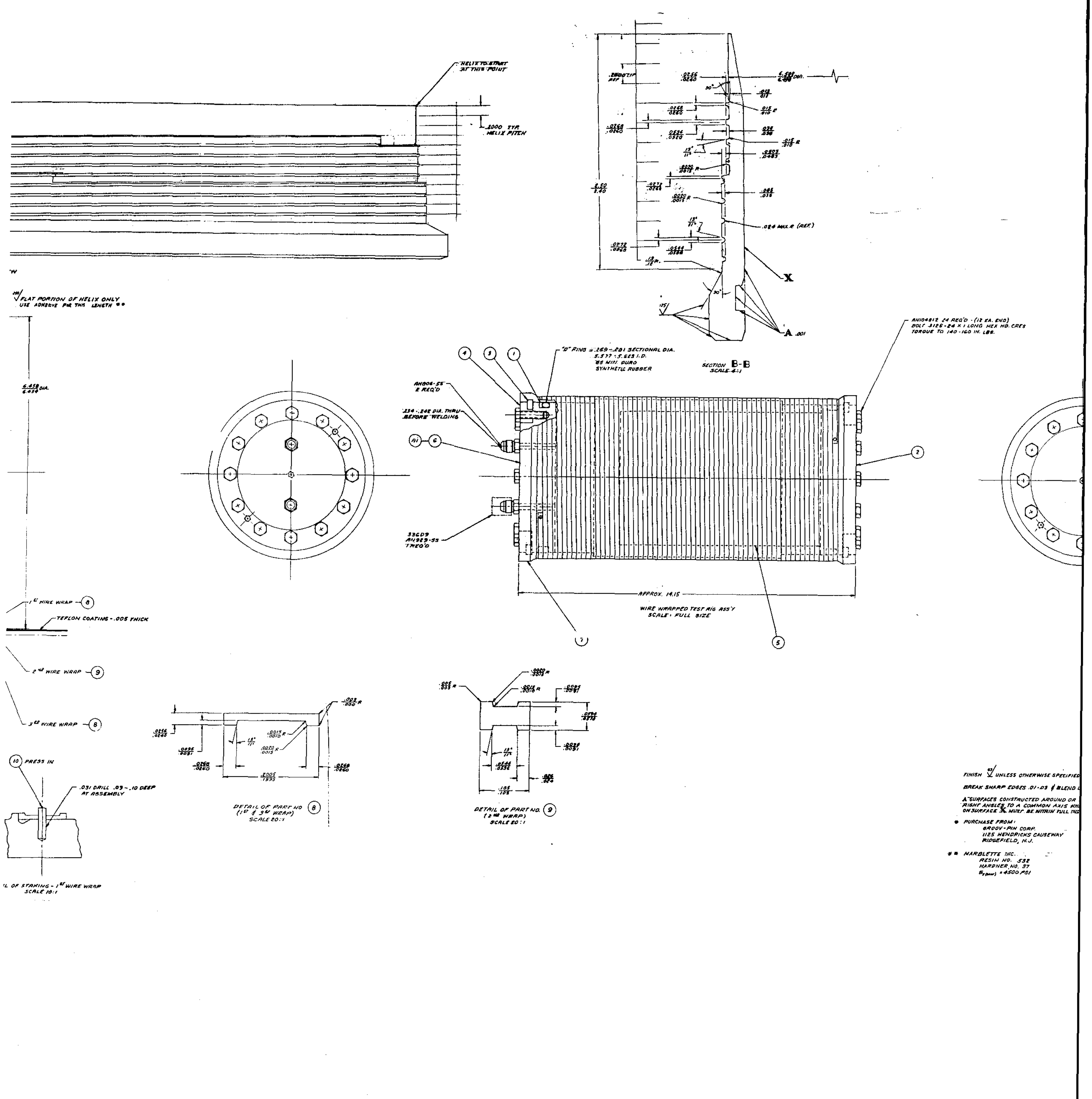

FINISH 63/ UNLESS OTHERWISE SPECIFIED

BREAK SHARP EDGES .01-.03 & BLEND

A SURFACES CONSTRUCTED AROUND OR RIGHT ANGLES TO A COMMON AXIS WHICH ON SURFACE X MUST BE WITHIN FULL IND.

* PURCHASE FROM: GROOV-PIN CORP. 1125 HENDRICKS CAUSEWAY RIDGEFIELD, N.J.

** MARBLETTE INC. RESIN NO. 532 HARDNER NO. 37 $E_{(bond)}$ = 4500 PSI

F

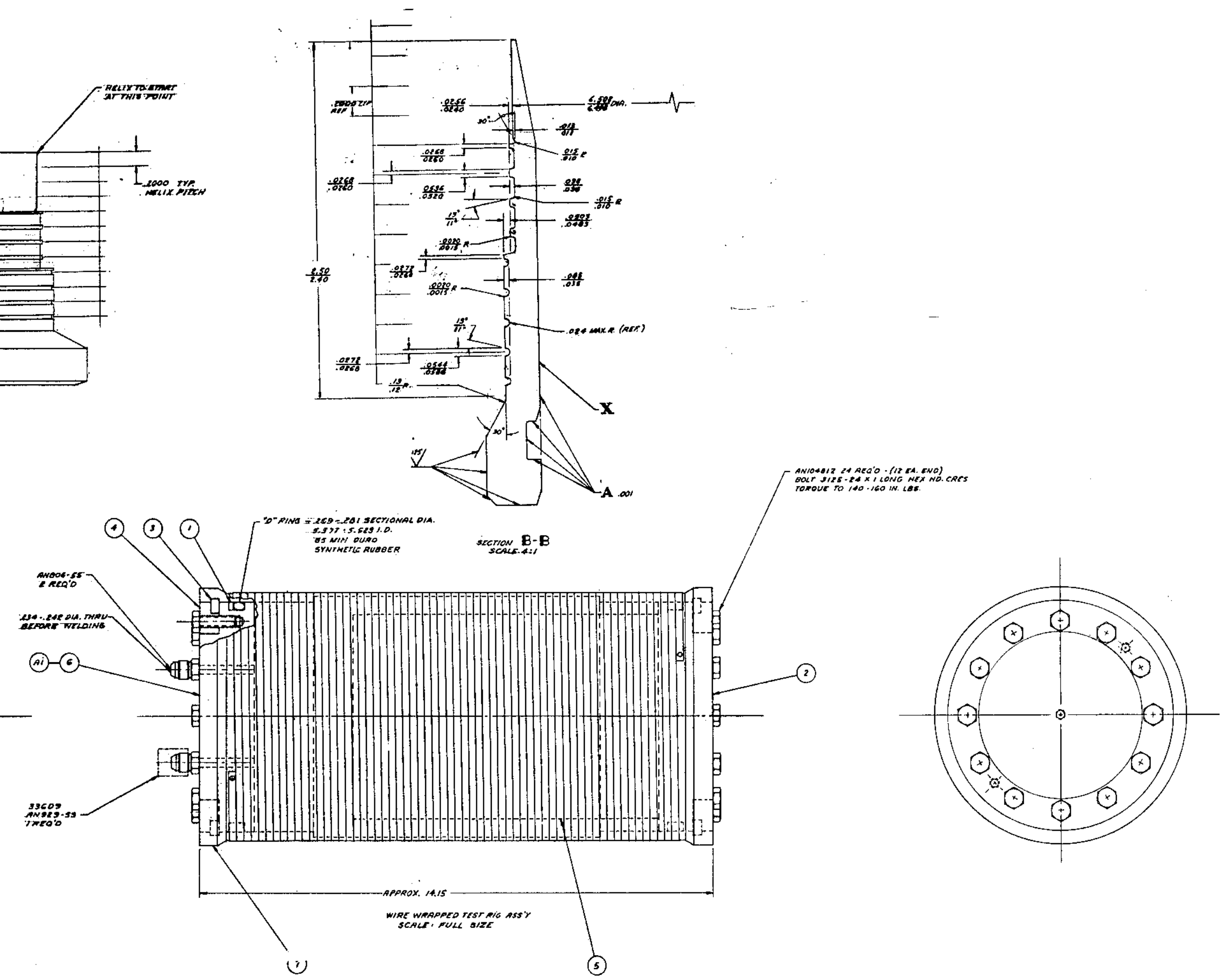

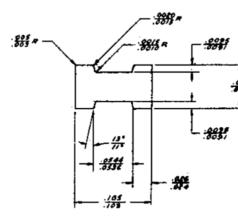

FINISH 63/ UNLESS OTHERWISE SPECIFIED.

BREAK SHARP EDGES .01-.03 & BLEND UNLESS OTHERWISE SPECIFIED.

A SURFACES CONSTRUCTED AROUND OR AT RIGHT ANGLES TO A COMMON AXIS WHEN PART IS MOUNTED ON SURFACE X MUST BE WITHIN FULL INDICATOR READING SPECIFIED.

* PURCHASE FROM:
GROOV-PIN CORP.
1125 HENDRICKS CAUSEWAY
RIDGEFIELD, N.J.

** MARBLETTE INC.
RESIN NO. 532
HARDNER NO. 37
$S_{s(bond)}$ = 4500 PSI

LS25439

ITEM NO.	PART NO (ADD)	ASS'Y	PART NO (REFERENCE)	PART NO (CANCEL)	QUAN	DESCRIPTION		MAT'L	OTHER SPECS	FORG. CAST W.B.
A1	LS23896A1				1	PLUG & FITTING ASS'Y				
11					2	ROUND HD DRIVE STUD NO. 0		SAE 6150	1/8 LONG	
10					4	GROOV-PIN TYPE 3 - 1/32 DIA *		SAE 6150	1/8 LONG	
9					AS REQ	WIRE - I-BEAM		B120VCA		
8					AS REQ	WIRE - CHANNEL		B120VCA		
7					2	ADAPTER - WIRE R_c 46-50		TAKENT OR EQUIVALENT		
	A929-5S				1	CAP ASS'Y - PRESS SEAL		CORR RESIST STEEL	TYPE 304L OR 347	
	AN806-5S	A1			2	PLUG - FLARED TUBE		CORR RESIST STEEL	TYPE 304L OR 347	
6	LS23896-7	A1			1	PLUG - INLET		SAE 4340 SAE 8740	RC 19-26	
5	LS23896-6				1	CYLINDER		OPTIONAL		
	AN104812				24	BOLT-HEX.HD. .3125-24 X 1" LG		C'RES		
					2	"O" RING - 5.600 I.D. .275 SECT. DIA		SYNTHETIC RUBBER	85 MIN DURO	
4	LS23896-5				2	PLATE - RESTRAINING		SAE 4340 SAE 8740	RC 19-26	
3	LS23896-4				6	RING - SEGMENT		SAE 4340 SAE 8740 SAE 52100	RC 47-51	
2	LS23896-3				1	PLUG - PLAIN		SAE 4340 SAE 8740	RC 19-26	
1	LS23896-2				2	RING - BACK-UP		LEATHER		

PARTS LIST

SCALE AS INDICATED
JOB NUMBER
DRAWN 2-1-60
CHECKED 3-1-60

CURTISS-WRIGHT CORP.
WRIGHT AERONAUTICAL DIV.
WOOD-RIDGE, NEW JERSEY, U.S.A.

TEST RIG - WIRE WRAPPED

LS25439

FIGURE 2

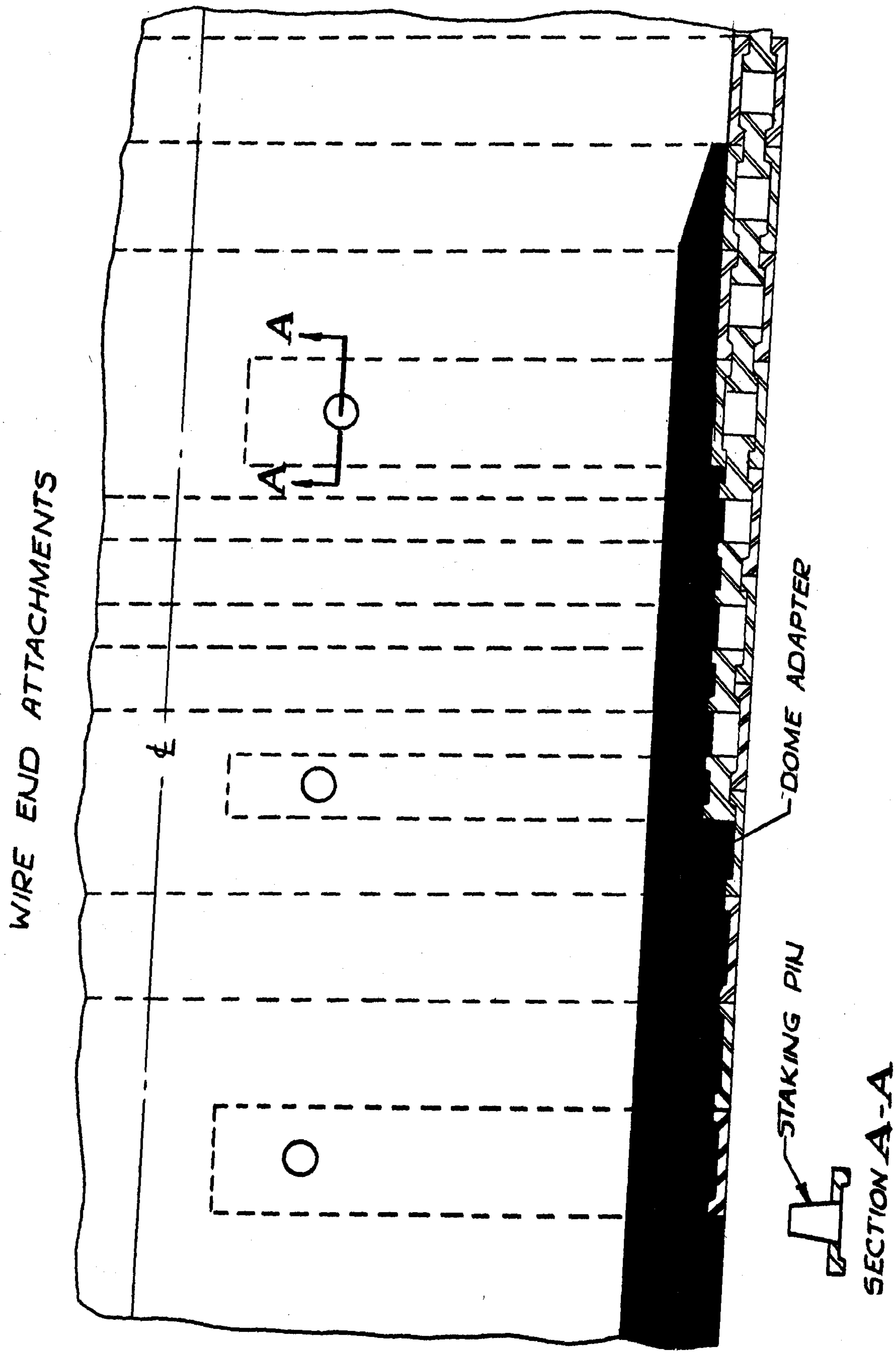

WIRE END ATTACHMENTS
A
A
DOME ADAPTER
STAKING PIN
SECTION A-A

FIGURE 3

WEIGHT COMPARISON

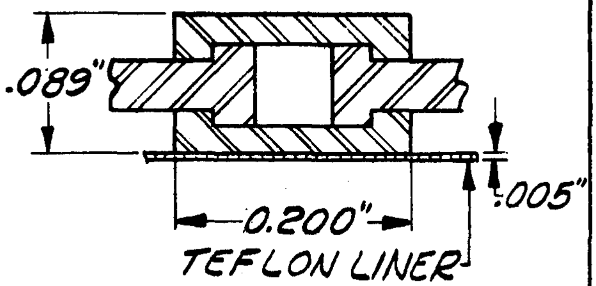

SEE FIGURE 3 FOR WIRE DIMENSIONS

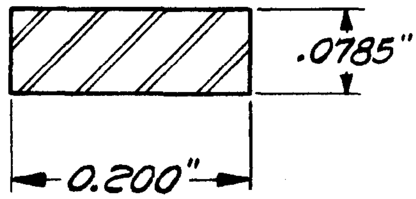

TITANIUM AT 250,000 PSI Y.S.	TRICENT AT 200,000 PSI Y.S.
CHANNEL (2) = .001269# DUMBELL (1) = .000897 LINER = .000069 .002235#	SHELL = .00453#

WEIGHT SAVING OVER CYLINDRICAL SECTION OF TRICENT MOTOR $= \dfrac{.00453-.002235}{.00453} = 50\%$

FIGURE 4

CHANNEL BREAKDOWN

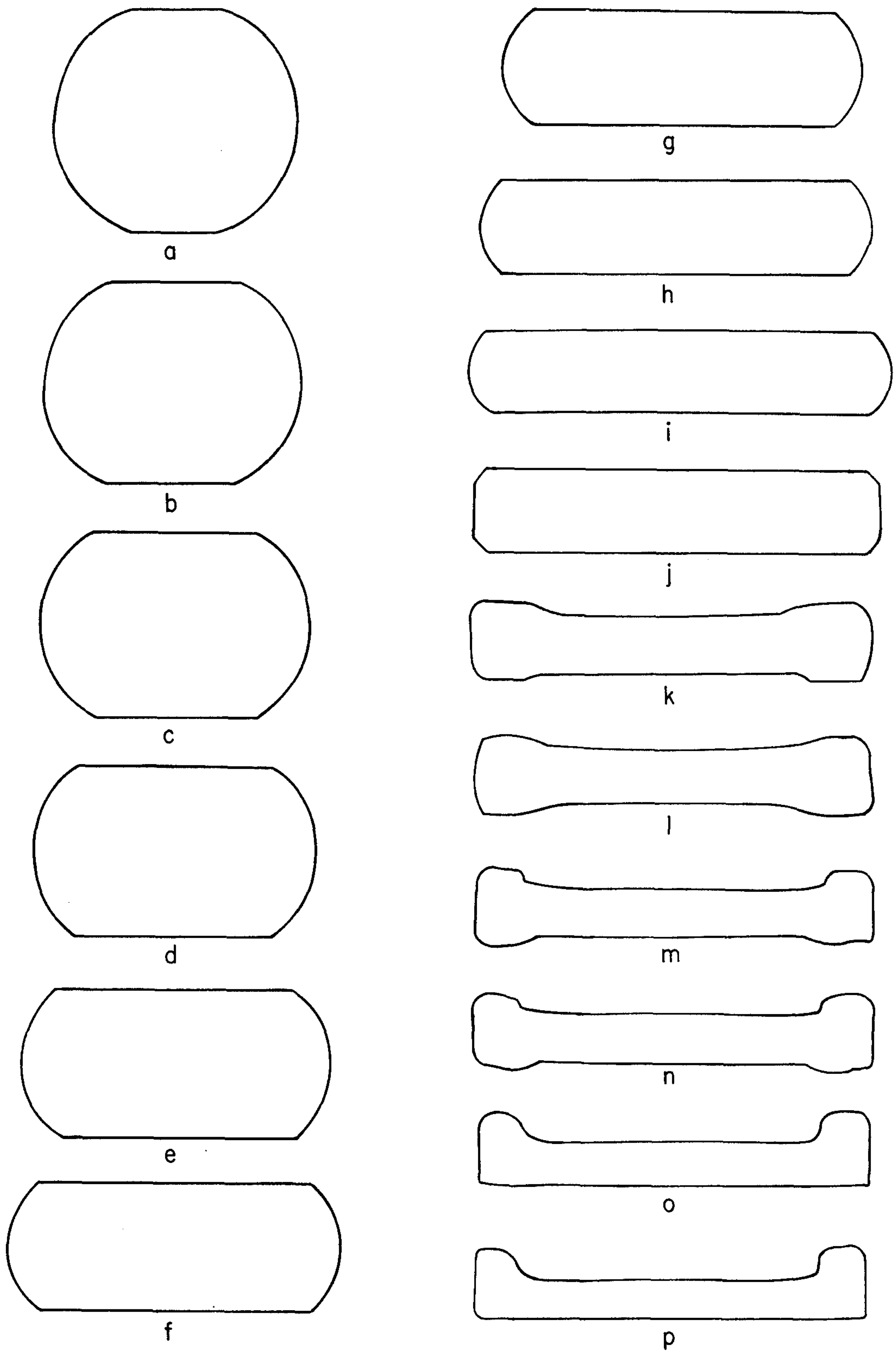

FIGURE 5

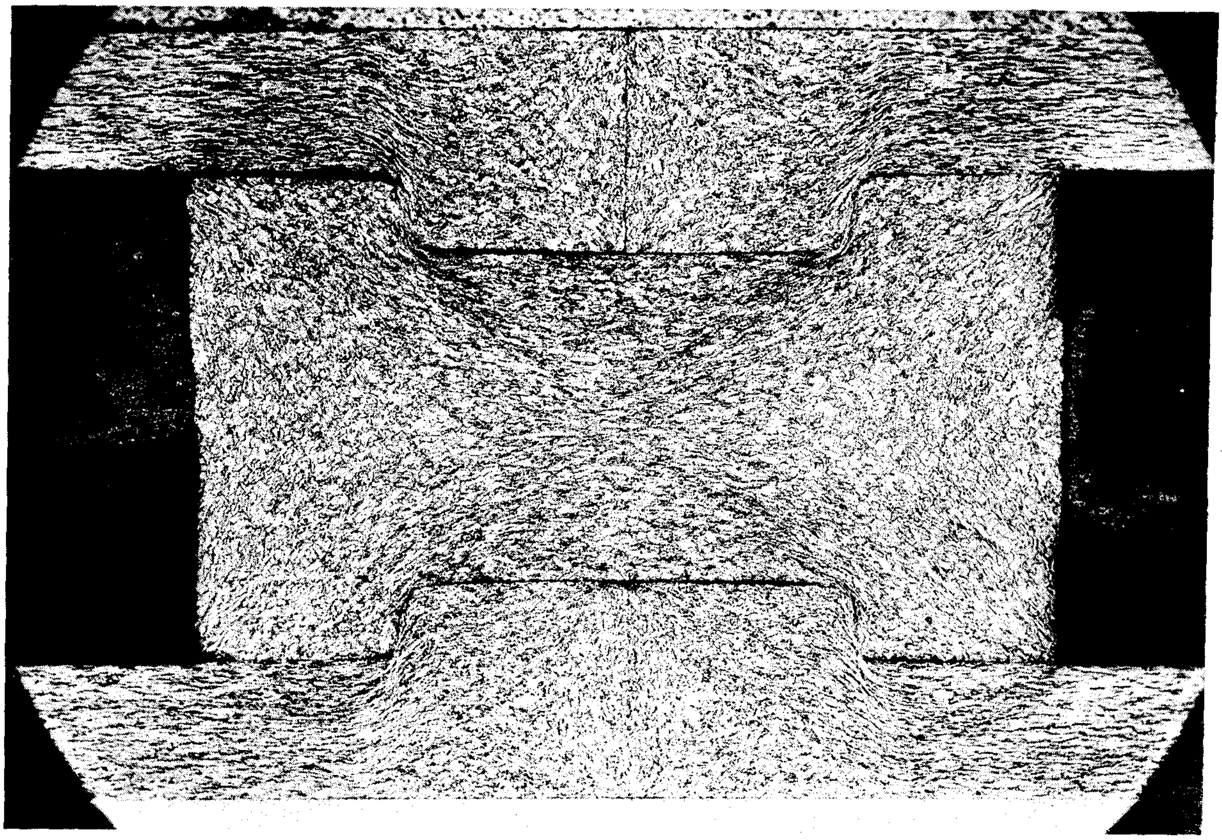

Three Layer Interference Fit

FIGURE 6

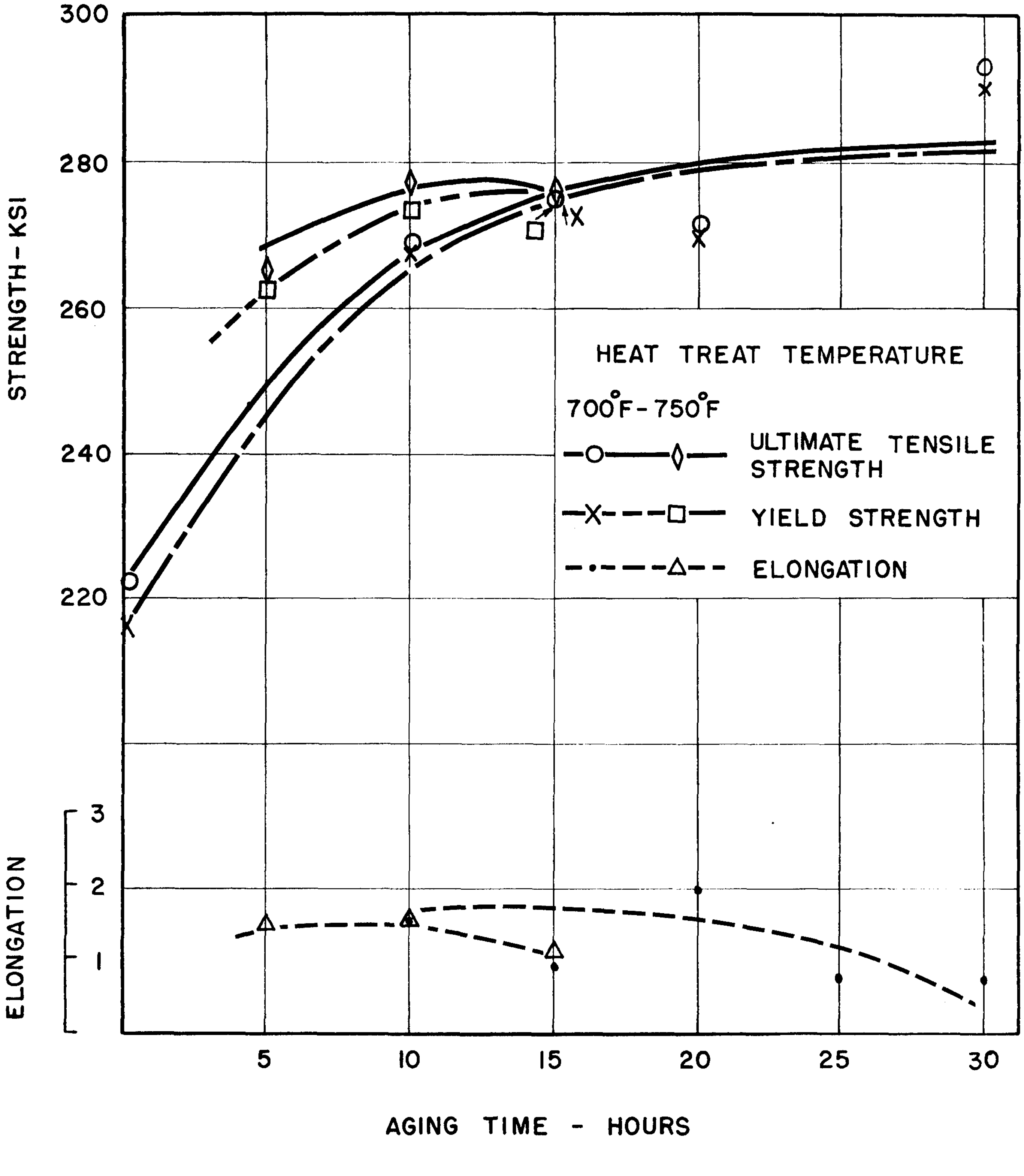
300
280
260
240
220
STRENGTH - KSI
3
2
1
ELONGATION
5
10
15
20
25
30
AGING TIME - HOURS
HEAT TREAT TEMPERATURE
700°F - 750°F
ULTIMATE TENSILE STRENGTH
YIELD STRENGTH
ELONGATION

FIGURE 7

HEAT TREAT RESPONSE OF "I" BEAM WIRE

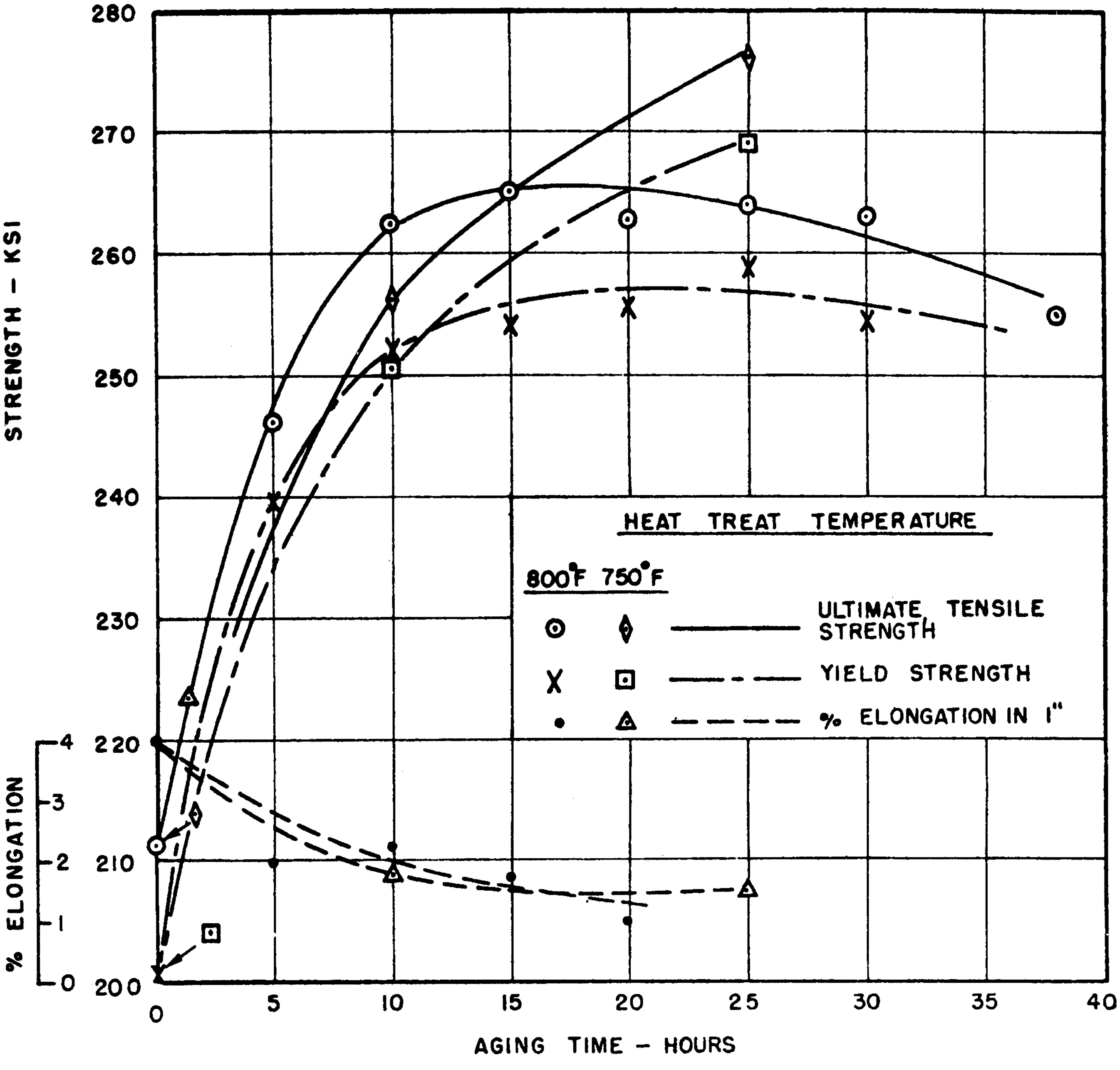

FIGURE 8

AGING RESPONSE VS. % R.A.

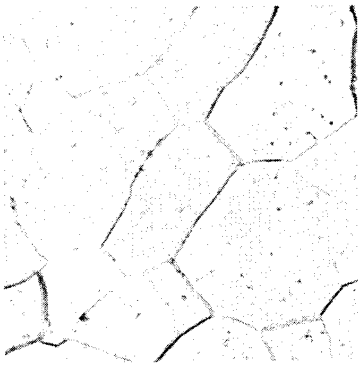

AS COLD ROLLED

6% RA

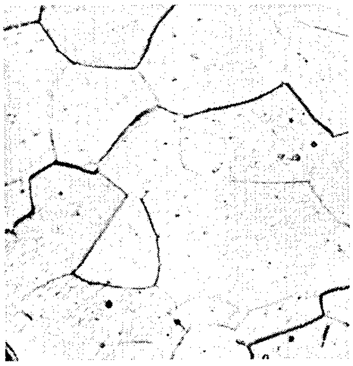

AS COLD ROLLED

19% RA

AS COLD ROLLED

63% RA

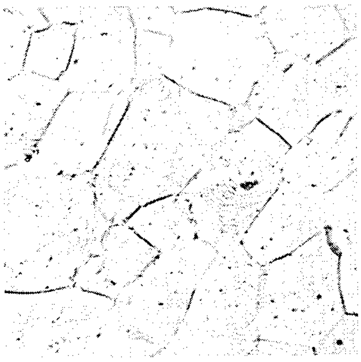

AGED 750°F - 20 HRS

6% RA

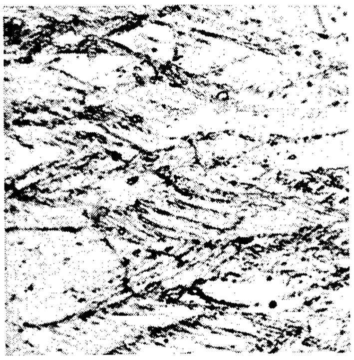

AGED 750°F - 20 HRS.

19% RA

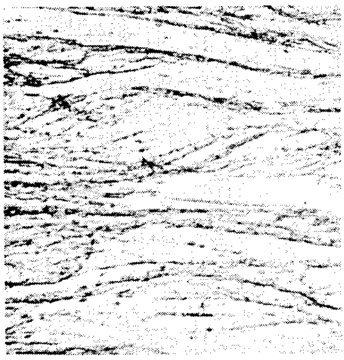

AGED 750°F - 20 HRS.

63% RA

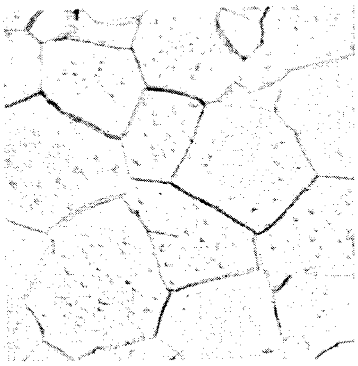

AGED 750°F - 47 HRS.

6% RA

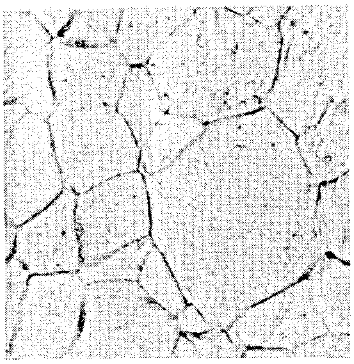

AGED 750°F - 47 HRS

19% RA

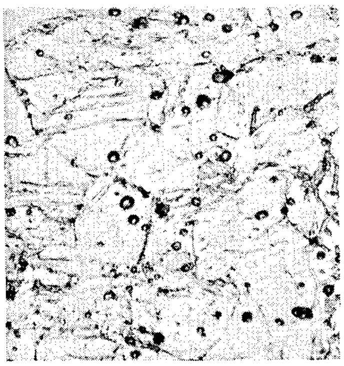

AGED 750°F - 47 HRS.

63% RA

FIGURE 9

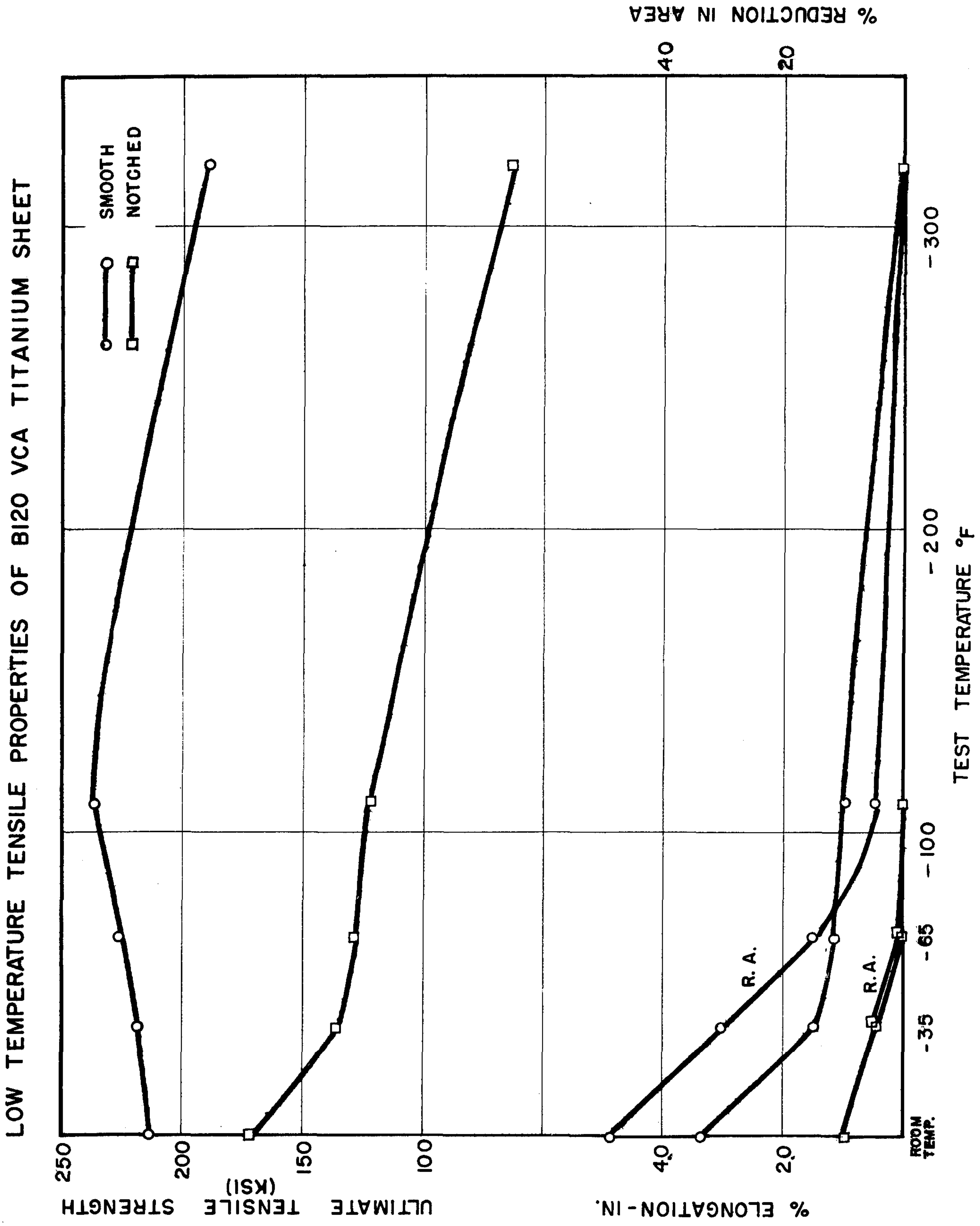
LOW TEMPERATURE TENSILE PROPERTIES OF B120 VCA TITANIUM SHEET
SMOOTH
NOTCHED
ULTIMATE TENSILE STRENGTH (KSI)
250
200
150
100
% ELONGATION - IN.
4.0
2.0
% REDUCTION IN AREA
40
20
R. A.
R. A.
ROOM TEMP.
-35
-65
-100
-200
-300
TEST TEMPERATURE °F

FIGURE 10

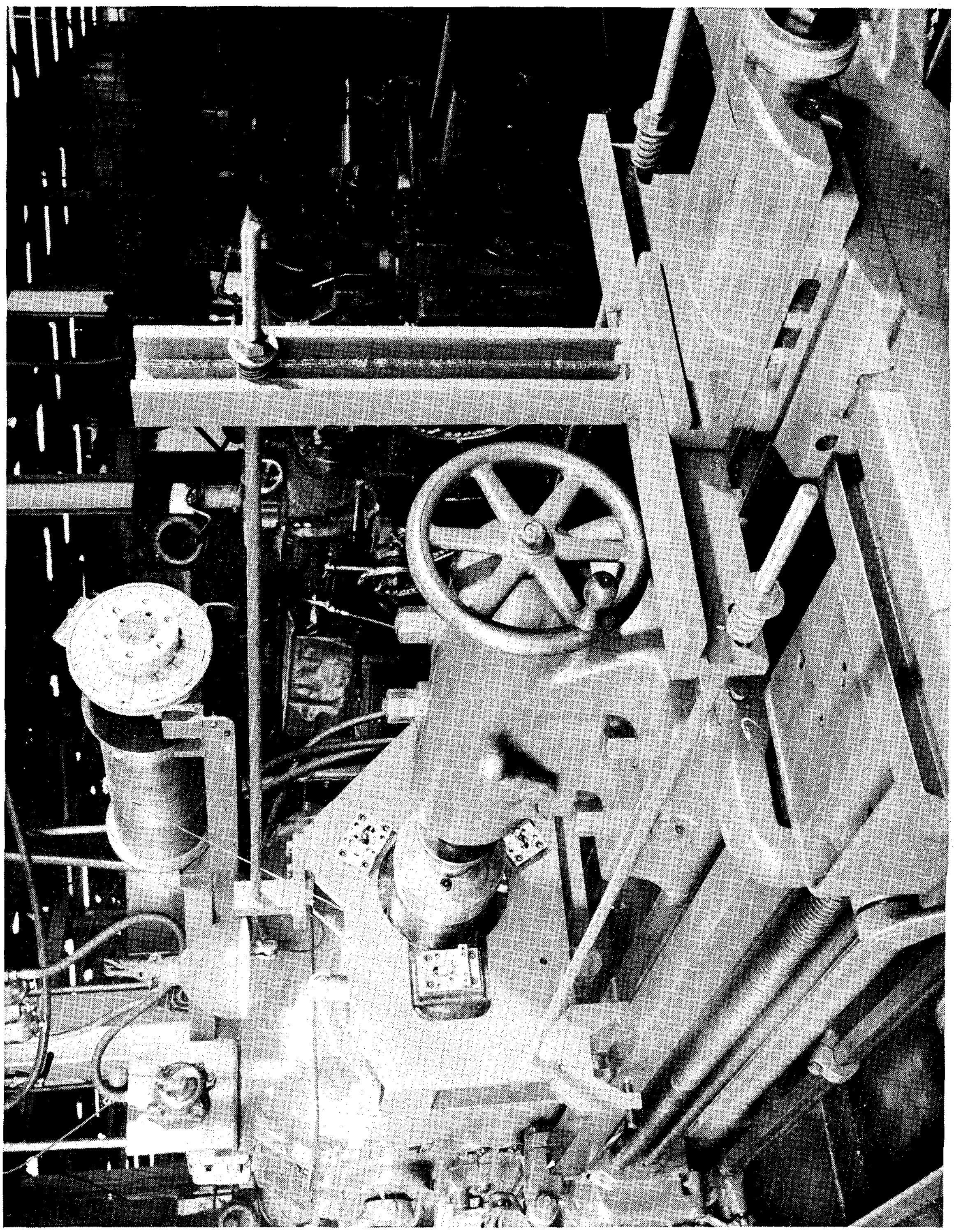

Wrapping Apparatus Modification

FIGURE 11

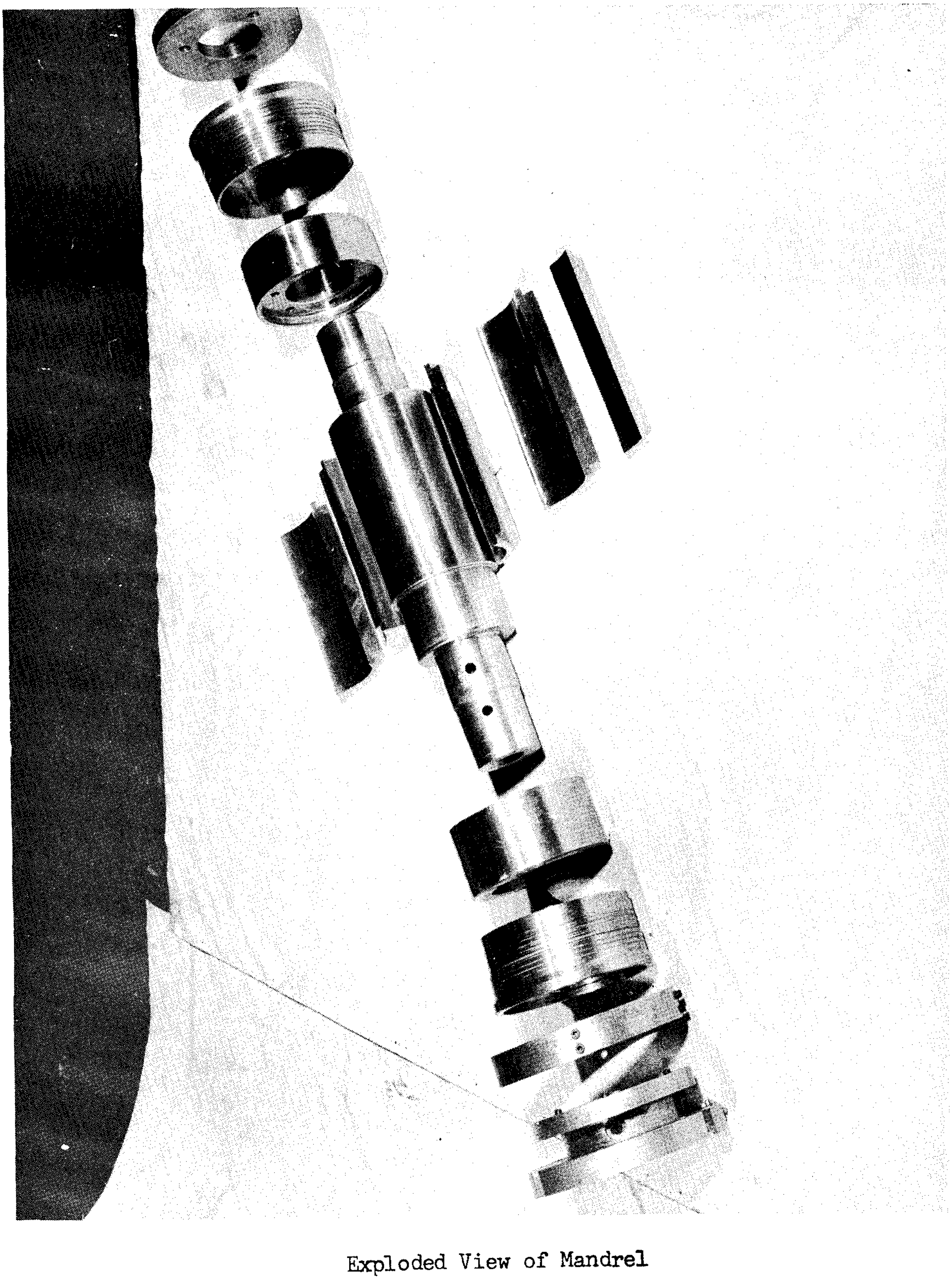

Exploded View of Mandrel

FIGURE 12

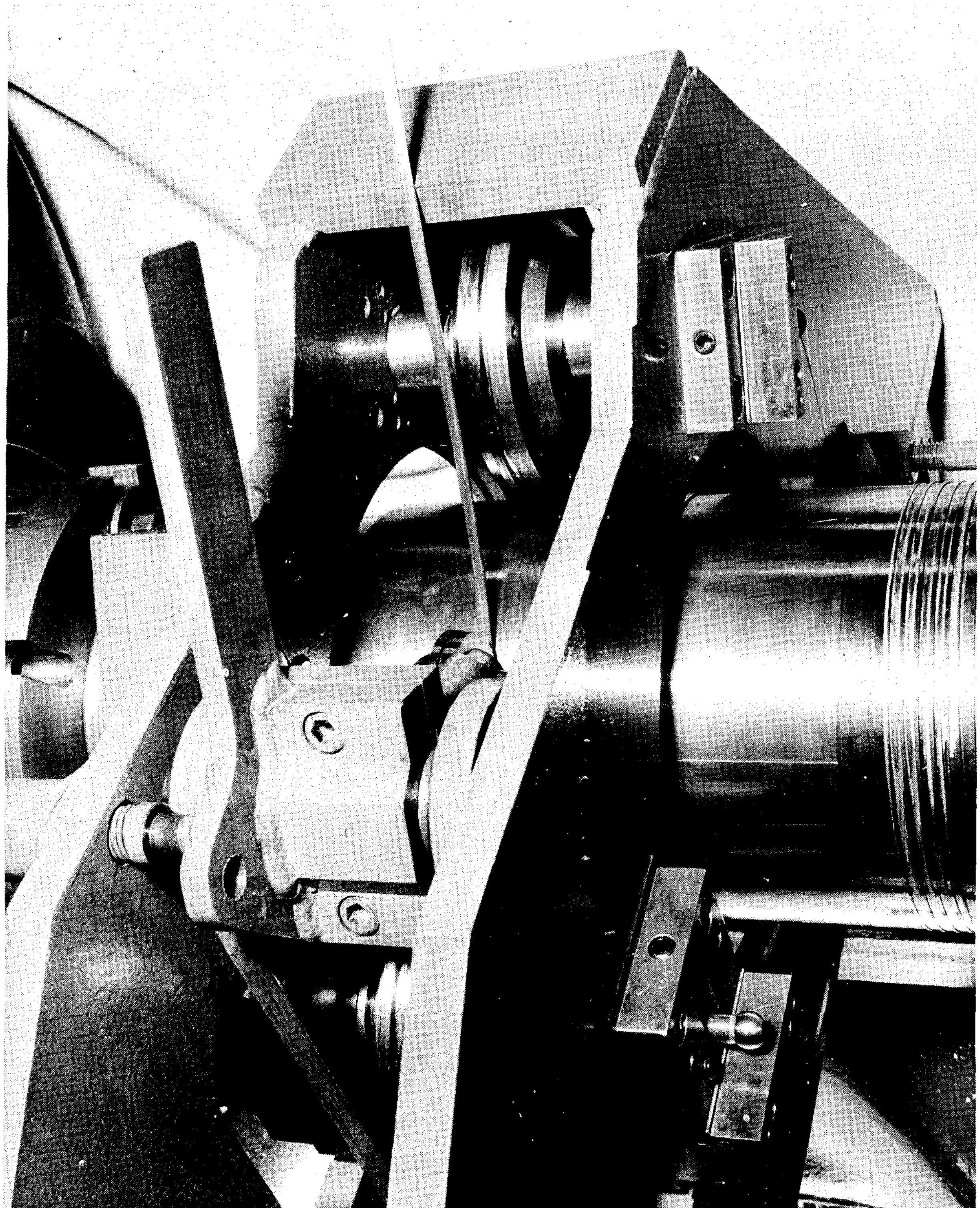

Wrapping Apparatus

FIGURE 13

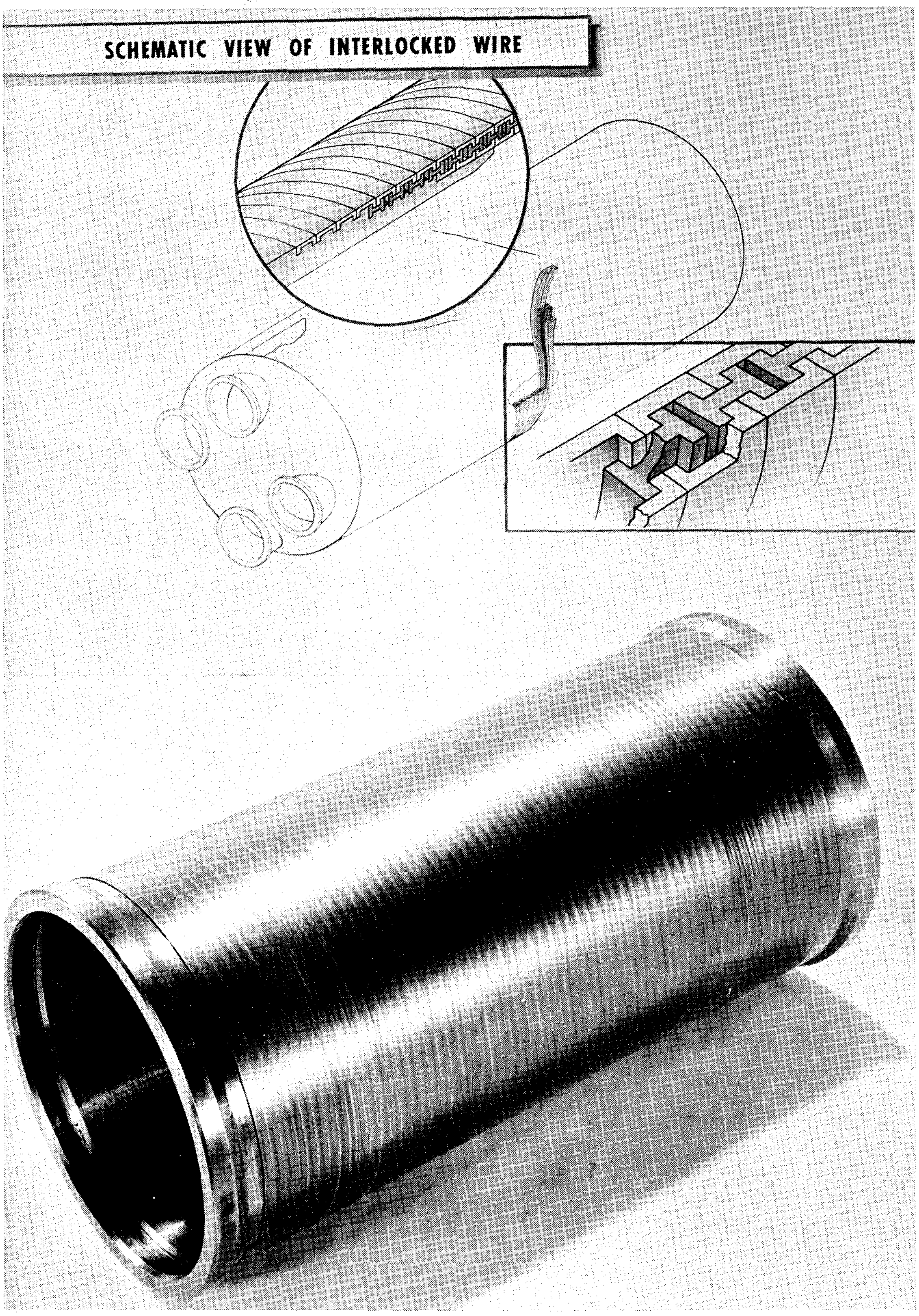

FIGURE 14

CHANNEL AND I-BEAM TAPE DESIGN

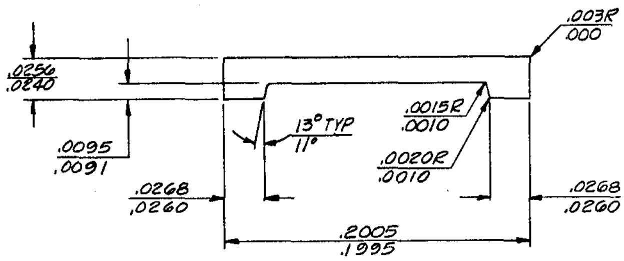

CHANNEL SHALLOW GROOVE

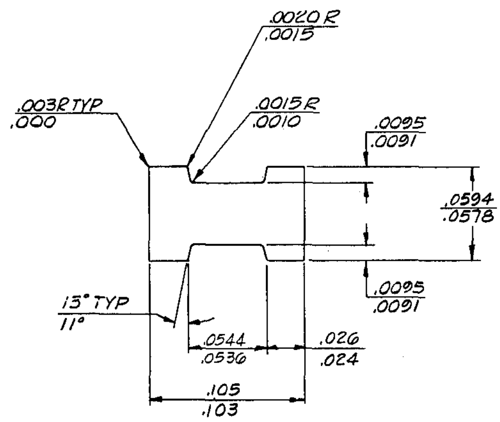

I-BEAM SHALLOW GROOVE

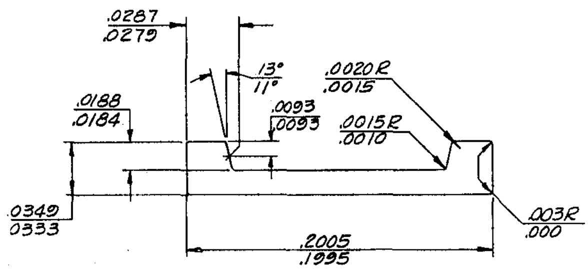

CHANNEL DEEP GROOVE

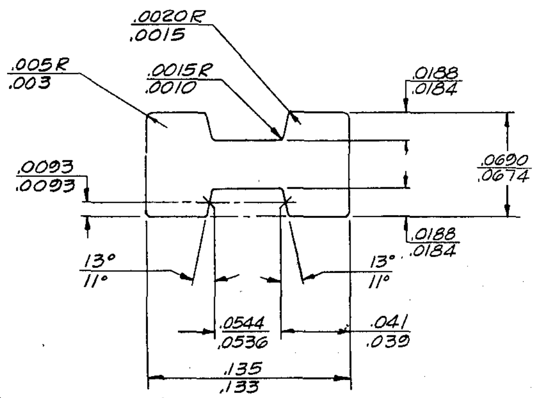

I-BEAM DEEP GROOVE

FIGURE 15

INSPECTION COMPARATOR

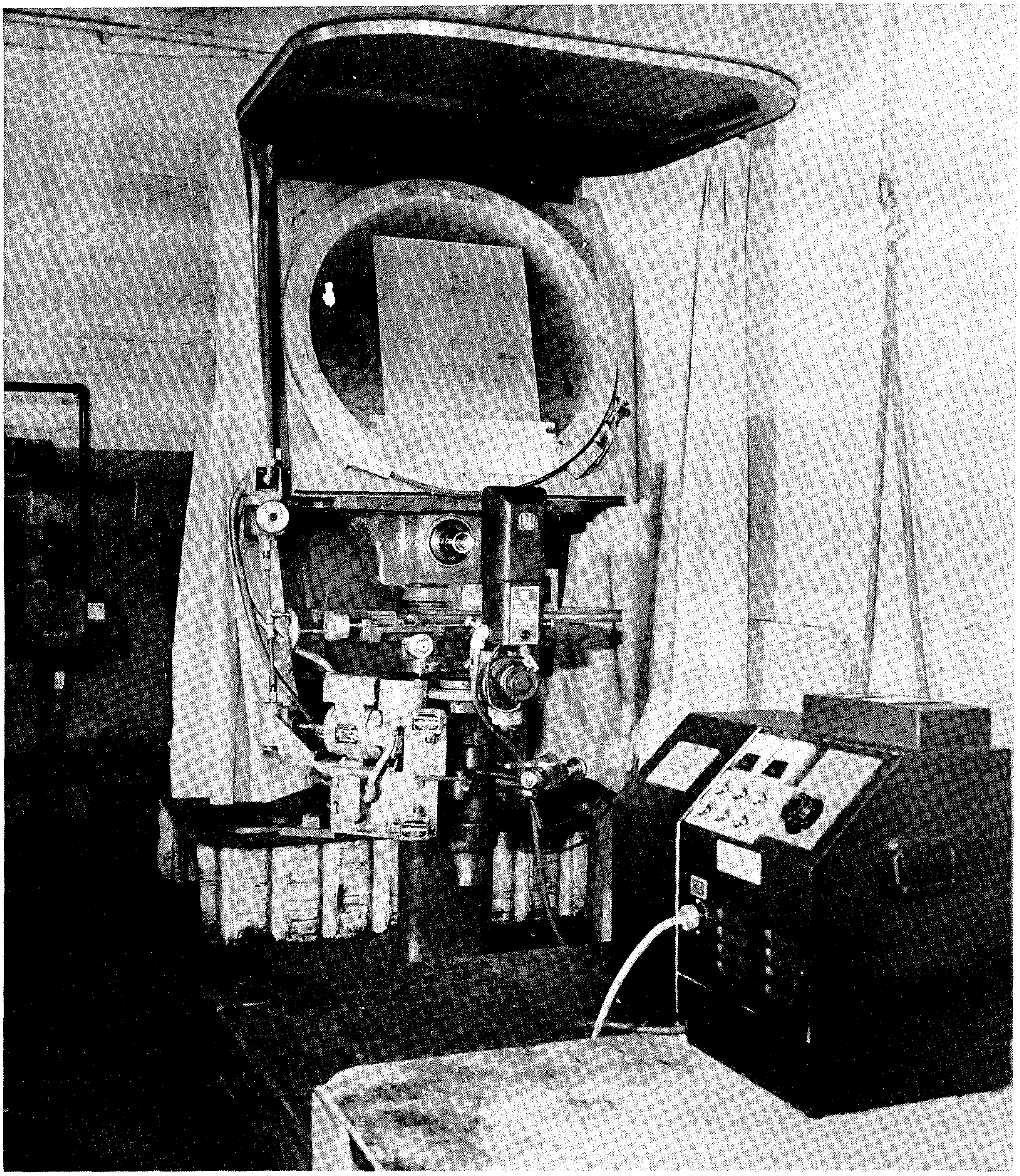

FIGURE 16

ALTERNATE DESIGN STUDIES

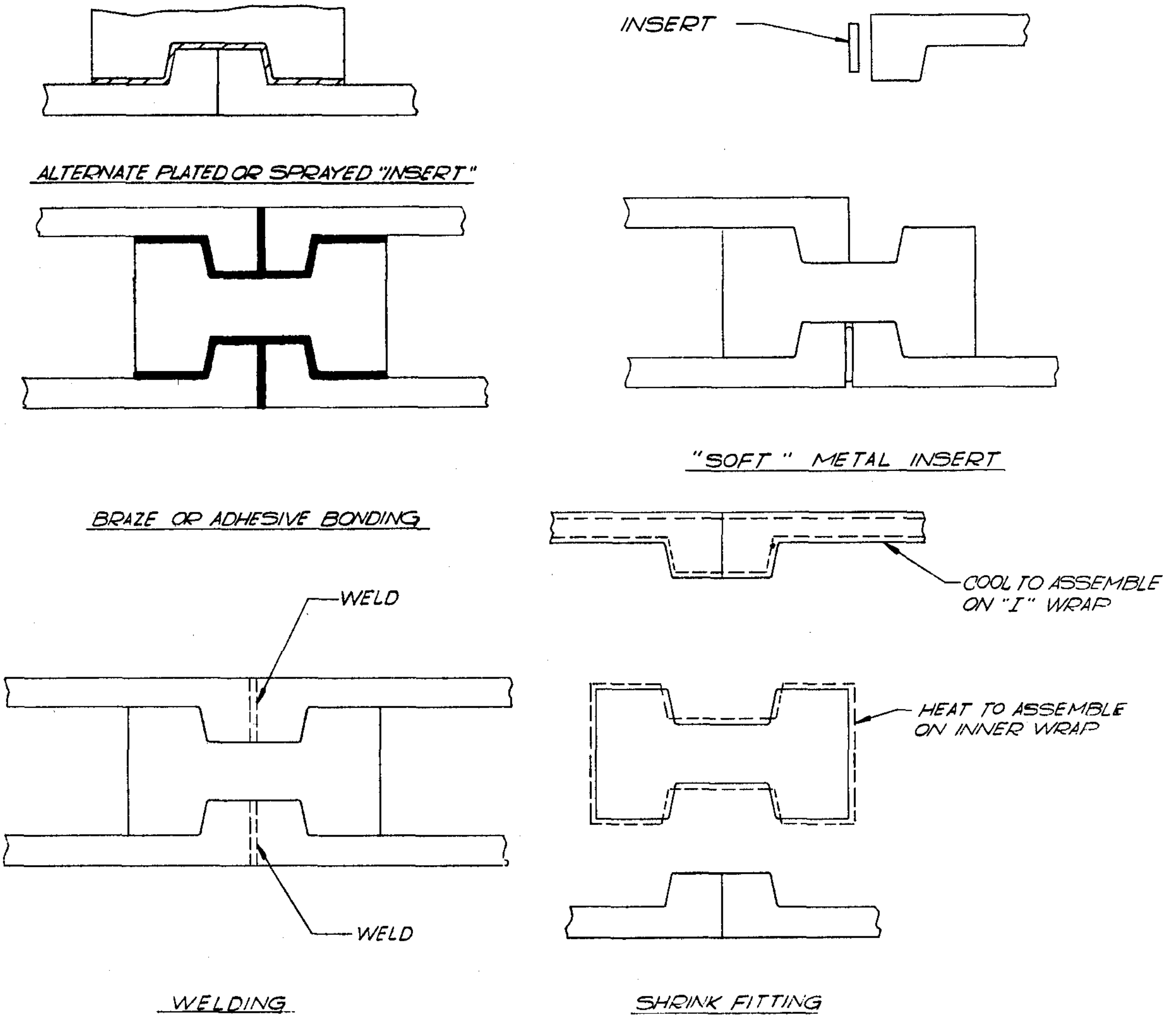

FIGURE 17

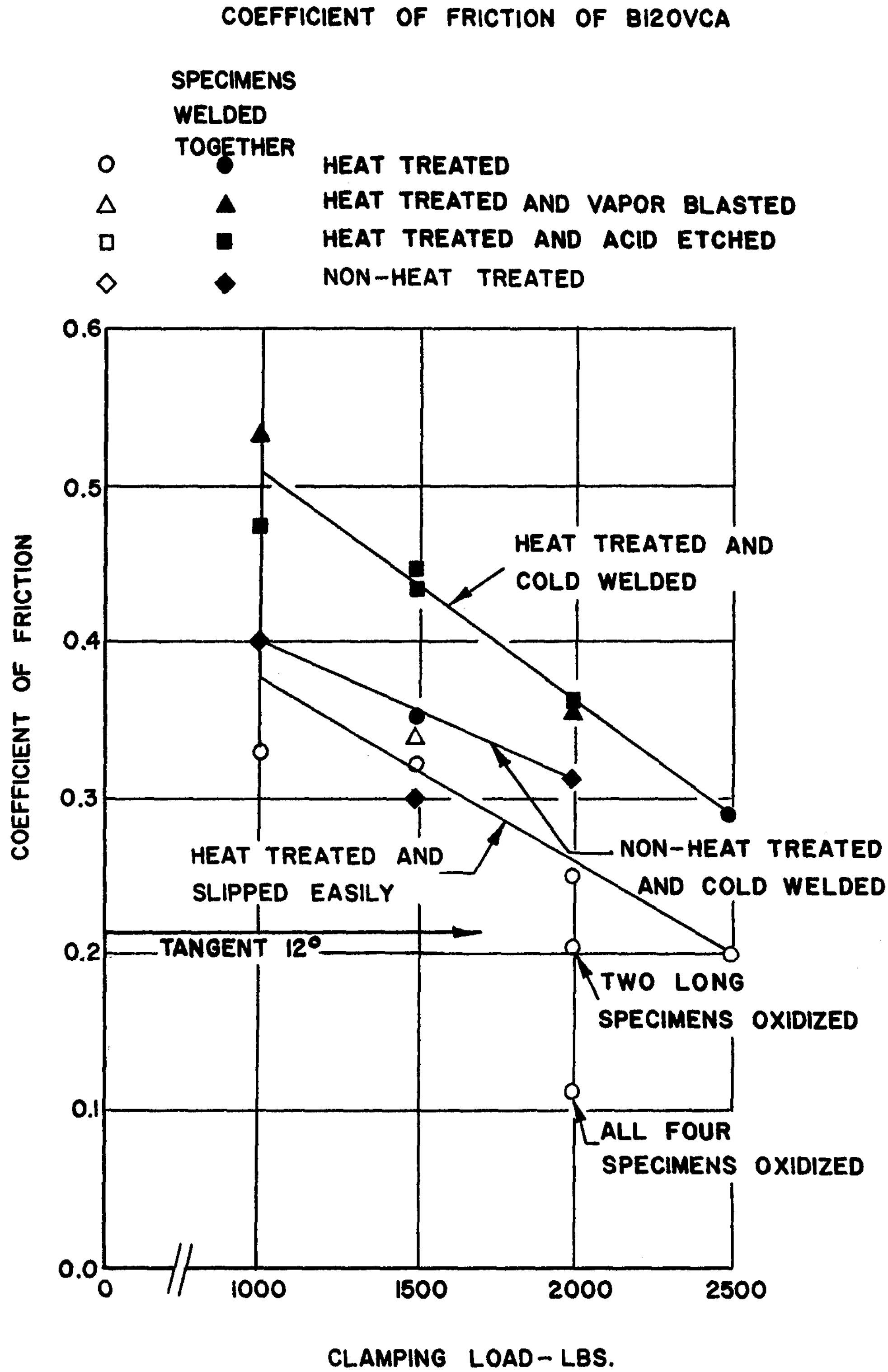
COEFFICIENT OF FRICTION OF B120VCA
SPECIMENS WELDED TOGETHER
HEAT TREATED
HEAT TREATED AND VAPOR BLASTED
HEAT TREATED AND ACID ETCHED
NON-HEAT TREATED
0.6
0.5
0.4
0.3
0.2
0.1
0.0
0
1000
1500
2000
2500
COEFFICIENT OF FRICTION
CLAMPING LOAD - LBS.
HEAT TREATED AND COLD WELDED
HEAT TREATED AND SLIPPED EASILY
NON-HEAT TREATED AND COLD WELDED
TANGENT 12°
TWO LONG SPECIMENS OXIDIZED
ALL FOUR SPECIMENS OXIDIZED

FIGURE 18

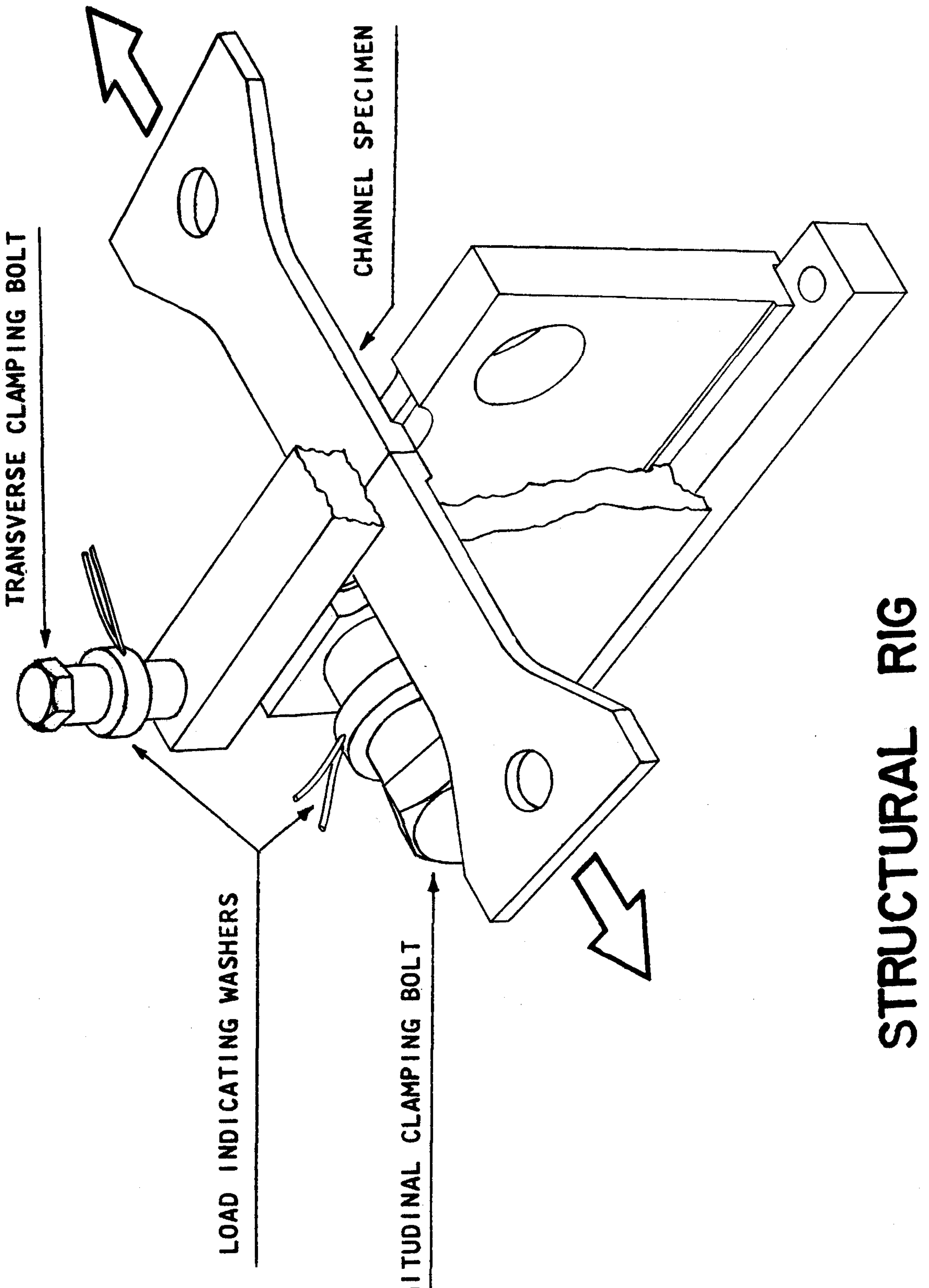

TRANSVERSE CLAMPING BOLT
CHANNEL SPECIMEN
LOAD INDICATING WASHERS
LONGITUDINAL CLAMPING BOLT
STRUCTURAL RIG

FIGURE 19

TURKS HEAD CHANNEL ROLLER DESIGN

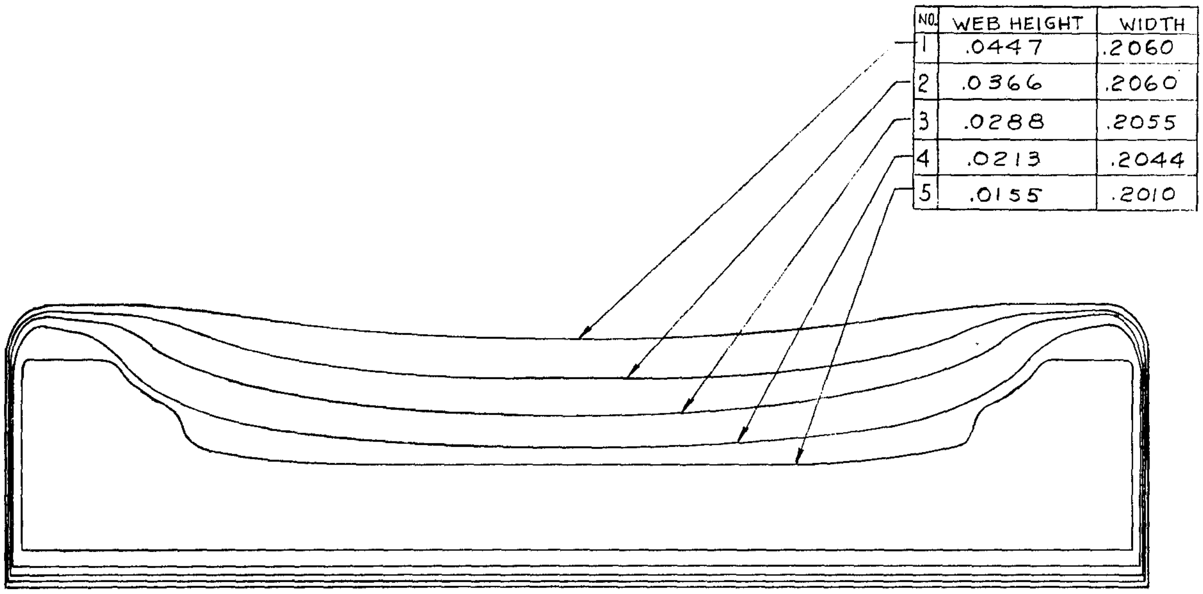

NO.	WEB HEIGHT	WIDTH
1	.0447	.2060
2	.0366	.2060
3	.0288	.2055
4	.0213	.2044
5	.0155	.2010

ROLLER BREAKDOWN

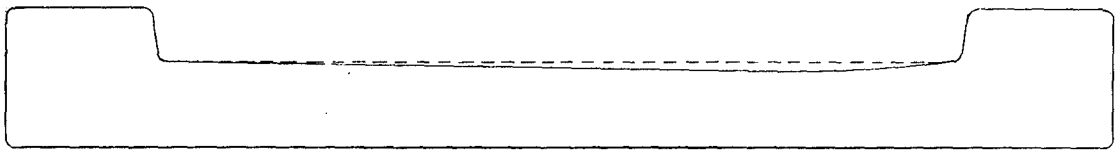

SHALLOW GROOVE FINISH ROLLER

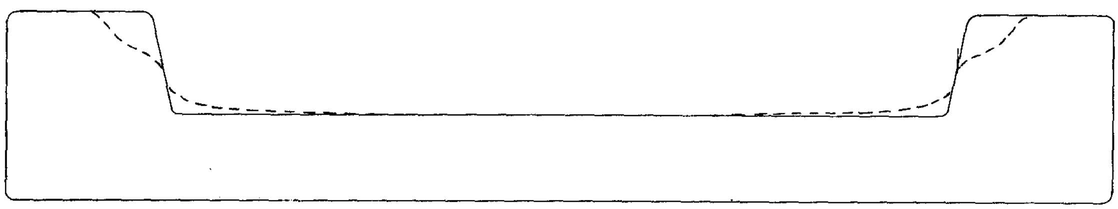

DEEP GROOVE FINISH ROLLER

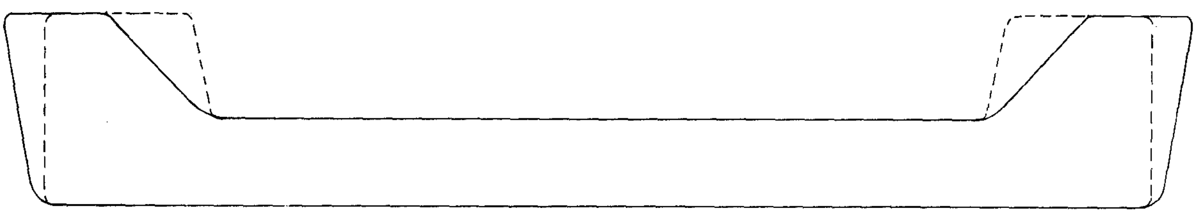

NEW FORM ROLLER DESIGN

FIGURE 20

DUCTILITY TESTS OF B120VCA TITANIUM

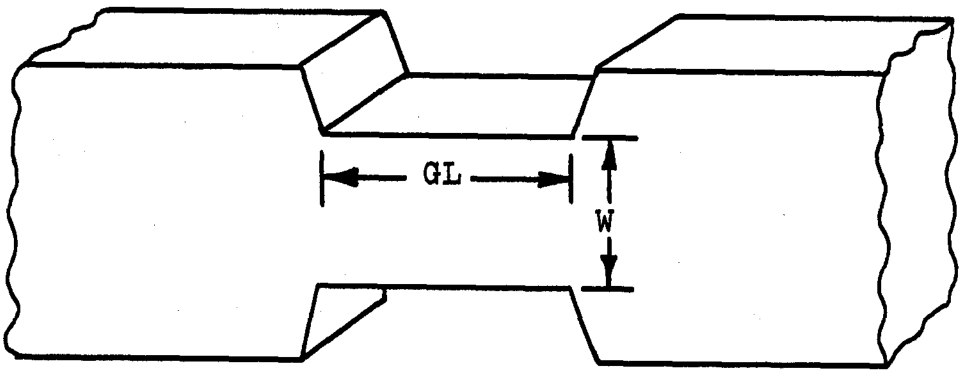

COLD WORKED WIRE

GL = .054 W = .031

NON HEAT TREATED = 22% ELONG.
HEAT TREATED = 4% ELONG.

SHEET STOCK

GL = .540 W = .310

NON HEAT TREATED = 17% ELONG.
HEAT TREATED = 7.8% ELONG.

FIGURE 21

NOTCH SENSITIVITY OF B120VCA TITANIUM

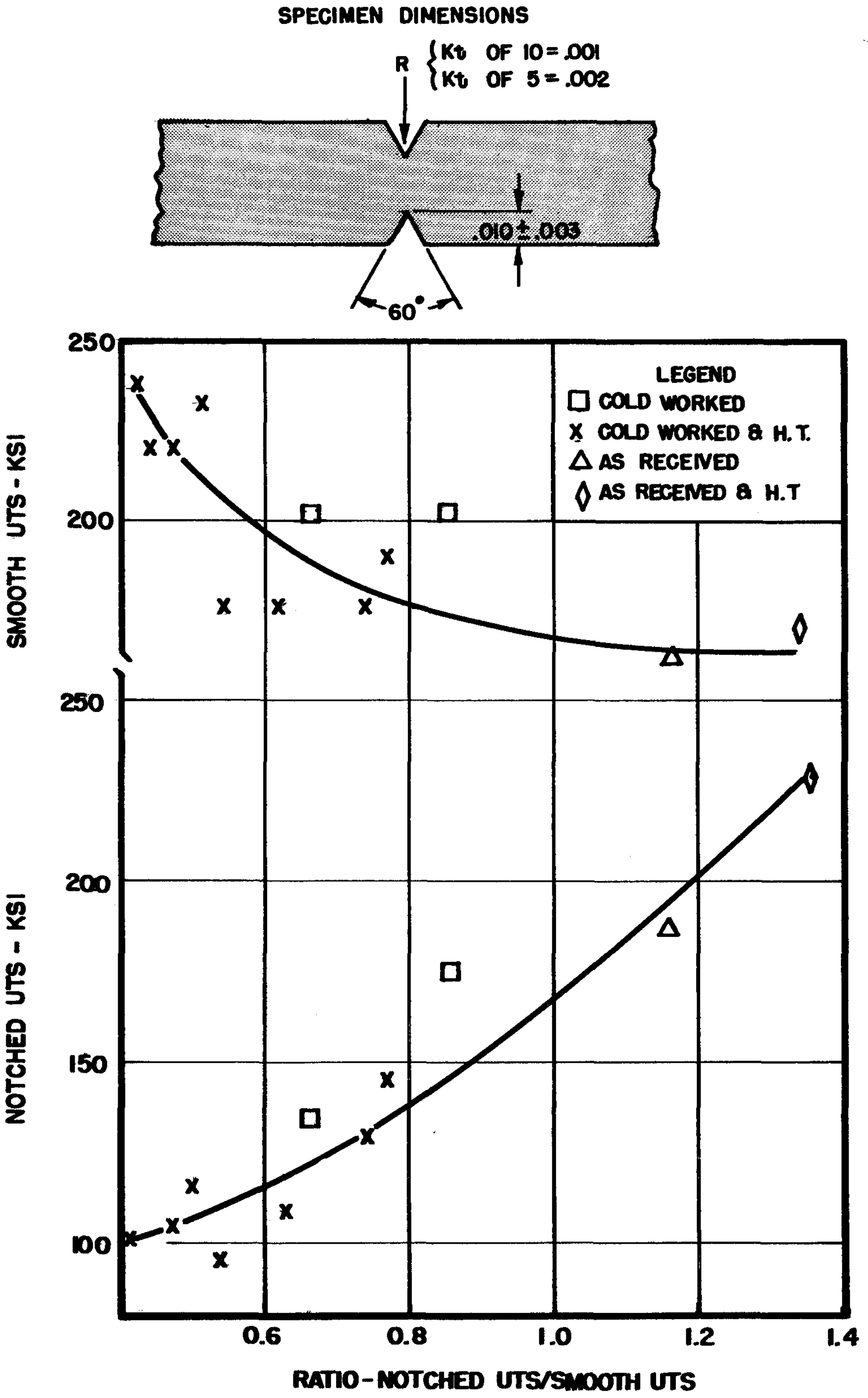

FIGURE 22

HEAT TREAT VACUUM VS ULTIMATE TENSILE STRENGTH FOR B120VCA TITANIUM

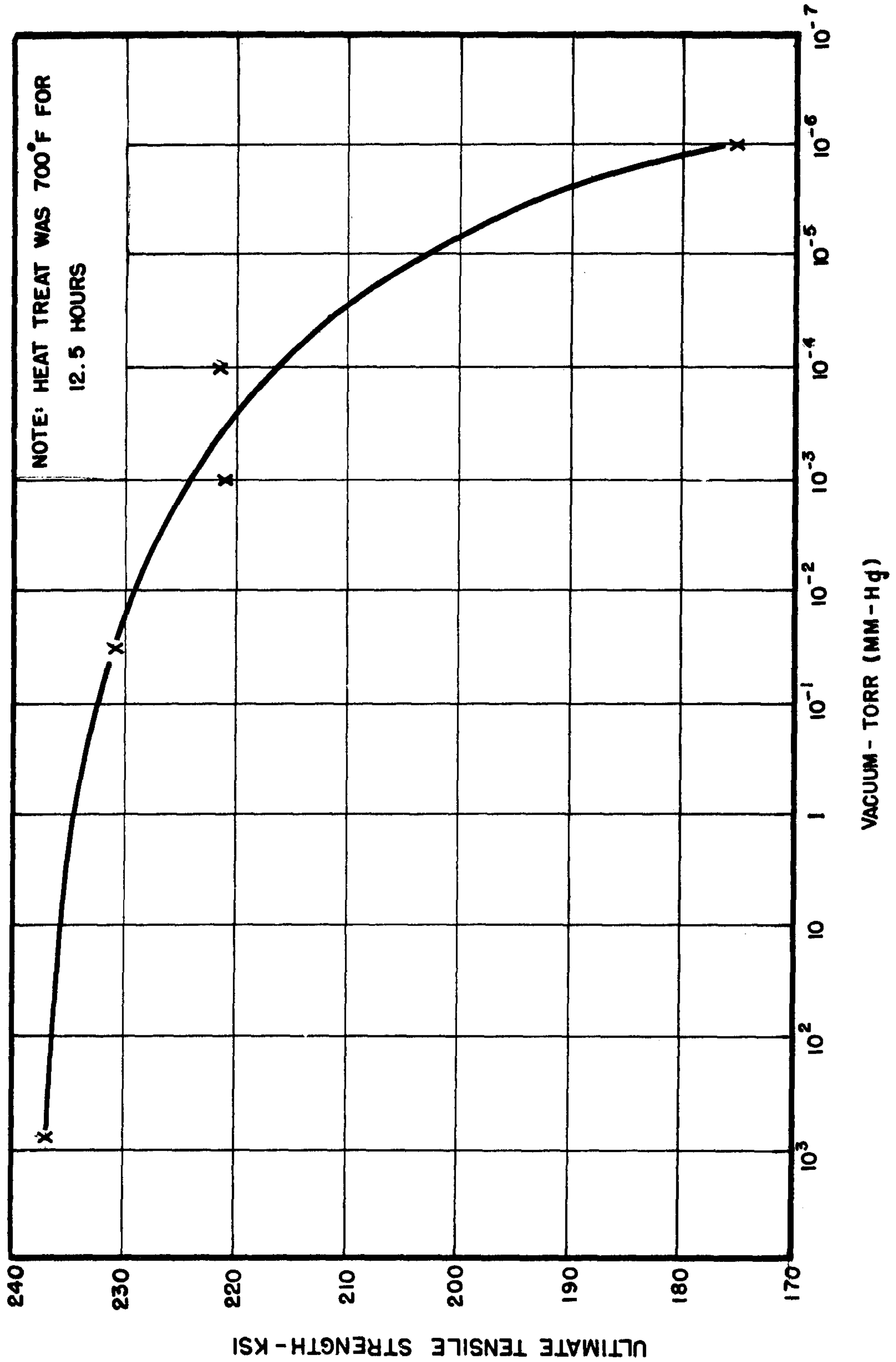

FIGURE 23

STRUCTURAL RIG

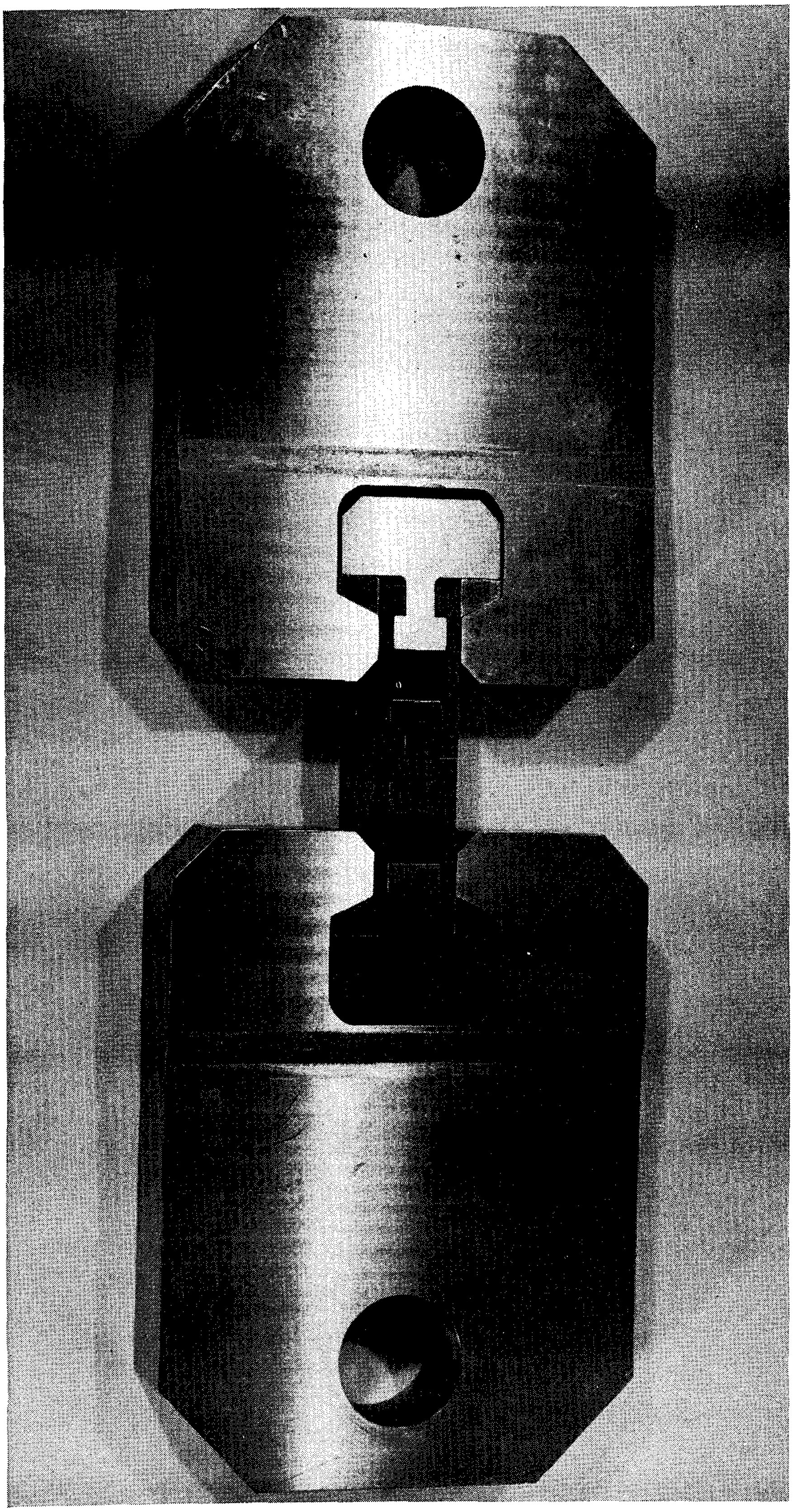

FIGURE 24

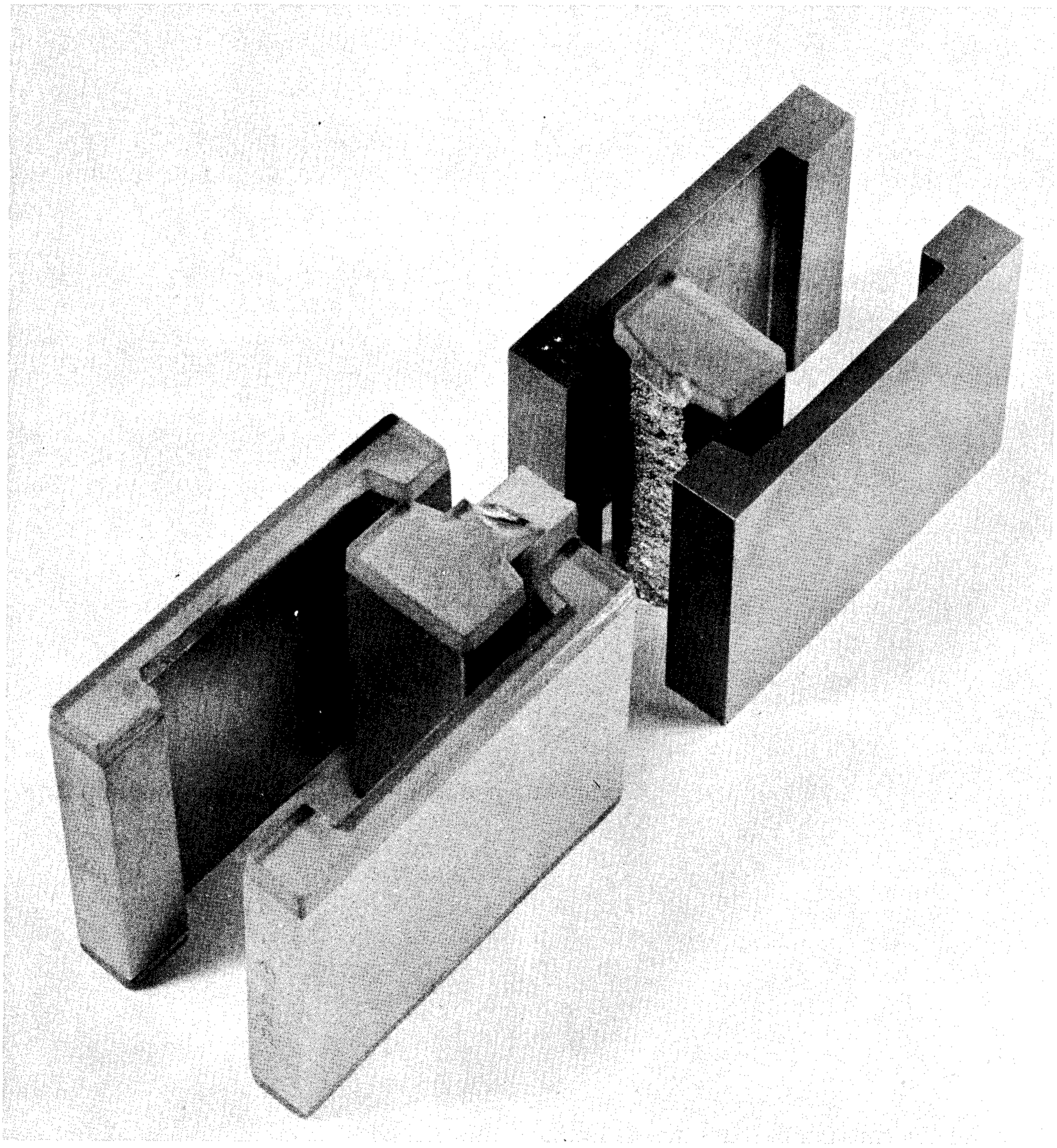

Interference Rig No. 1 - Failure of I-Beam

FIGURE 25

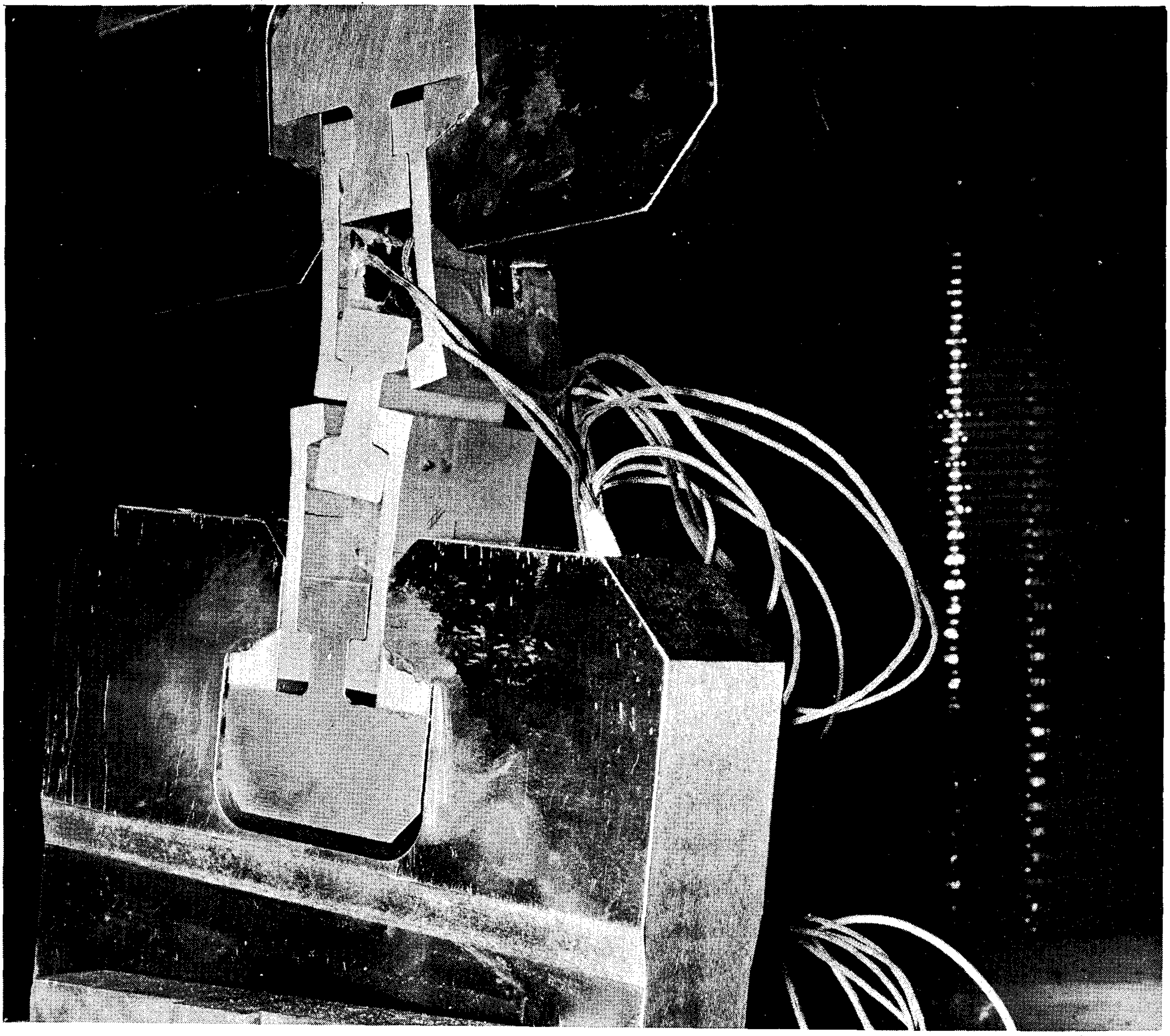

Wire Wrap Interference Test Rig No. 2 Failure of Interlock

FIGURE 26

PROPOSED REVISED DESIGN OF TAPE INTERLOCK

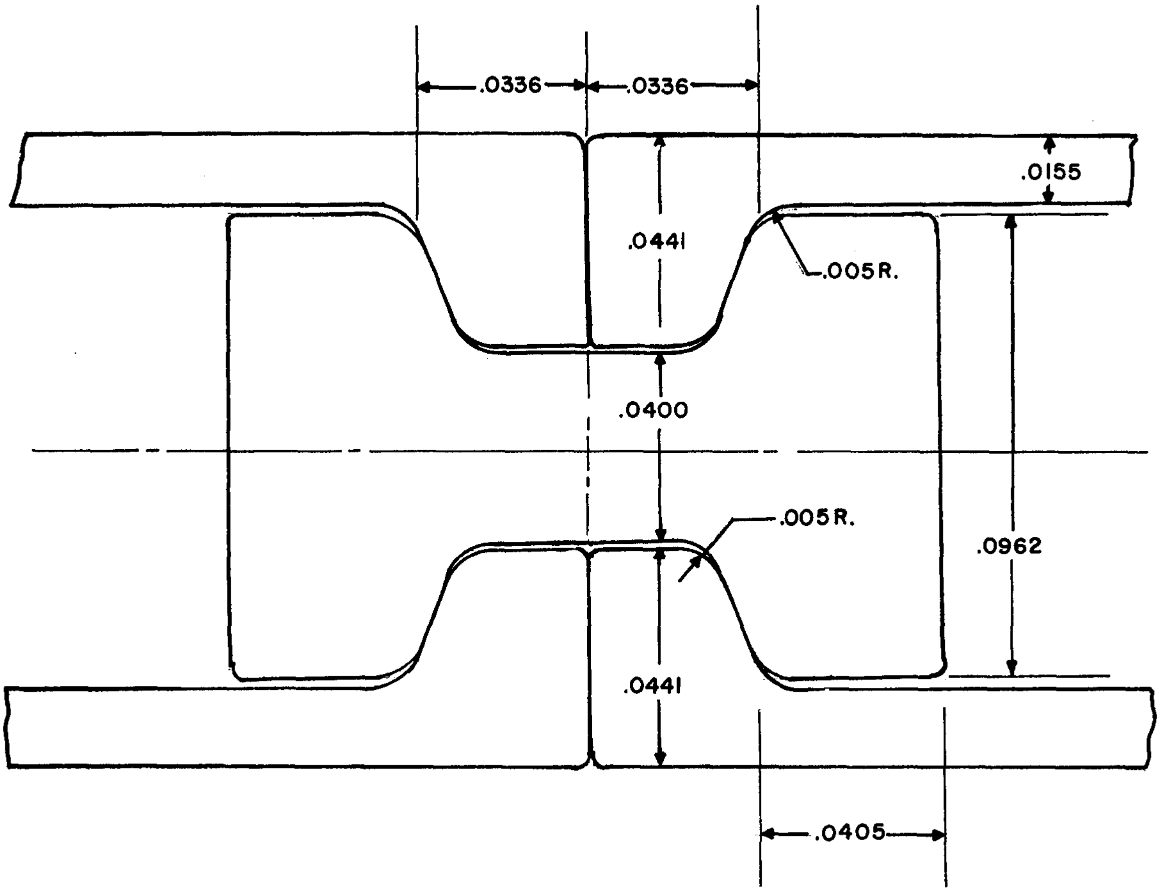

FIGURE 27

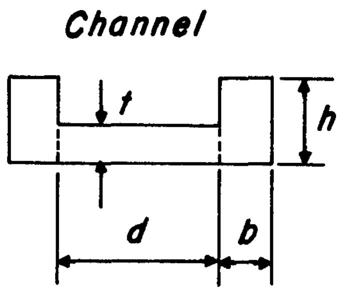

(a)

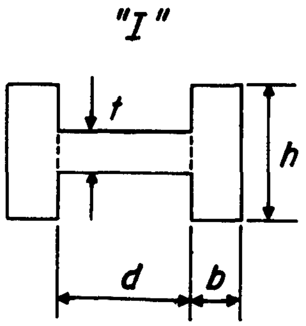

(b)

	DEEP	SHALLOW
t	0.0155	0.0155
d	0.1434	0.1450
b	0.0283	0.0275
h	0.0341	0.0248

	DEEP	SHALLOW
t	0.0312	0.0400
d	0.0540	0.0518
b	0.0400	0.0261
h	0.0684	0.0586

CONFIGURATIONS OF SHALLOW AND DEEP WIRES

FIGURE 28

Free-Body of Wire Subjected to End Moments

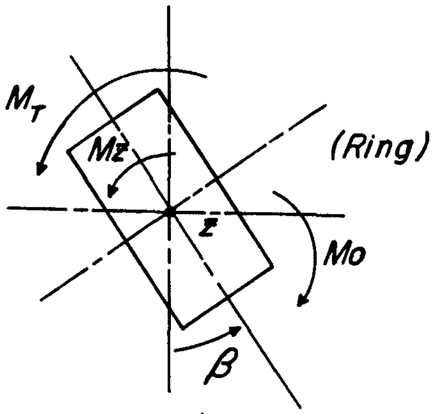

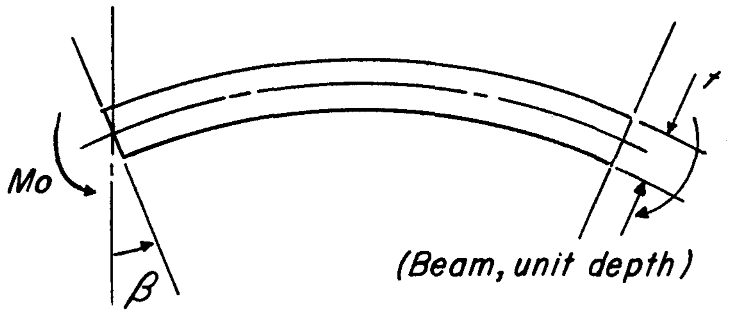

M_z = Moment req'd to twist unrestrained ring

M_o = Restraining moment

$M_T = M_o + M_z$

$$M_z = \frac{\beta E I y'}{R^2}\left(\frac{\text{in-lb}}{\text{in}}\right) \times 2\pi R(\text{in})$$

$$M_z = \frac{2\pi \beta E I y'}{R} \ (\text{in-lb})$$

$$M_T = 2\pi E\left(\frac{\beta I y'}{R} + \frac{2 I_o R \beta}{d}\right)$$

$$U_z = \int_0^{2\pi} \frac{R (M_T)^2 \, d\theta}{2 E I y'}$$

$$U_z = \frac{\pi R (M_T)^2}{E I y'}$$

$$\beta = \frac{M_o \ell}{2\pi I_o} \qquad \ell = d$$

$$M_o = \frac{2\beta E I_o}{d}\left(\frac{\text{in-lb}}{\text{in}}\right) \times 2\pi R$$

$$M_o = \frac{4\pi E I_o R \beta}{d} \ (\text{in-lb})$$

$$U_o = \frac{\int_0^{2\pi} (M_o)^2 R \, d\theta}{2EI}$$

$$U_o = \frac{\pi R (M_o)^2}{E I_o}$$

FIGURE 29

Free Body of Wire Subjected to Bending

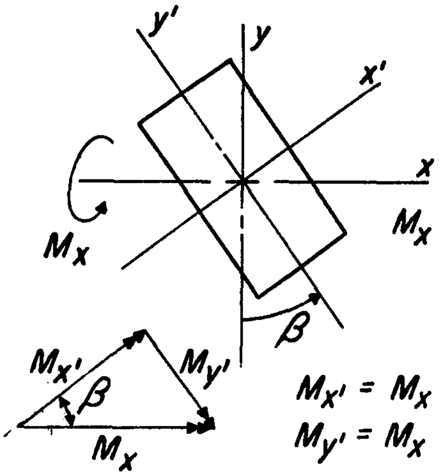

$$M_x = \frac{EI_x}{R_x}$$

$$M_{x'} = M_x \cos\beta$$
$$M_{y'} = M_x \sin\beta$$

$$I_x = \frac{1}{12}\, bh^3$$

$$M_{x'} = \frac{Ebh^3}{12R}\cos\beta$$

$$M_{y'} = \frac{Ebh^3}{12R}\sin\beta$$

$$U_{x'} = \frac{\pi R (M_{x'})^2}{EI_{x'}}$$

$$U_{y'} = \frac{\pi R (M_{y'})^2}{EI_{x'}}$$

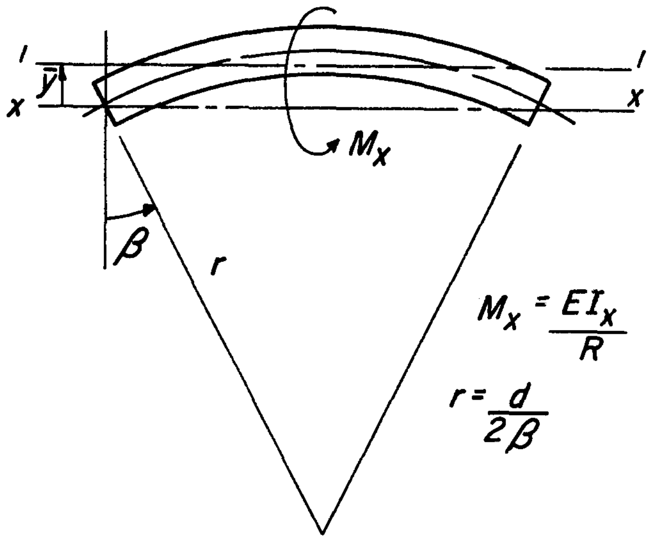

$$M_x = \frac{EI_x}{R}$$

$$r = \frac{d}{2\beta}$$

$$\left.\begin{aligned} A &= 2\beta r t \\ I_{1-1} &= r^3 t\left(\beta + \sin\beta\cos\beta - \frac{2\sin^2\beta}{\beta}\right) \\ \bar{y} &= r\left(\frac{\sin\beta}{\beta} - \cos\beta\right) \end{aligned}\right\}*$$

$$I_{x-x} = I_{1-1} + A\bar{y}^2$$

$$I_{x-x} = \frac{d^3 t}{8}\left(\frac{1}{\beta^2} - \frac{3}{\beta^3}\sin\beta\cos\beta + \frac{2}{\beta^2}\cos^2\beta\right)$$

$$M_x = \frac{Ed^3 t}{8R}\left(\frac{1}{\beta^2} - \frac{3}{\beta^3}\sin\beta\cos\beta + \frac{2}{\beta^2}\cos^2\beta\right)$$

$$U_x = \frac{\pi R (M_x)^2}{EI_x}$$

*From Roark, "Formulas for Stress and Strain" 3rd Ed., p.72

FIGURE 30

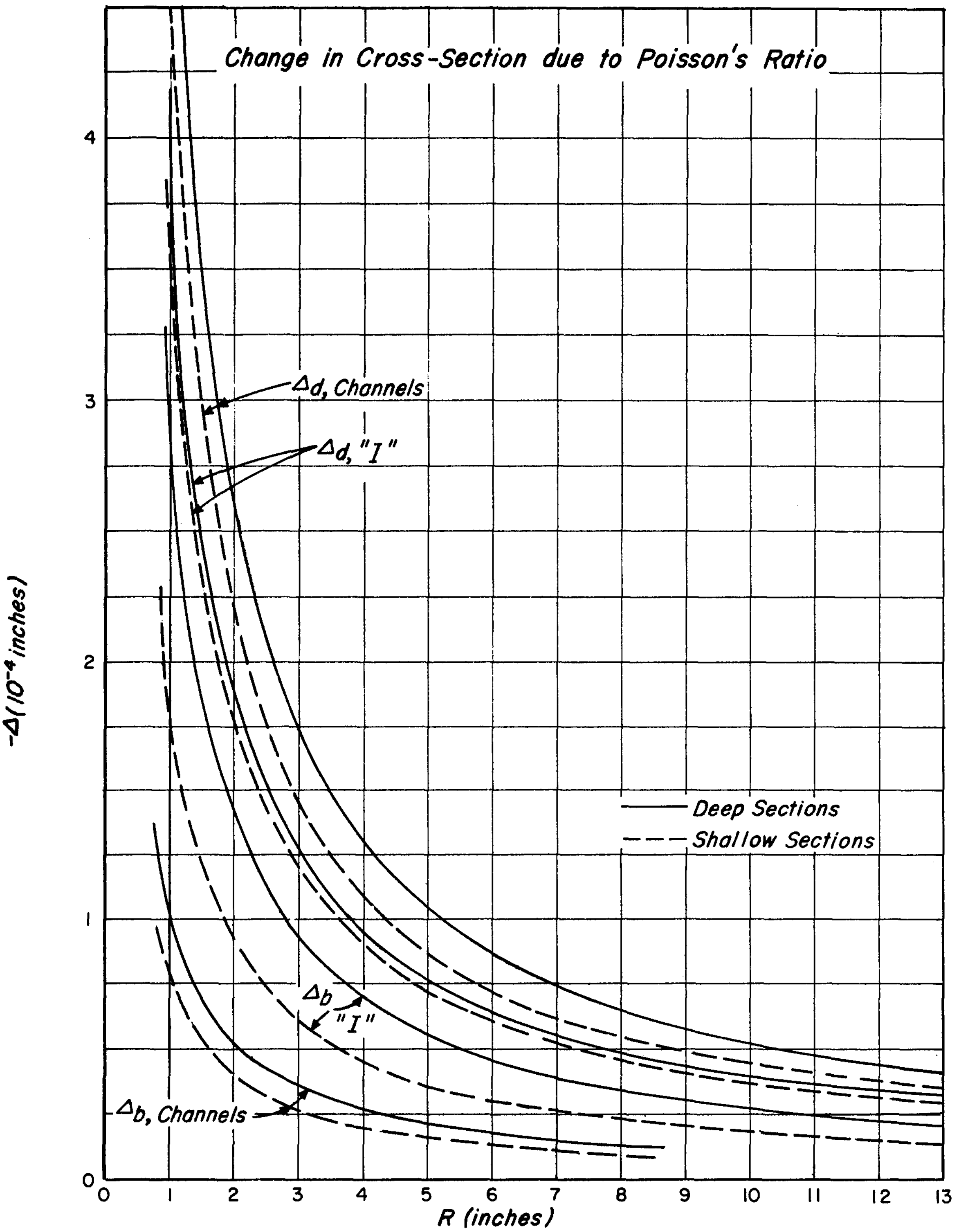
Change in Cross-Section due to Poisson's Ratio
Δ_d, Channels
Δ_d, "I"
Δ_b
"I"
Δ_b, Channels
Deep Sections
Shallow Sections
$-\Delta(10^{-4}$ inches)
R (inches)
0
1
2
3
4
5
6
7
8
9
10
11
12
13

FIGURE 31

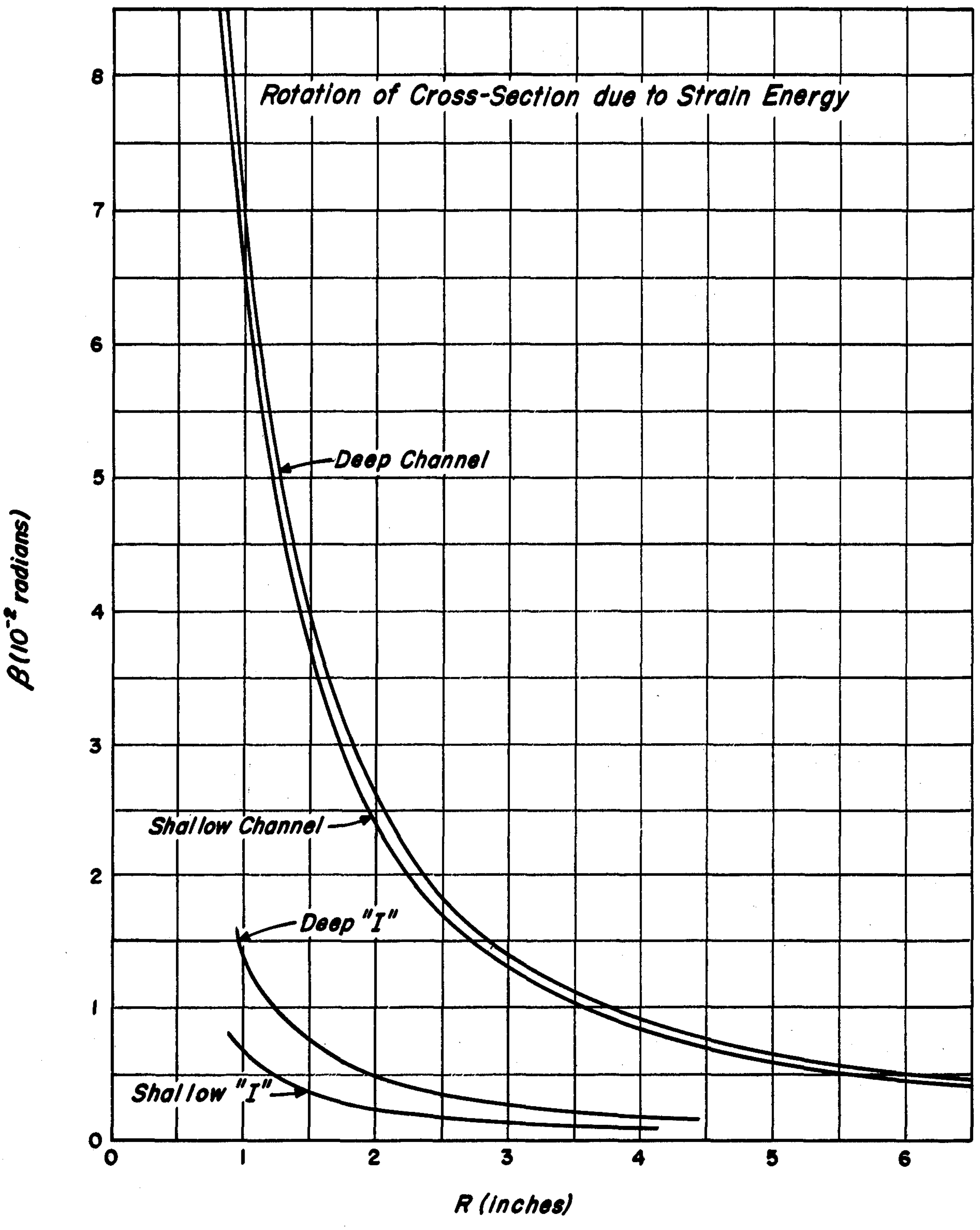
Rotation of Cross-Section due to Strain Energy
Deep Channel
Shallow Channel
Deep "I"
Shallow "I"
β (10⁻² radians)
R (inches)
0
1
2
3
4
5
6
7
8

FIGURE 32

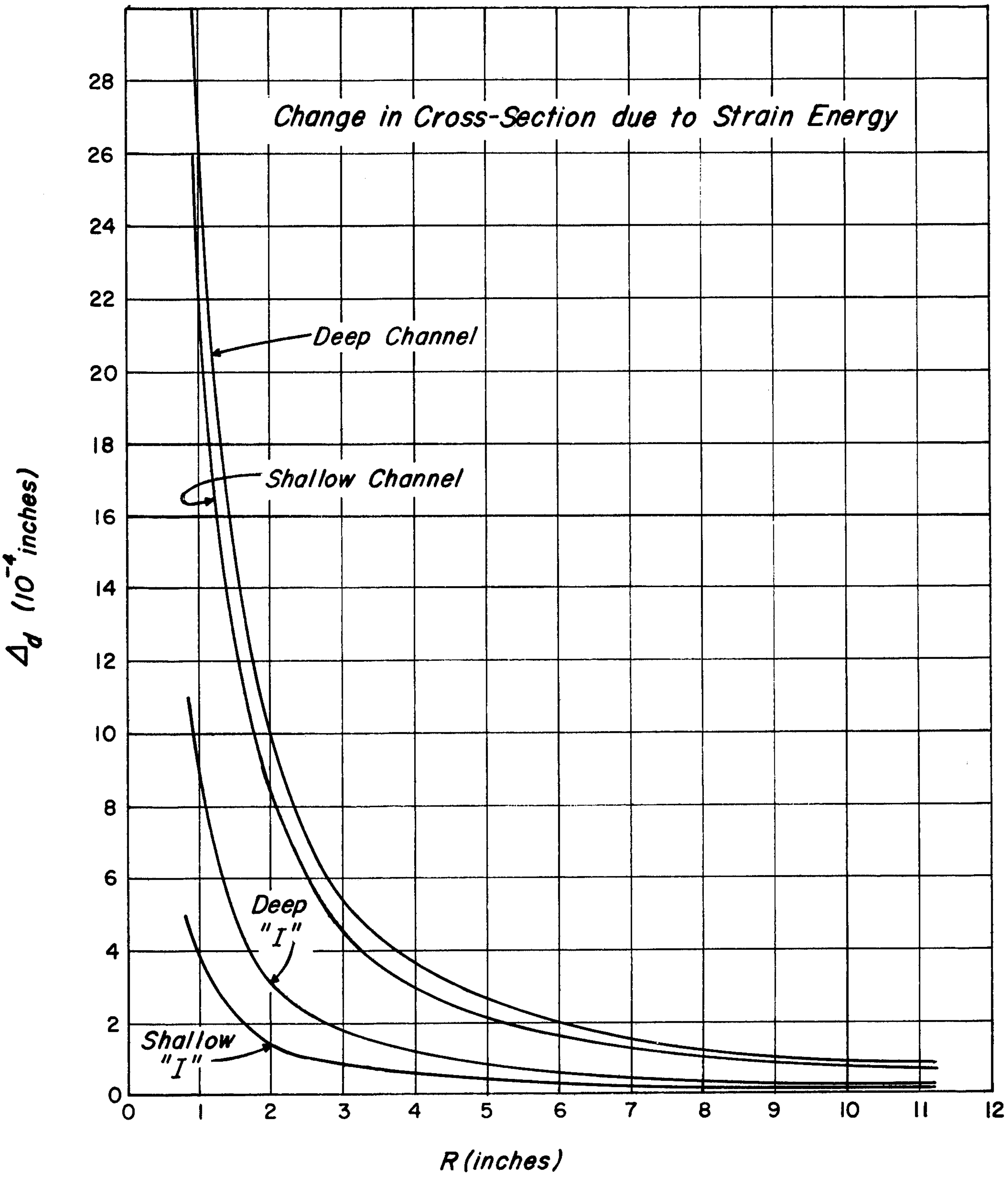

Change in Cross-Section due to Strain Energy
Deep Channel
Shallow Channel
Deep "I"
Shallow "I"
Δ_d (10^{-4} inches)
R (inches)
0
2
4
6
8
10
12
14
16
18
20
22
24
26
28
0
1
2
3
4
5
6
7
8
9
10
11
12

FIGURE 33

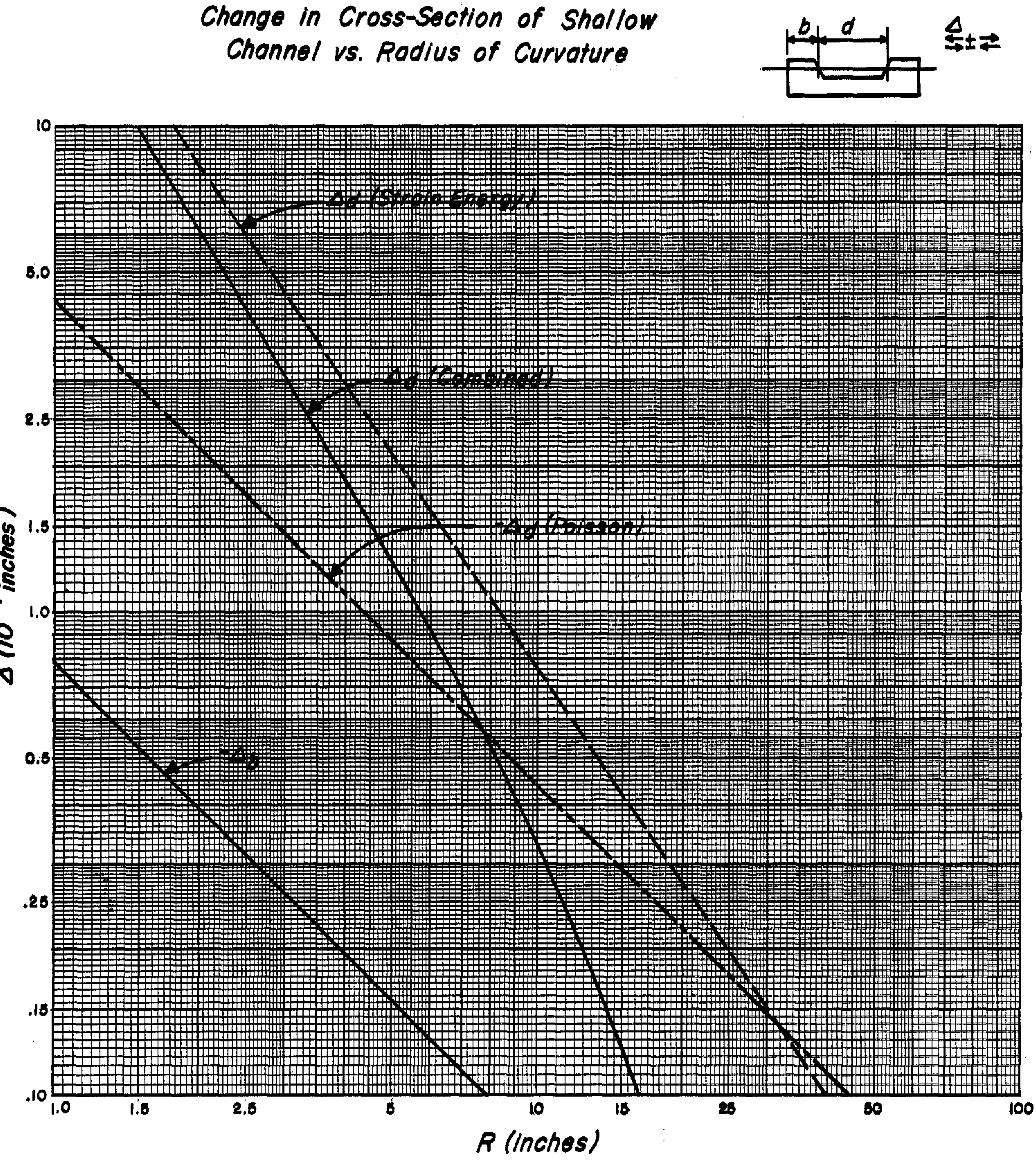
Change in Cross-Section of Shallow Channel vs. Radius of Curvature
b
d
Δ
Δ_d (Strain Energy)
Δ_d (Combined)
$-\Delta_d$ (Poisson)
$-\Delta_b$
Δ (10^{-4} inches)
10
5.0
2.5
1.5
1.0
0.5
.25
.15
.10
1.0
1.5
2.5
5
10
15
25
50
100
R (inches)

FIGURE 34

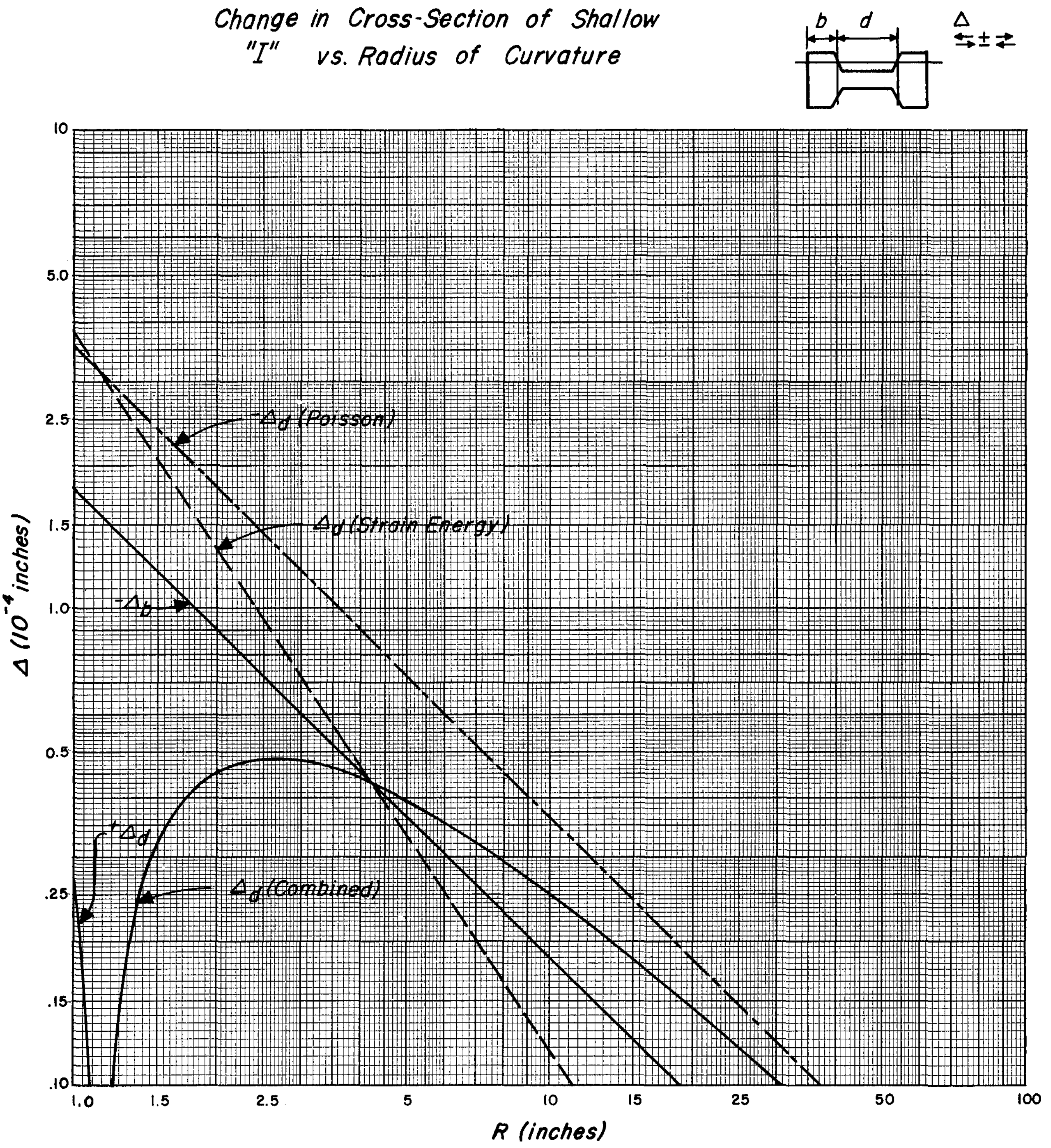
Change in Cross-Section of Shallow "I" vs. Radius of Curvature
b
d
Δ
$^{-}\Delta_d$ (Poisson)
Δ_d (Strain Energy)
$^{-}\Delta_b$
$^{+}\Delta_d$
Δ_d (Combined)
Δ (10⁻⁴ inches)
R (inches)
10
5.0
2.5
1.5
1.0
0.5
.25
.15
.10
1.0
1.5
2.5
5
10
15
25
50
100

FIGURE 35

Change in Cross-Section of Deep Channel vs. Radius of Curvature

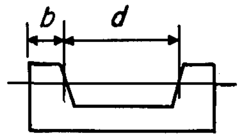

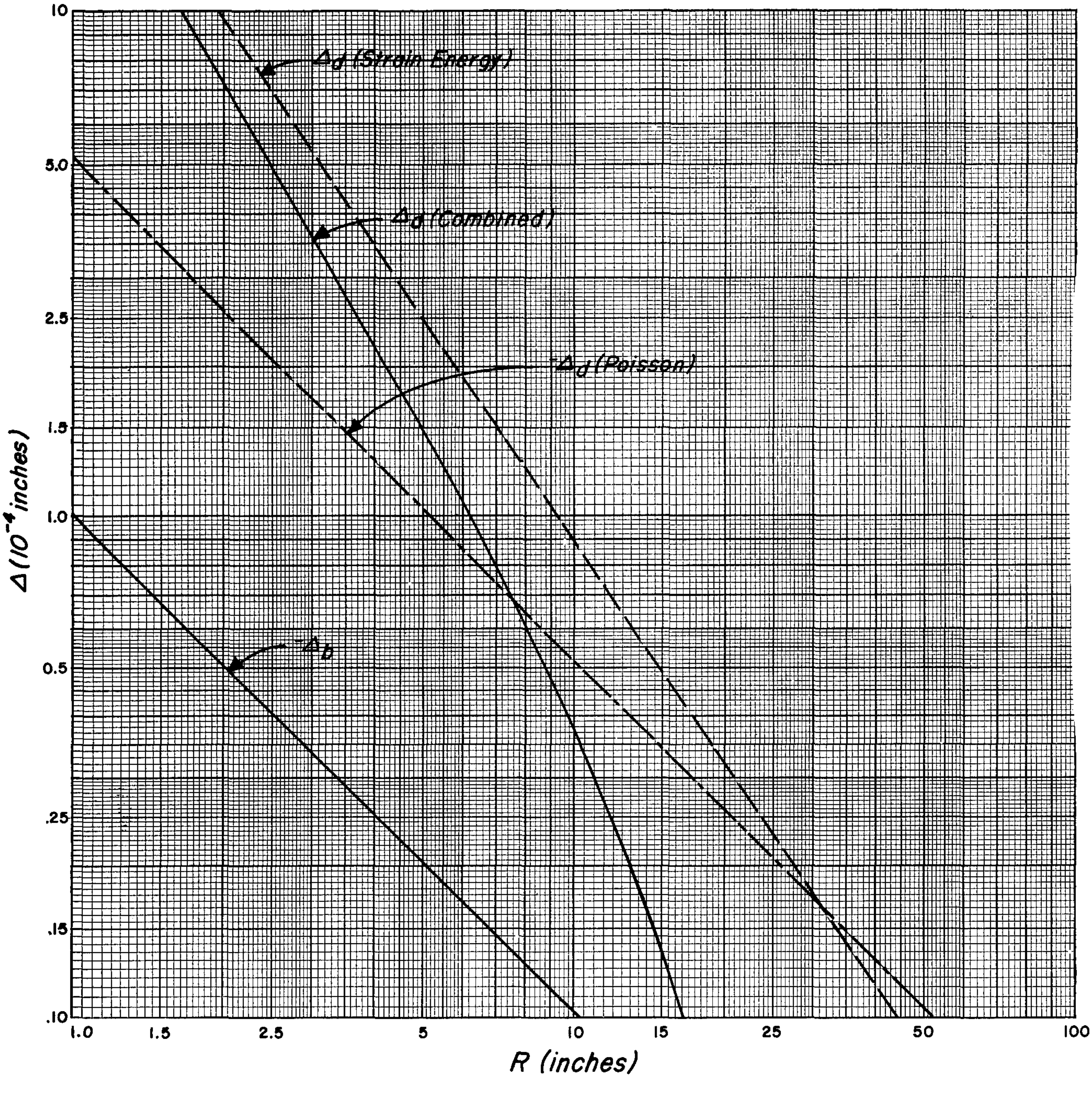

DEPARTMENT OF DEFENSE
PLASTICS TECHNICAL EVALUATION CENTER
PICATINNY ARSENAL, DOVER, N. J.

FIGURE 36

Change in Cross-Section of Deep "I" vs. Radius of Curvature

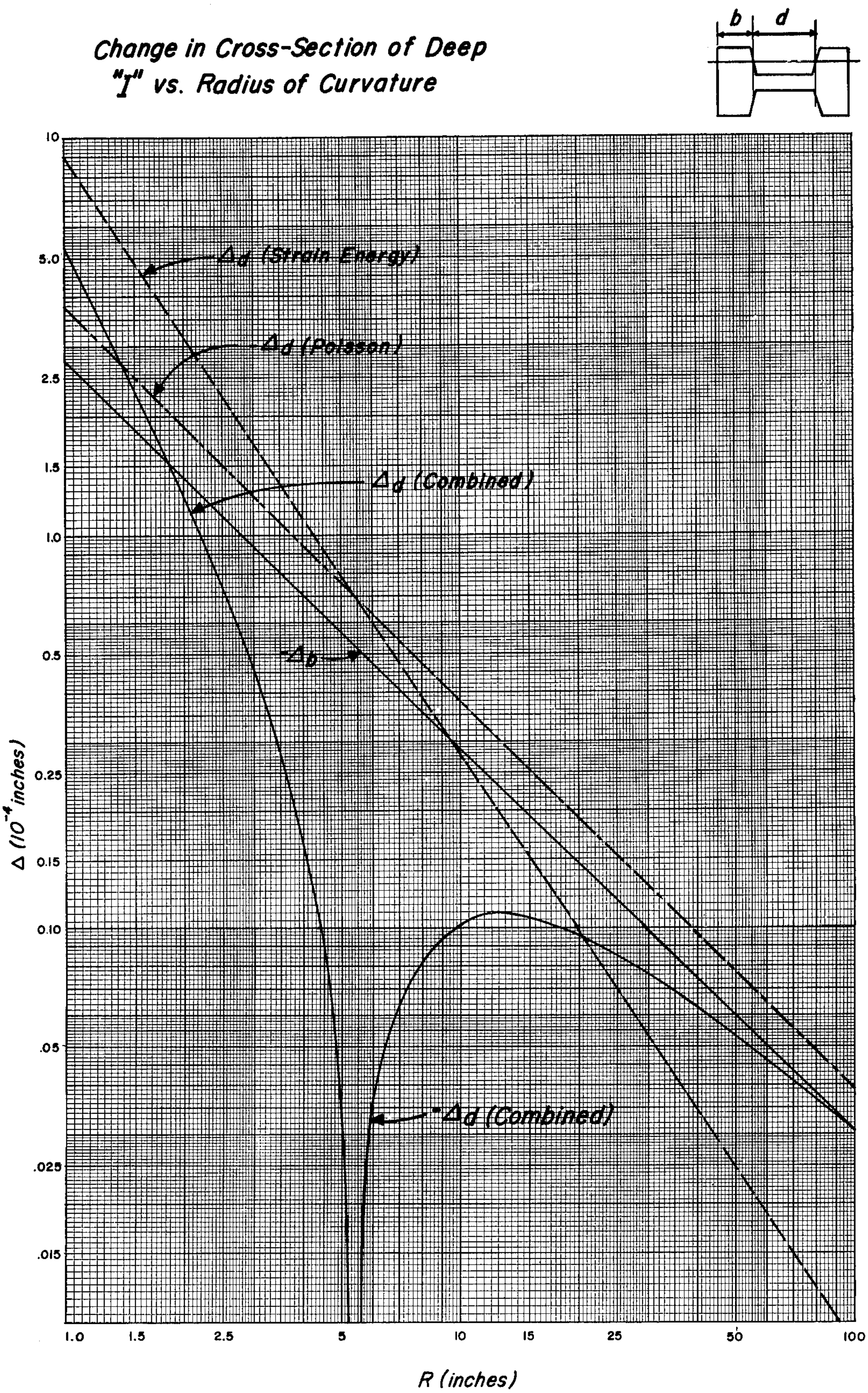

FIGURE 37

Loads on Helical Coil of one turn

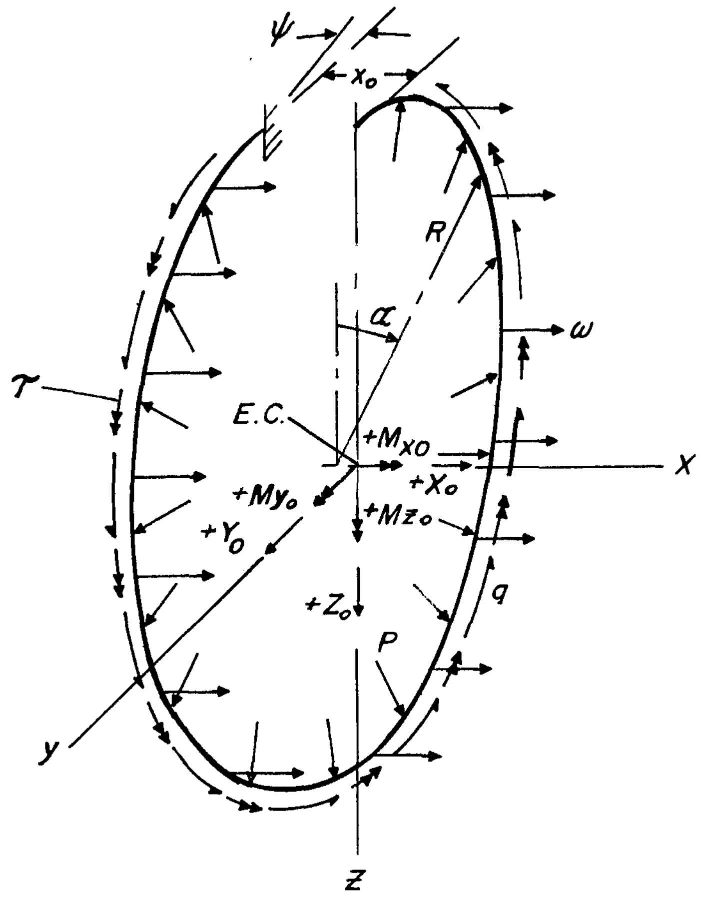

FIGURE 38

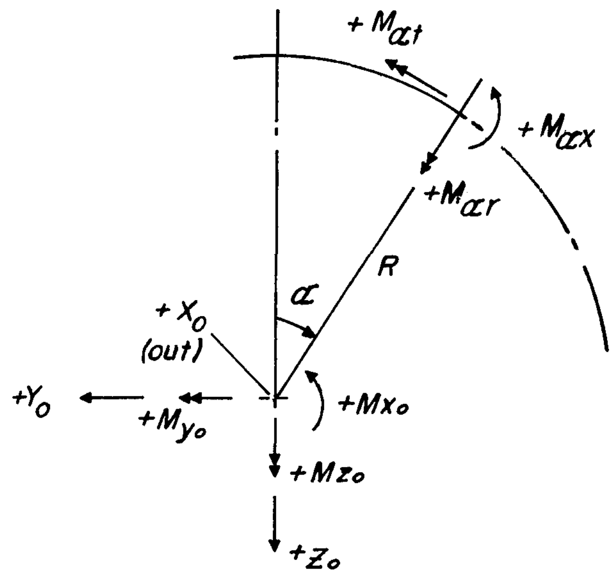

Moments in Coil due to Redundant Forces

FIGURE 39

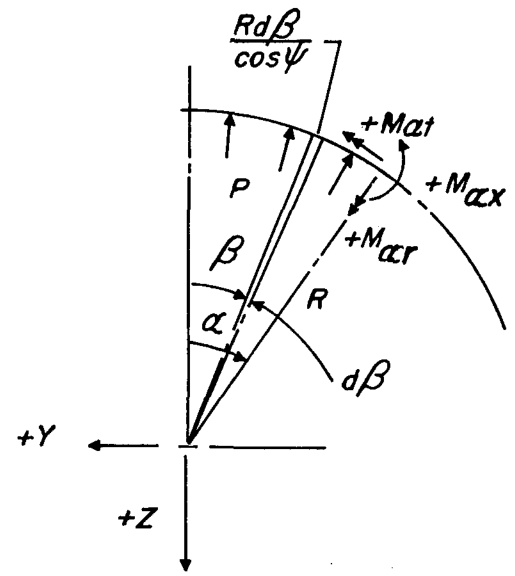

Moments in Coil due to Pressure Load

FIGURE 40

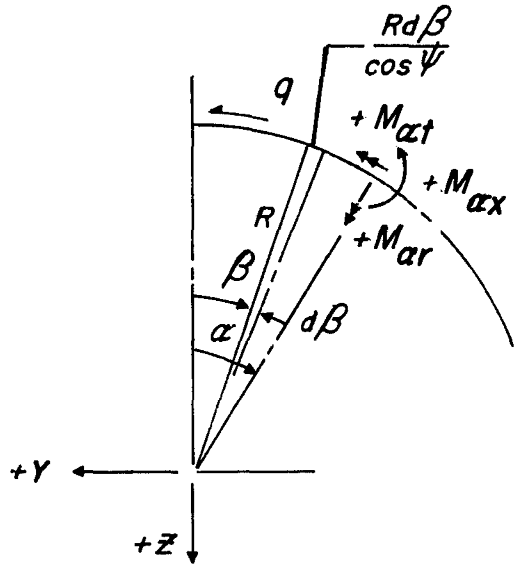

Moments in Coil due to Circumferential Shear

FIGURE 41

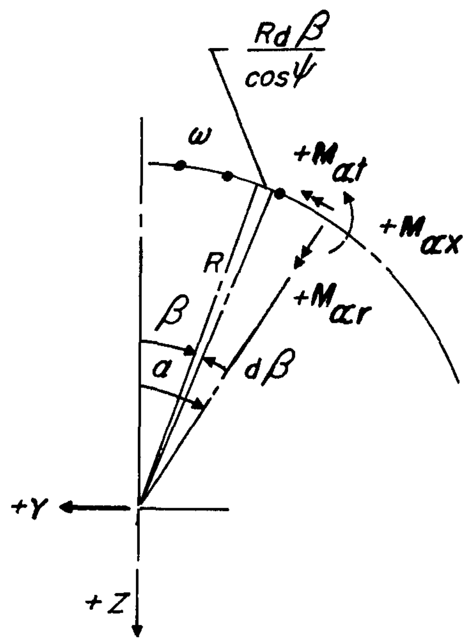

Moments in Coil due to Axial Load

FIGURE 42

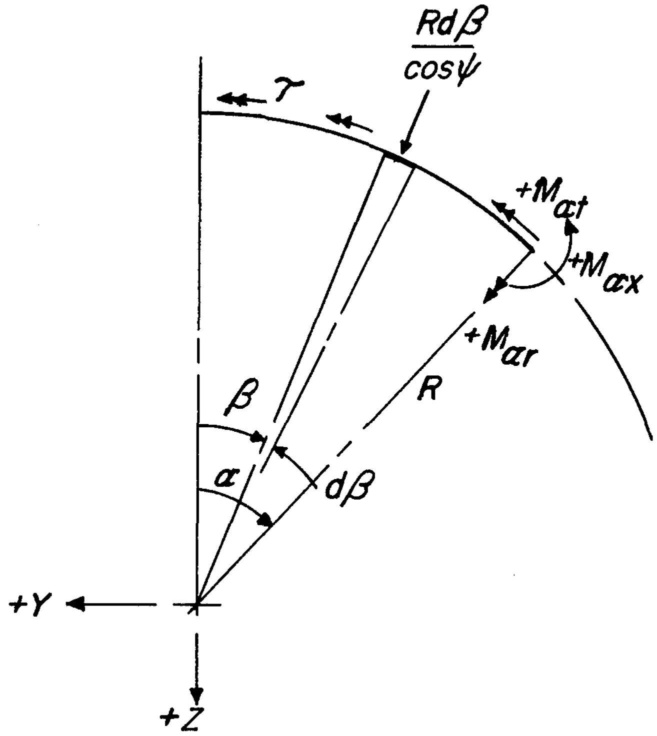

Moments in Coil due to Torsional Moment

FIGURE 43

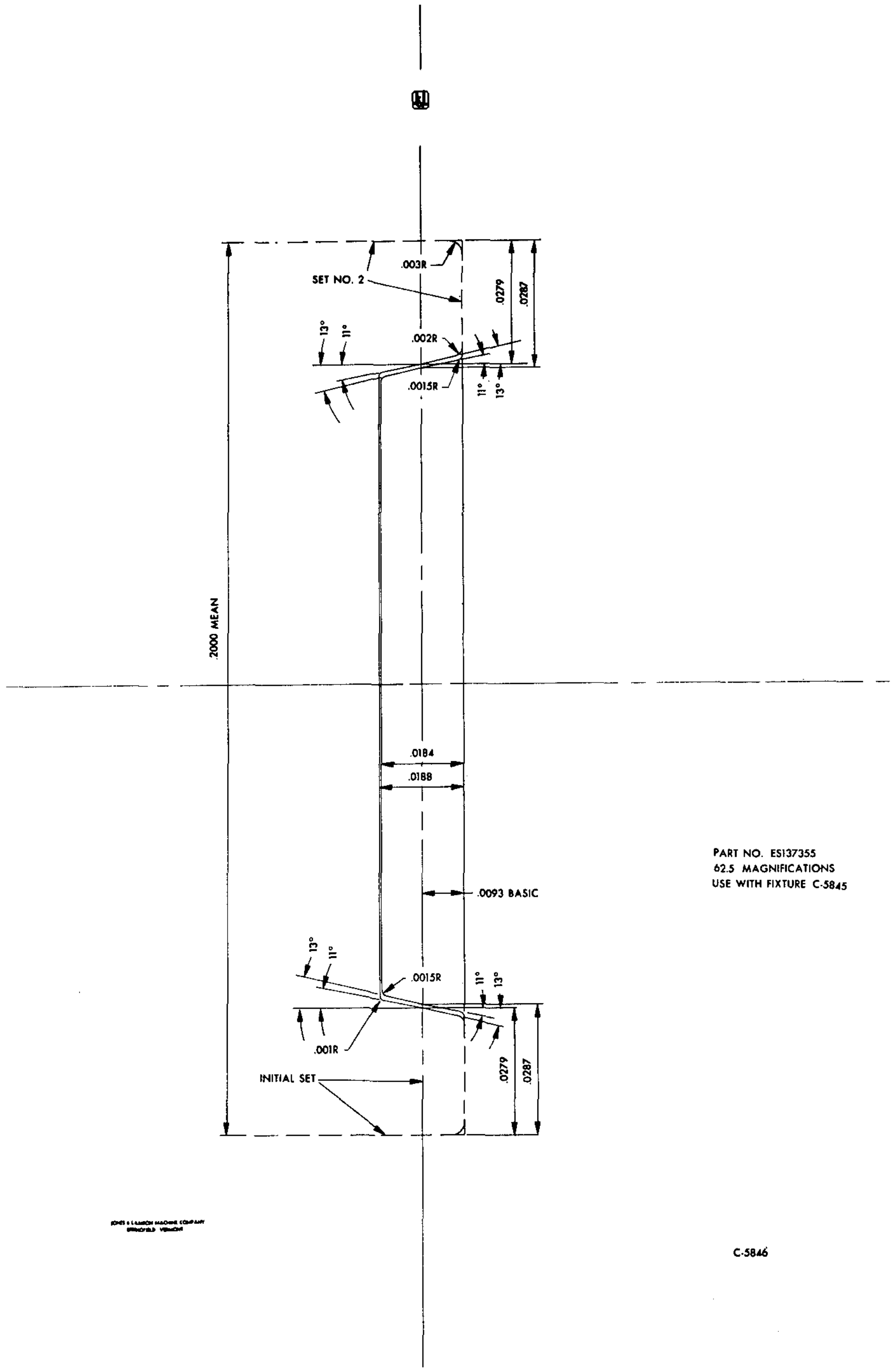

COMPARATOR CHART

FIGURE 44

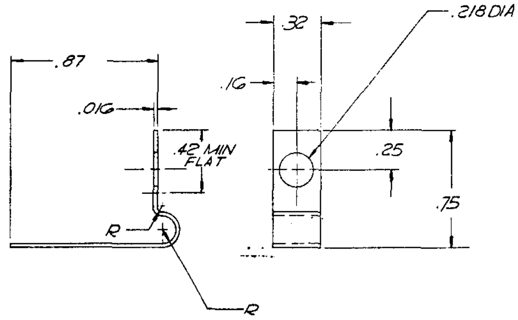

DETAIL OF ITEM 3
MAT'L - STEEL
(4 REQ'D)

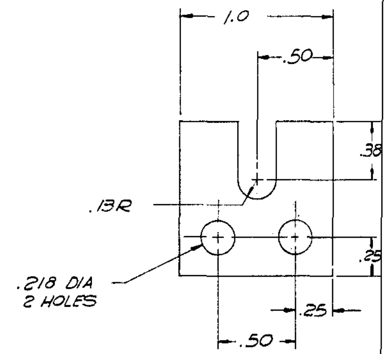

DETAIL OF I
MAT'L - ST
(2 REQ'D)

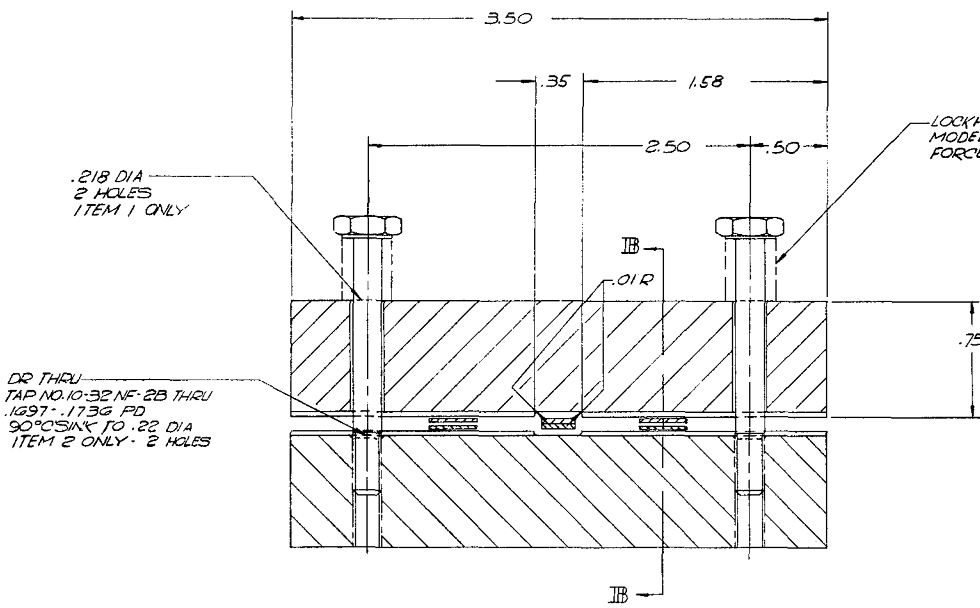

SECT C-C
ITEM 5 REMOVED

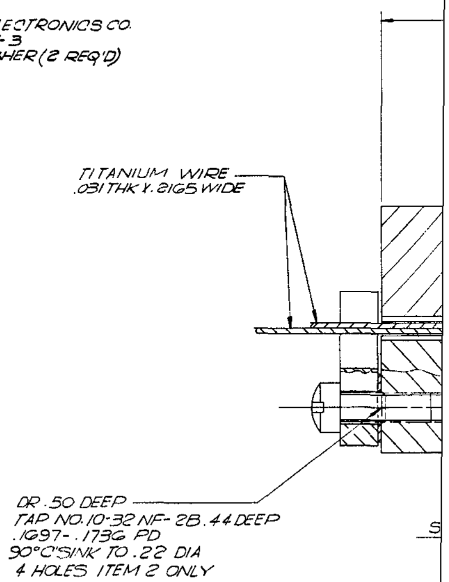

S

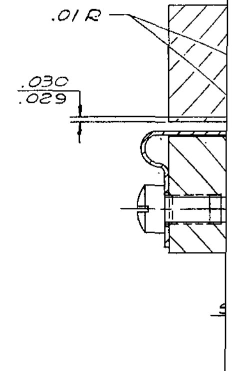

S

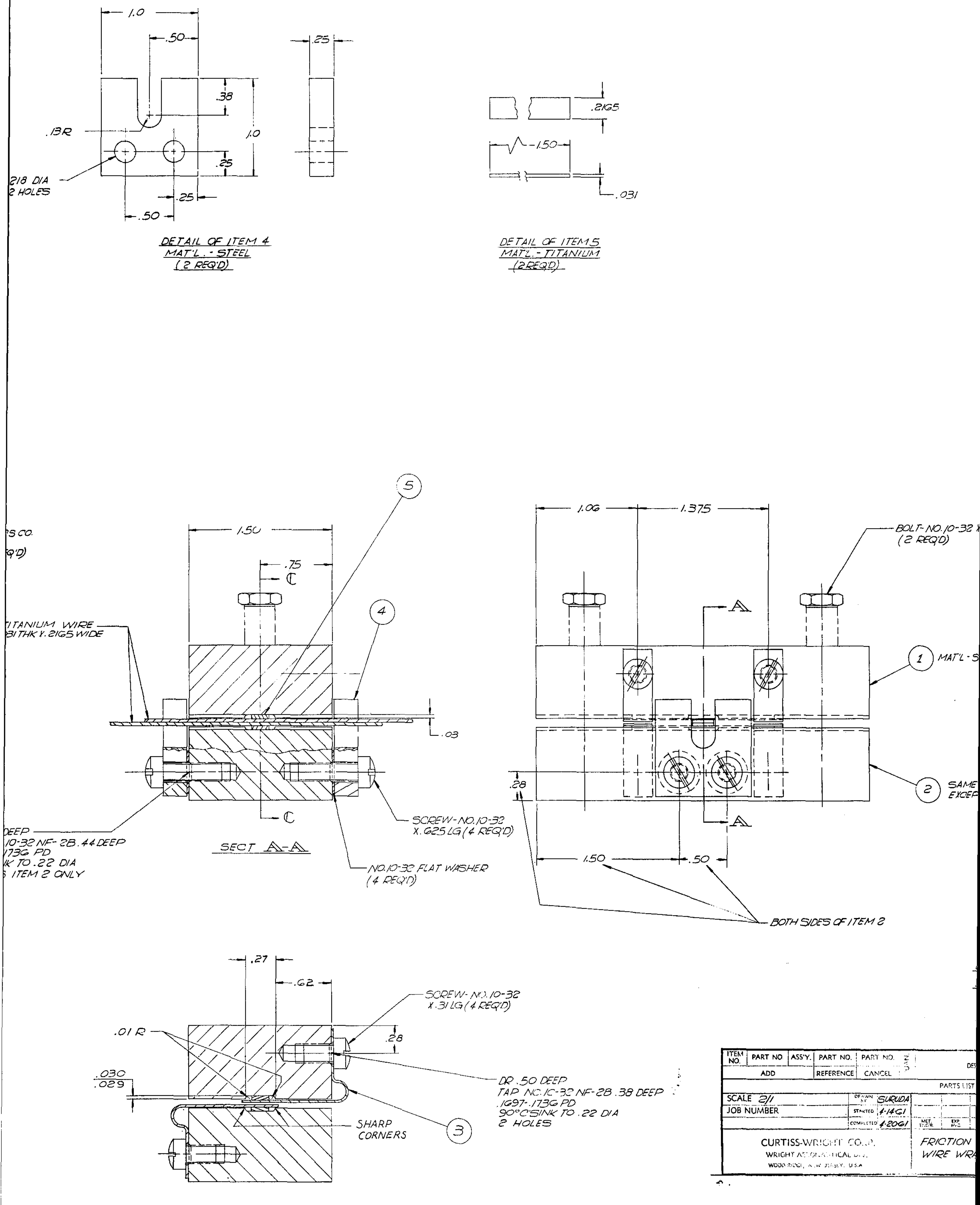
DETAIL OF ITEM 4
MAT'L. - STEEL
(2 REQ'D)
.13R
.218 DIA
2 HOLES
DETAIL OF ITEM 5
MAT'L. - TITANIUM
(2 REQ'D)
.2165
1.50
.031
TITANIUM WIRE
.031 THK X .2165 WIDE
SECT A-A
SCREW-NO.10-32
X .625 LG (4 REQ'D)
NO.10-32 FLAT WASHER
(4 REQ'D)
10-32 NF-2B .44 DEEP
.1736 PD
TO .22 DIA
ITEM 2 ONLY
BOLT-NO.10-32 X
(2 REQ'D)
MAT'L - S
SAME
EXCEP
BOTH SIDES OF ITEM 2
.01 R
SCREW-NO.10-32
X .31 LG (4 REQ'D)
DR .50 DEEP
TAP NO.10-32 NF-2B .38 DEEP
.1697-.1736 PD
90° C'SINK TO .22 DIA
2 HOLES
SHARP
CORNERS
SECT B-B
ITEM NO.
PART NO
ASS'Y.
PART NO.
ADD
REFERENCE
CANCEL
PARTS LIST
SCALE 2/1
JOB NUMBER
SURUDA
4-14-61
4-20-61
CURTISS-WRIGHT CORP.
WRIGHT AERONAUTICAL DIV.
WOOD RIDGE, NEW JERSEY, U.S.A.
FRICTION
WIRE WR

FIGURE

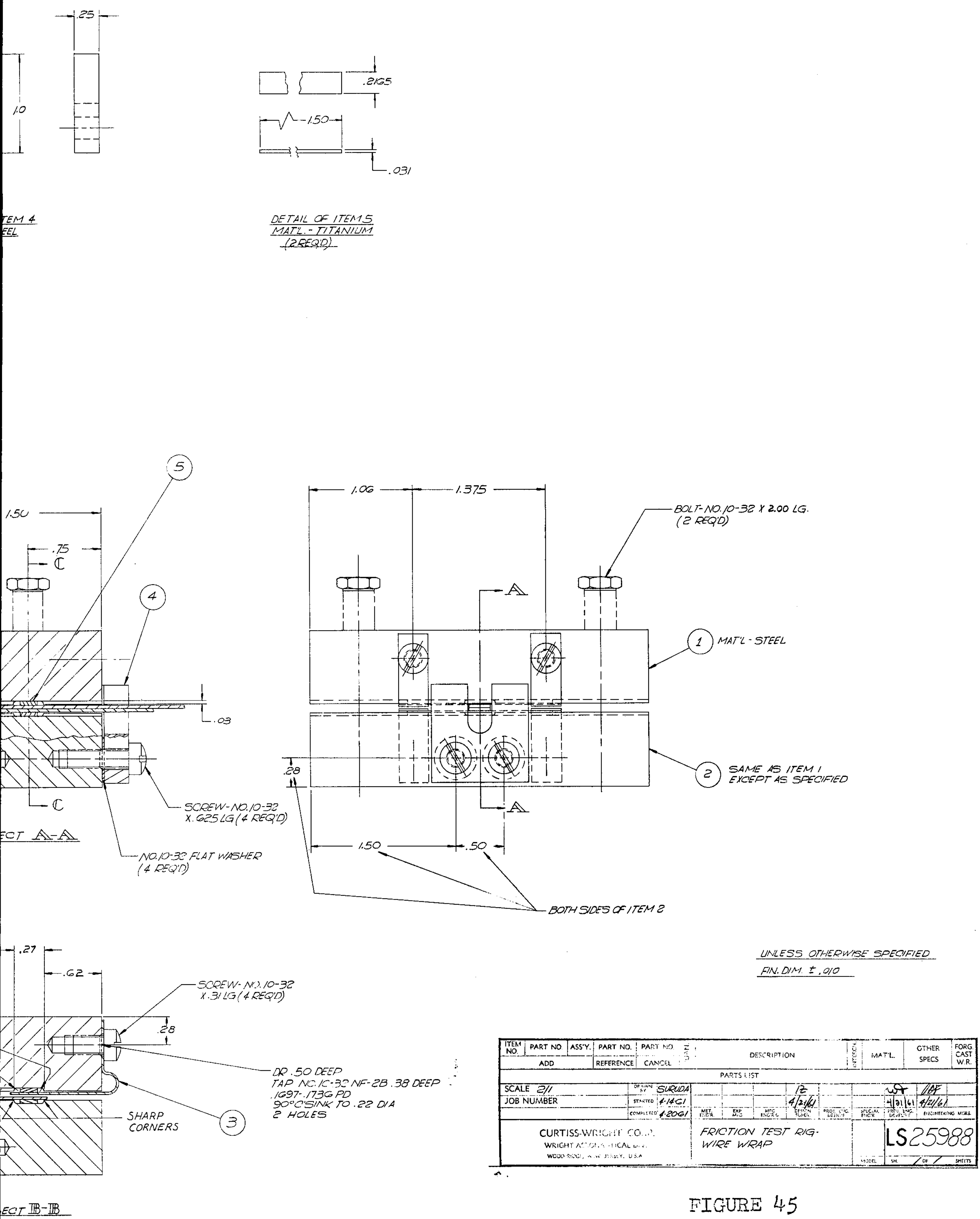

.25
1.0
ITEM 4
EEL
.2165
1.50
.031
DETAIL OF ITEM 5
MAT'L. - TITANIUM
(2 REQ'D)
5
1.50
.75
4
.03
SCREW-NO.10-32
X.625 LG (4 REQ'D)
SECT A-A
NO.10-32 FLAT WASHER
(4 REQ'D)
1.06
1.375
BOLT-NO.10-32 X 2.00 LG.
(2 REQ'D)
A
1
MAT'L - STEEL
.28
2
SAME AS ITEM 1
EXCEPT AS SPECIFIED
1.50
.50
BOTH SIDES OF ITEM 2
.27
.62
SCREW-NO.10-32
X.31 LG (4 REQ'D)
.28
DR .50 DEEP
TAP NO.10-32 NF-2B .38 DEEP
.1697-.1736 PD
90°C'SINK TO .22 DIA
2 HOLES
SHARP
CORNERS
3
SECT B-B
UNLESS OTHERWISE SPECIFIED
FIN. DIM. ± .010
ITEM NO.
PART NO
ASS'Y.
PART NO.
PART NO.
ADD
REFERENCE
CANCEL
DESCRIPTION
MAT'L.
OTHER SPECS
FORG. CAST W.R.
PARTS LIST
SCALE 2/1
JOB NUMBER
DRAWN BY SURUDA
STARTED 4-14-61
COMPLETED 4-20-61
CURTISS-WRIGHT CORP.
WRIGHT AERONAUTICAL DIV.
WOOD RIDGE, NEW JERSEY, U.S.A.
FRICTION TEST RIG-
WIRE WRAP
LS25988

FIGURE 45

FRICTION TEST RIG

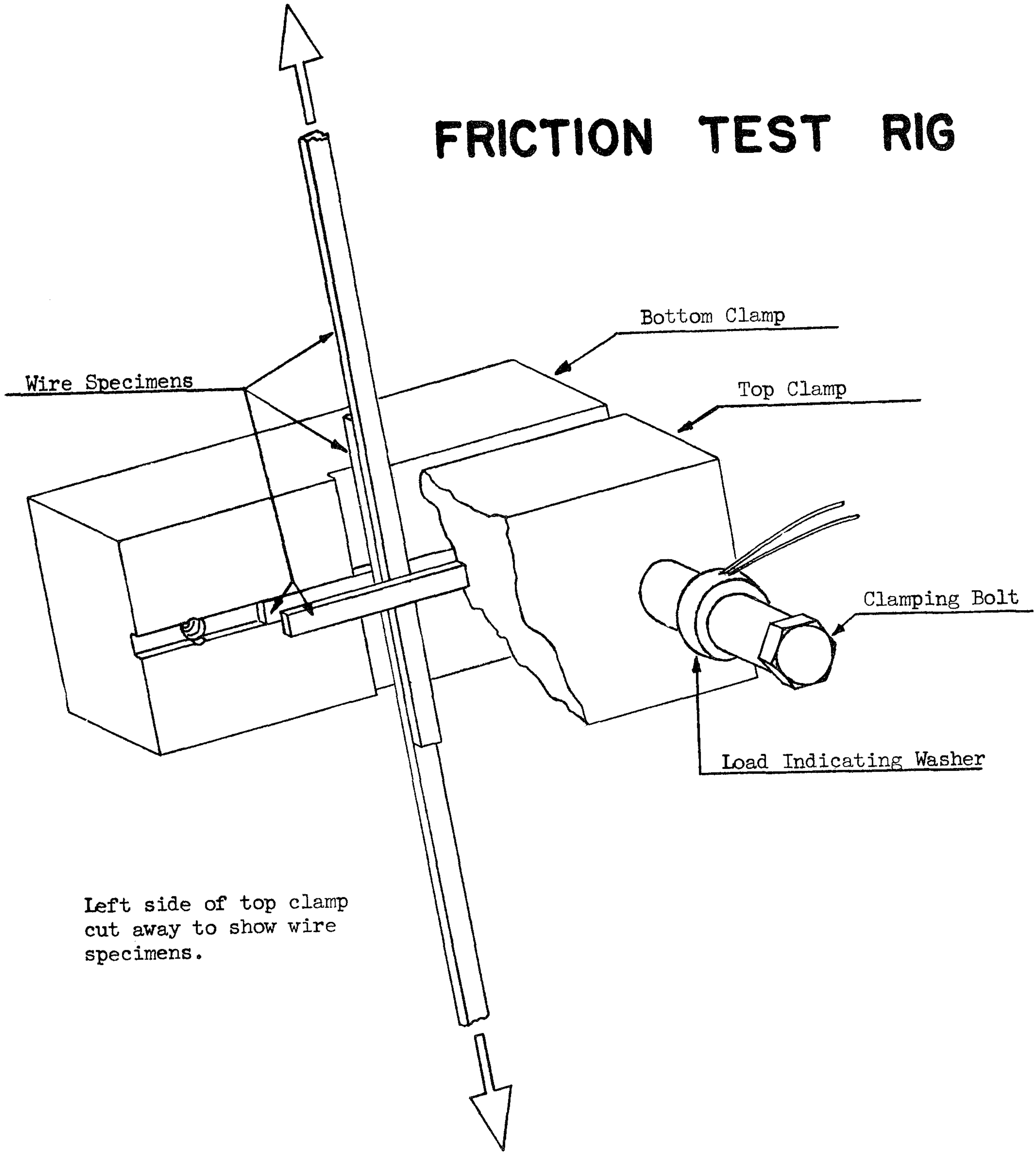

FIGURE 46

COLD WELDED FRICTION SPECIMENS

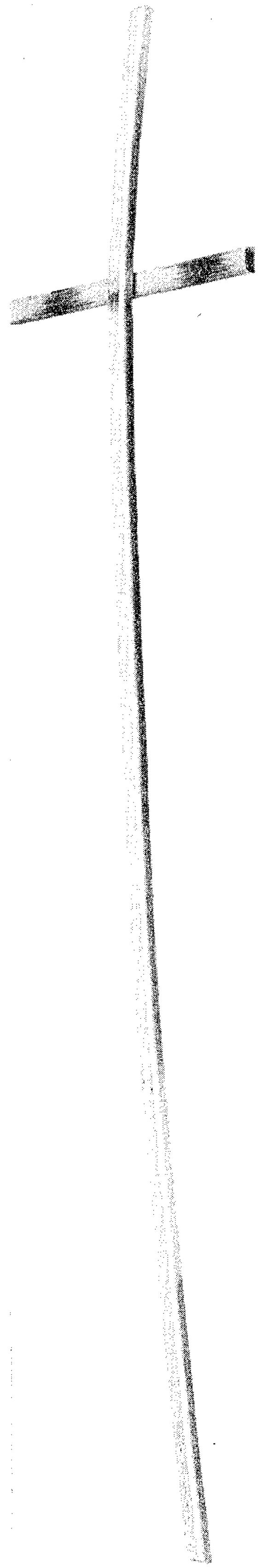

FIGURE 47

FREEBODY DIAGRAM

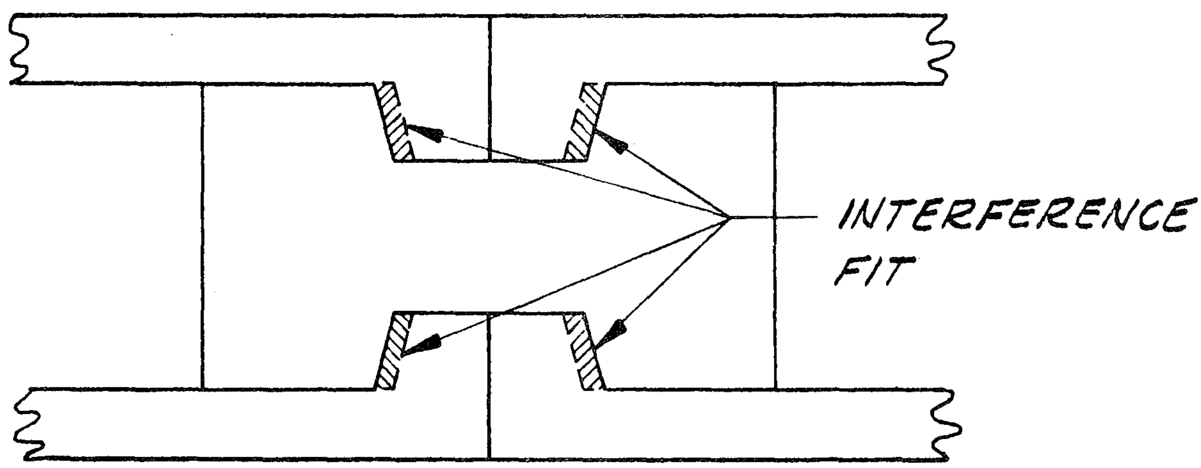

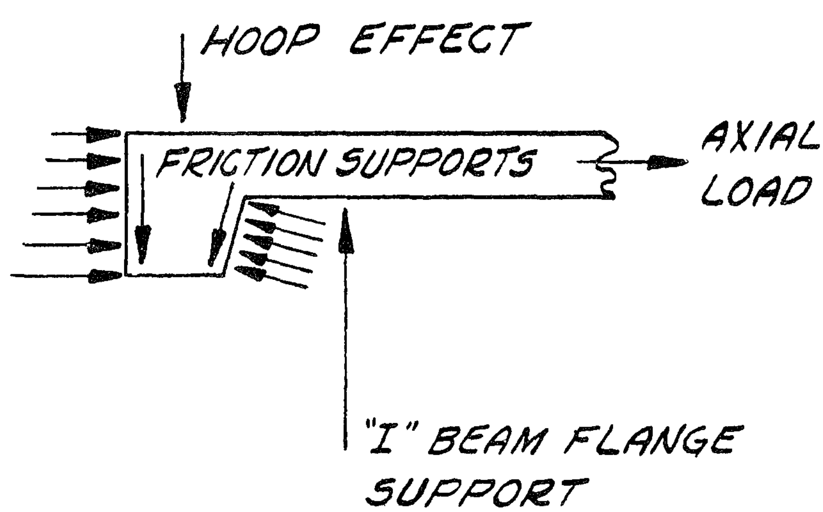

FIGURE 48

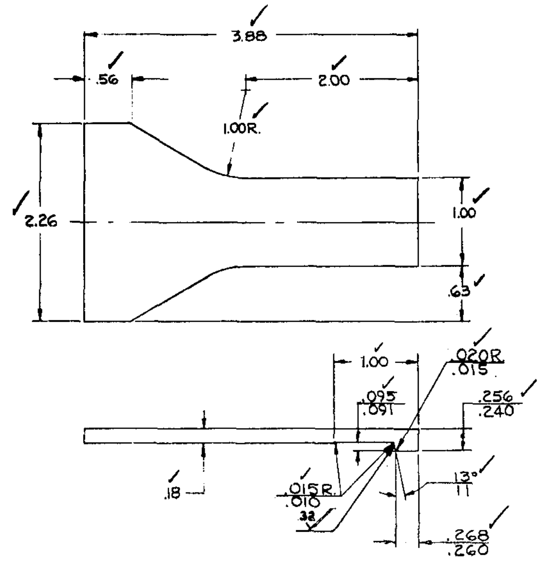

ITEM NO. 1

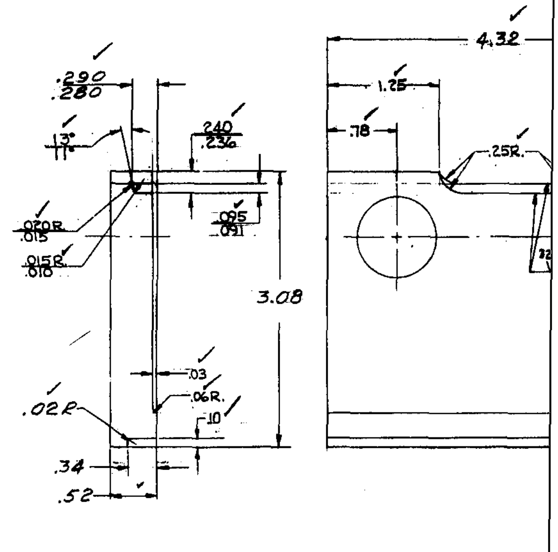

ITEM N

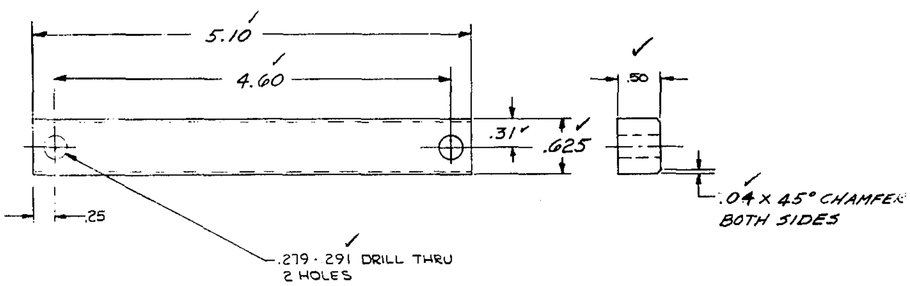

ITEM NO. 3

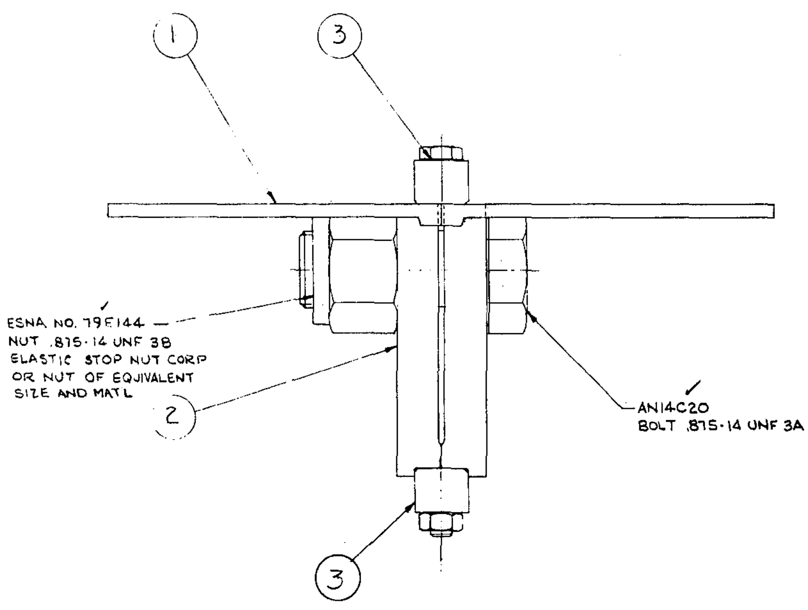

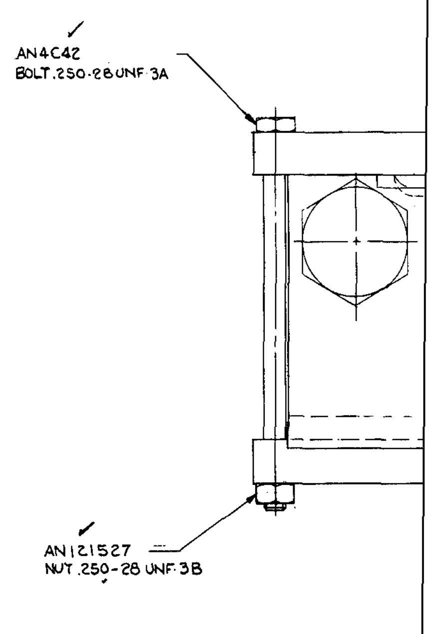

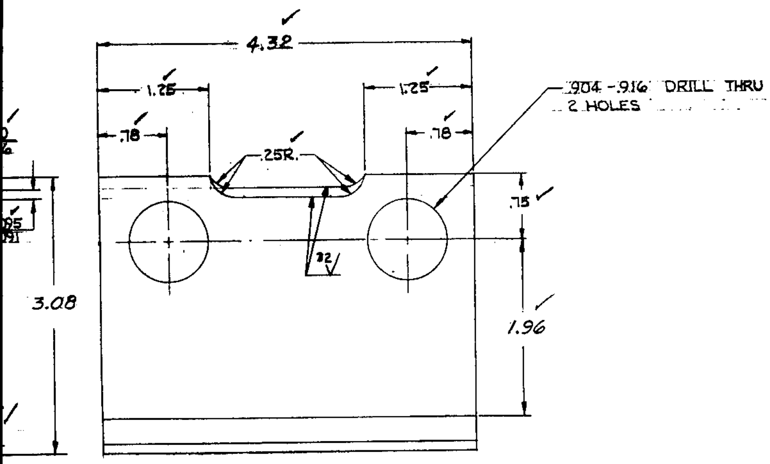

ITEM NO. 2

MFER

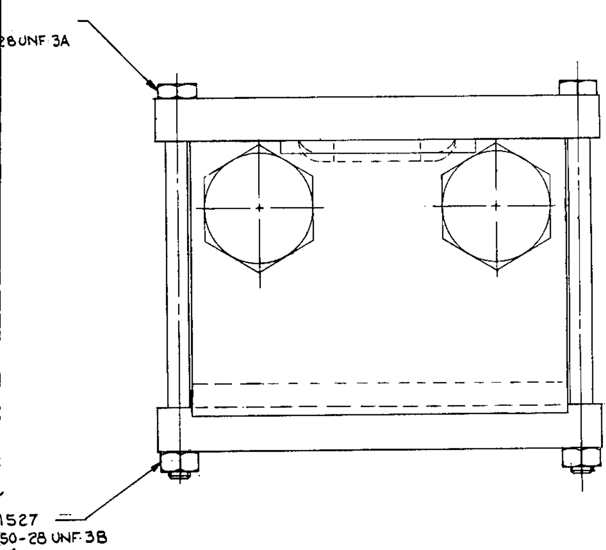

FINISH 125

BREAK SHARP E
.005-.015 APPR
FINISHED DIM. ±.0
ALL ANGLES ± 2
ALL NOTES APPLY
UNLESS OTHERWISE

	AN14C20				2	BOLT - .875-14 UNF
	ESNA NO. 79E144 OR EQUIVALENT				2	NUT - .875-14 UNF 3
	AN4C42				2	BLOT - .250-28 UNF
	AN121527				2	NUT - .250-28UNF
3					2	PLATE - SPECIN
2					2	CLAMP - "I" BEAM
1					2	SPECIMEN - CHAN
ITEM NO.	PART NO.	ASS'Y	PART NO.	PART NO.	QUAN.	DESCR
	ADD		REFERENCE	CANCEL		

PARTS LIST

SCALE FULL	DRAWN BY ZAWONSKI	H.H.
JOB NUMBER 650032	STARTED 10-25-60	11-1-60
	COMPLETED 10-27-60	MET. ENG'R / EXP. MFG.
CURTISS-WRIGHT CORP. WRIGHT		INTER-LOCKING WIRE C CHANNEL & "I" B

CHG. LTR.

FI

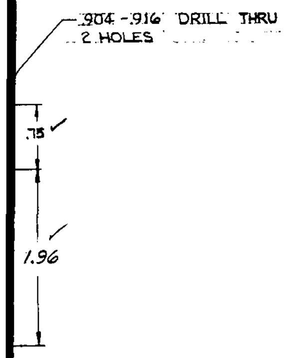

REVISIONS			
CHG. LTR.	DESCRIPTION	DATE	ENGRS.

FINISH $\overset{125}{\sqrt{}}$

BREAK SHARP EDGES
.005-.015 APPROX R

FINISHED DIM. ±.010
ALL ANGLES ± 2°

ALL NOTES APPLY
UNLESS OTHERWISE SPECIFIED

LS 25810

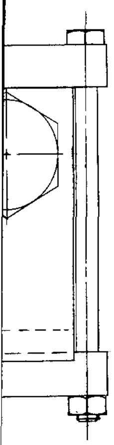

ITEM NO.	PART NO. (ADD)	ASS'Y	PART NO. (REFERENCE)	PART NO. (CANCEL)	QUAN.	DESCRIPTION	INTERCH.	MAT'L.	OTHER SPECS	FORG. CAST W.R.
	AN14C20				2	BOLT-.875-14 UNF 3A 2 3/16 LENGTH		CORROSION RESISTANT STEEL		
	ESNA NO. 192144 OR EQUIVALENT				2	NUT-.875-14 UNF 3B (SEE NOTE)		STAINLESS STEEL		
	AN4C42				2	BLOT-.250-28 UNF-3A 4 5/32 LENGTH		CORROSION RESISTANT STEEL		
	AN121527				2	NUT-.250-28UNF3B		CORROSION RESISTANT STEEL		
3					2	PLATE - SPECIMEN CLAMP		AISI 431	RC 32-36	
2					2	CLAMP - 'I' BEAM		TITANIUM B120VCA	180,000 Min. yield	
1					2	SPECIMEN-CHANNEL10/1 WIRE SIZE		TITANIUM B120VCA	180,000 Min. yield	

PARTS LIST

SCALE FULL	DRAWN BY ZAWONSKI	H.H.			J.L.			*[illegible]*	
JOB NUMBER 650032	STARTED 10-25-60	11-1-60			11-1-60			*11/3/60*	
	COMPLETED 10-27-60	MET. ENGR.	EXP. MGR.	MFG. ENGRG.	DETAIL SUPER.	PROJ. ENG. DESIGN	SPECIAL ENGR.	PROJ. ENG. DEVEL'PT.	ENGINEERING MGRS.

CURTISS-WRIGHT CORP. WRIGHT	INTER-LOCKING TITANIUM WIRE CASE - CHANNEL & 'I' BEAM JOINT RIG	MODEL	LS 25810 SH. 1 OF 1 SHEETS

FIGURE 49

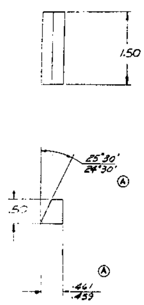

DETAIL OF ITEM 10
MATERIAL: D2C OR H-11 TOOL STEEL
300,000 PSI MIN YIELD (4 REQ'D)

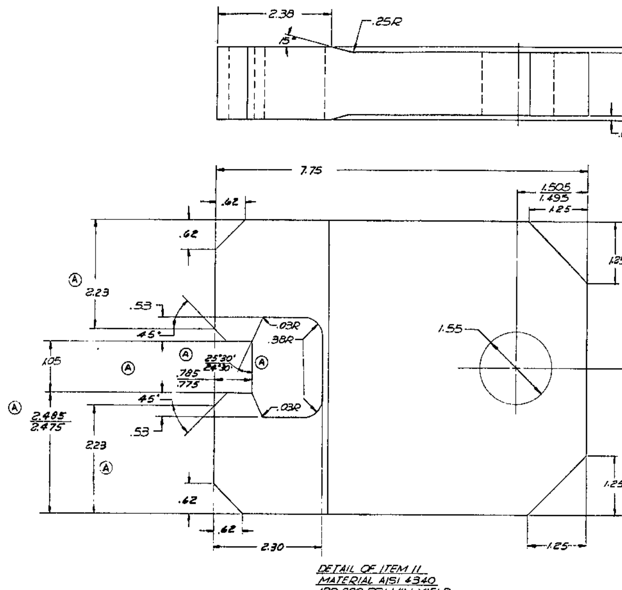

DETAIL OF ITEM 11
MATERIAL AISI 4340
120,000 PSI MIN YIELD
(4 REQ'D)

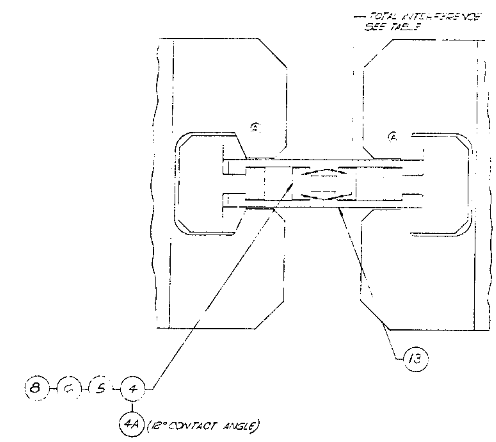

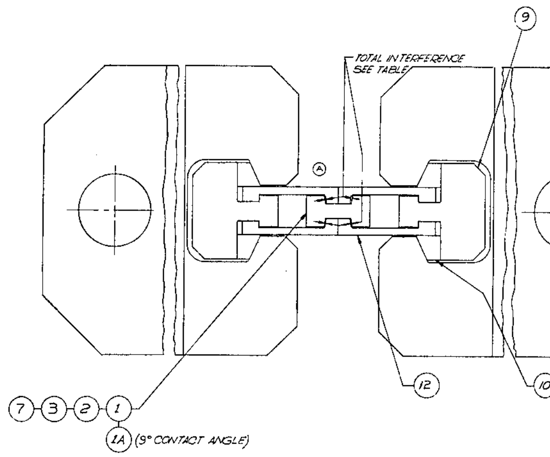

DETAIL OF ITEM 13
SAME AS ITEM 12 EXCEPT
AS SHOWN (4 REQ'D)

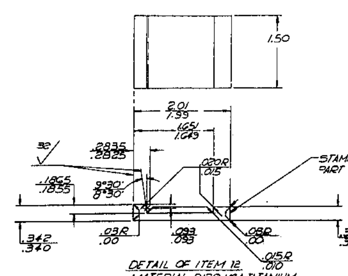

DETAIL OF ITEM 12
MATERIAL: B120-VCA TITANIUM
180,000 PSI MIN YIELD (4 REQ'D)

ITEM NO.	X	Y	TOTAL INTERFERENCE
1 & 4	.5545 / .5535	.40 / .38	.012
2 & 5	.5265 / .5255	.41 / .39	.040
3 & 6	.4865 / .4855	.43 / .41	.080
7 & 8	.6045 / .6035	.42 / .40	.012 WITH .050 SHIM

Ⓑ

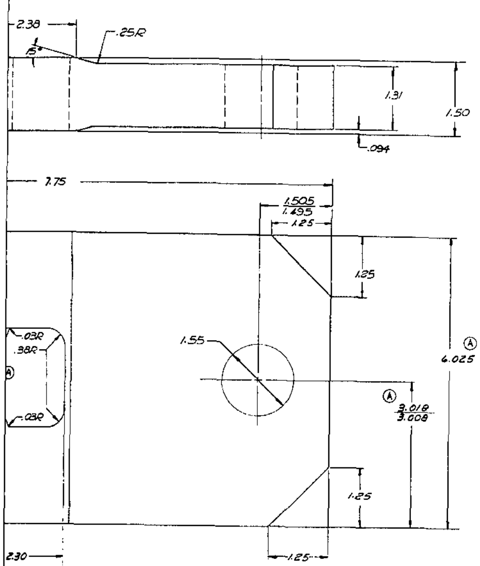

DETAIL OF ITEM 11
MATERIAL AISI 4340
120,000 PSI MIN YIELD
(2 REQ'D)

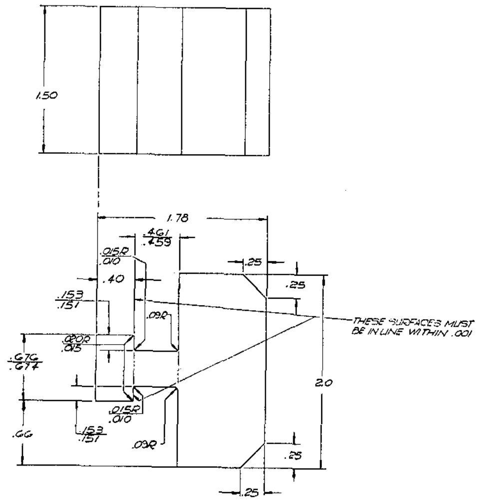

DETAIL OF ITEM 9
MATERIAL - DGC OR H-11 TOOL STEEL
200,000 PSI MIN YIELD (2 REQ'D)
SCALE 2/1

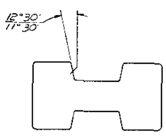

DETAIL OF ITEMS 4,5,6 & 8
SAME AS ITEMS 1,2,& 3 EXCEPT
AS SHOWN (1 OF EACH REQ'D)
SCALE 2/1

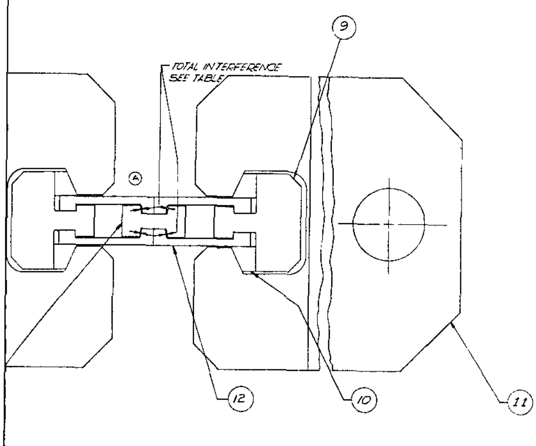

(... OT ANGLE)

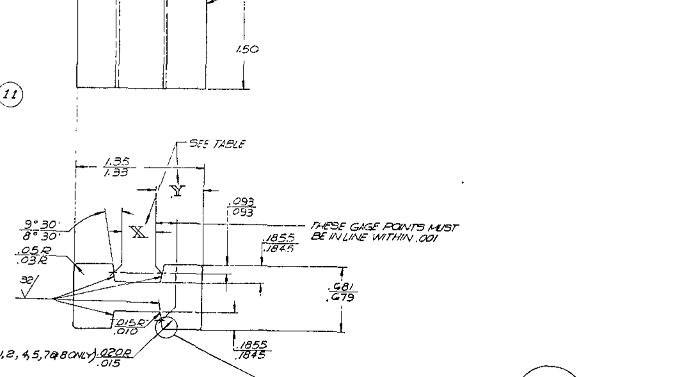

DETAIL OF ITEMS 1,2,3 & 7
MATERIAL: B120 VCA TITANIUM-180,000 PSI MIN YIELD
(1 OF EACH REQ'D)
SCALE 2/1

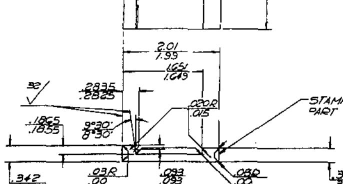

DETAIL OF ITEM 12
MATERIAL - B120-VCA TITANIUM
180,000 PSI MIN YIELD (4 REQ'D)

UNL...
FINI...
ALL...
FINI...
BRE...

ITEM NO.	PART NO.	ASSY.	PART NO.	PART NO.	QUAN.
	ADD		REFERENCE	CANCEL	

SCALE 1/1
JOB NUMBER
DRAWN BY BURUDA H.H.
STARTED 7-3-61
COMPLETED 7-10-61

CURTISS-WRIGHT CORP
WRIGHT AERONAUTICAL D...
WOOD-RIDGE, N.W. JERSEY, U.S.A.

WIRE...
TEST...

STRUCTURAL RIG

ITEM NO.	X	Y	TOTAL INTERFERENCE
1 & 4	.5545 / .5535	.40 / .38	.012
2 & 5	.5265 / .5255	.41 / .39	.040
3 & 6	.4865 / .4855	.43 / .41	.080
7 & 8	.6045 / .6035	.42 / .40	.018 WITH .050 SHIM

Ⓑ

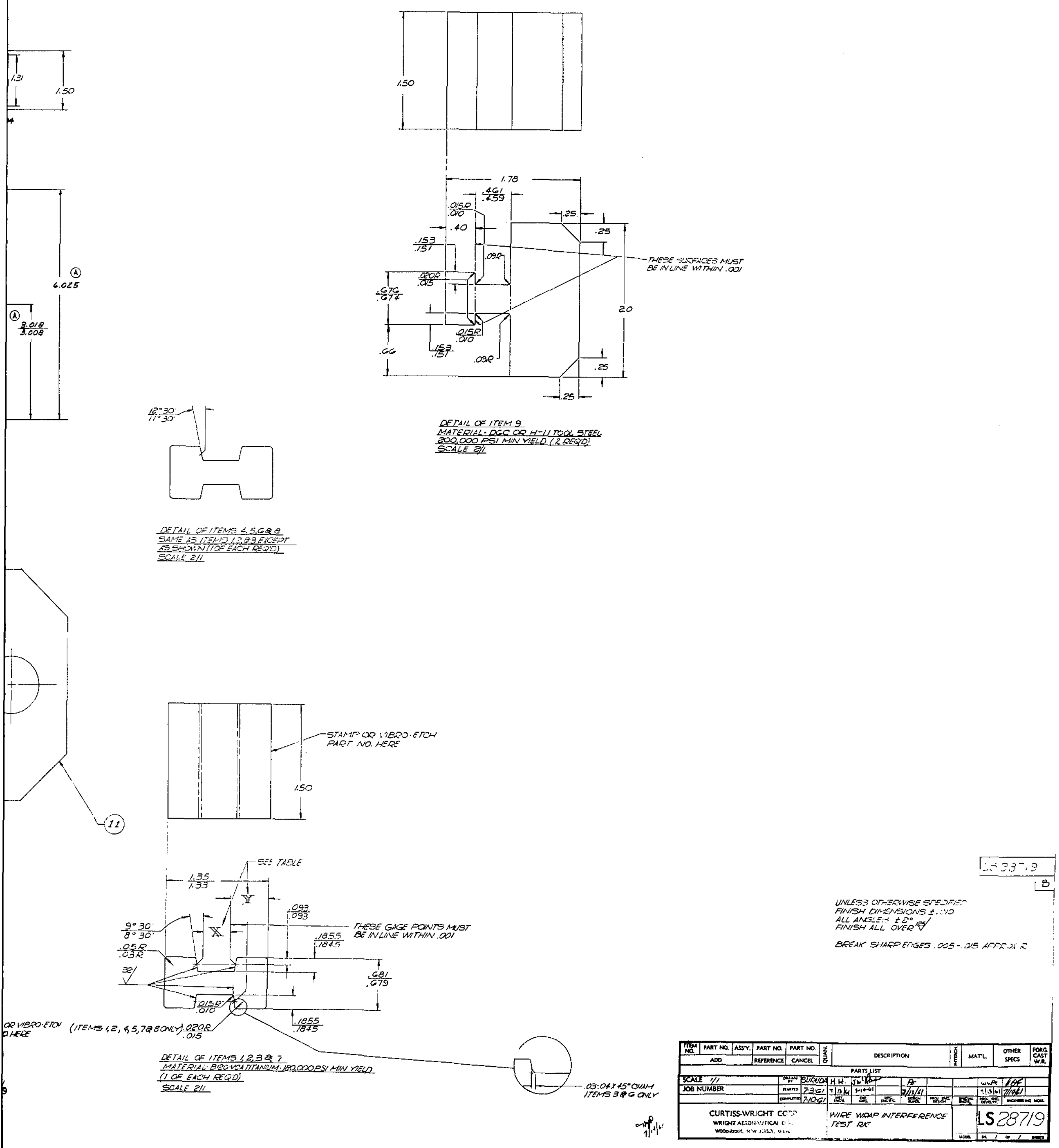

FIGURE 50

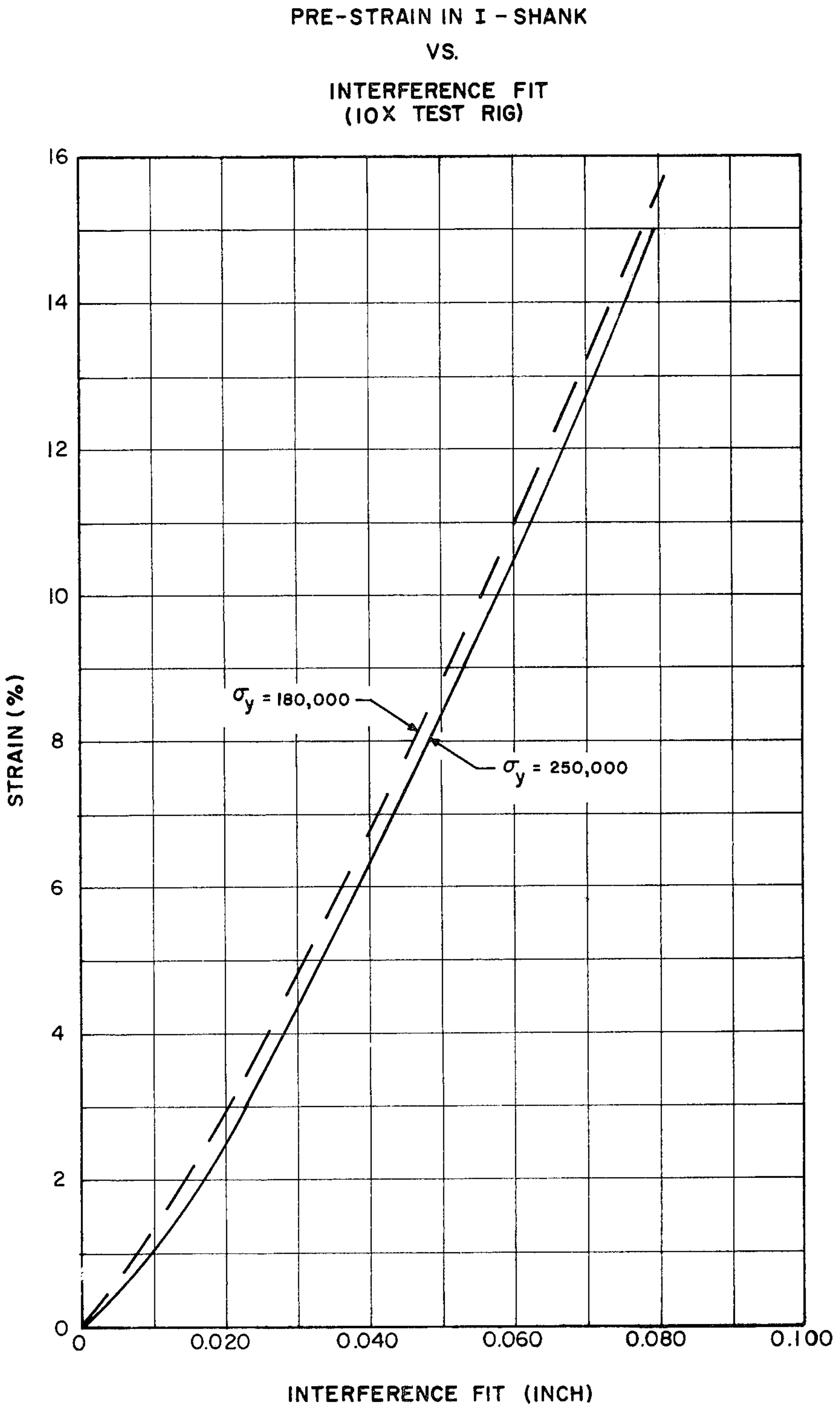

PRE-STRAIN IN I - SHANK
VS.
INTERFERENCE FIT
(10X TEST RIG)
16
14
12
10
8
6
4
2
0
STRAIN (%)
σ_y = 180,000
σ_y = 250,000
0
0.020
0.040
0.060
0.080
0.100
INTERFERENCE FIT (INCH)

FIGURE 51

10X TEST RIG ASSEMBLY

THEORETICAL MAXIMUM CAPACITY
VS.
YIELD STRENGTH OF TITANIUM

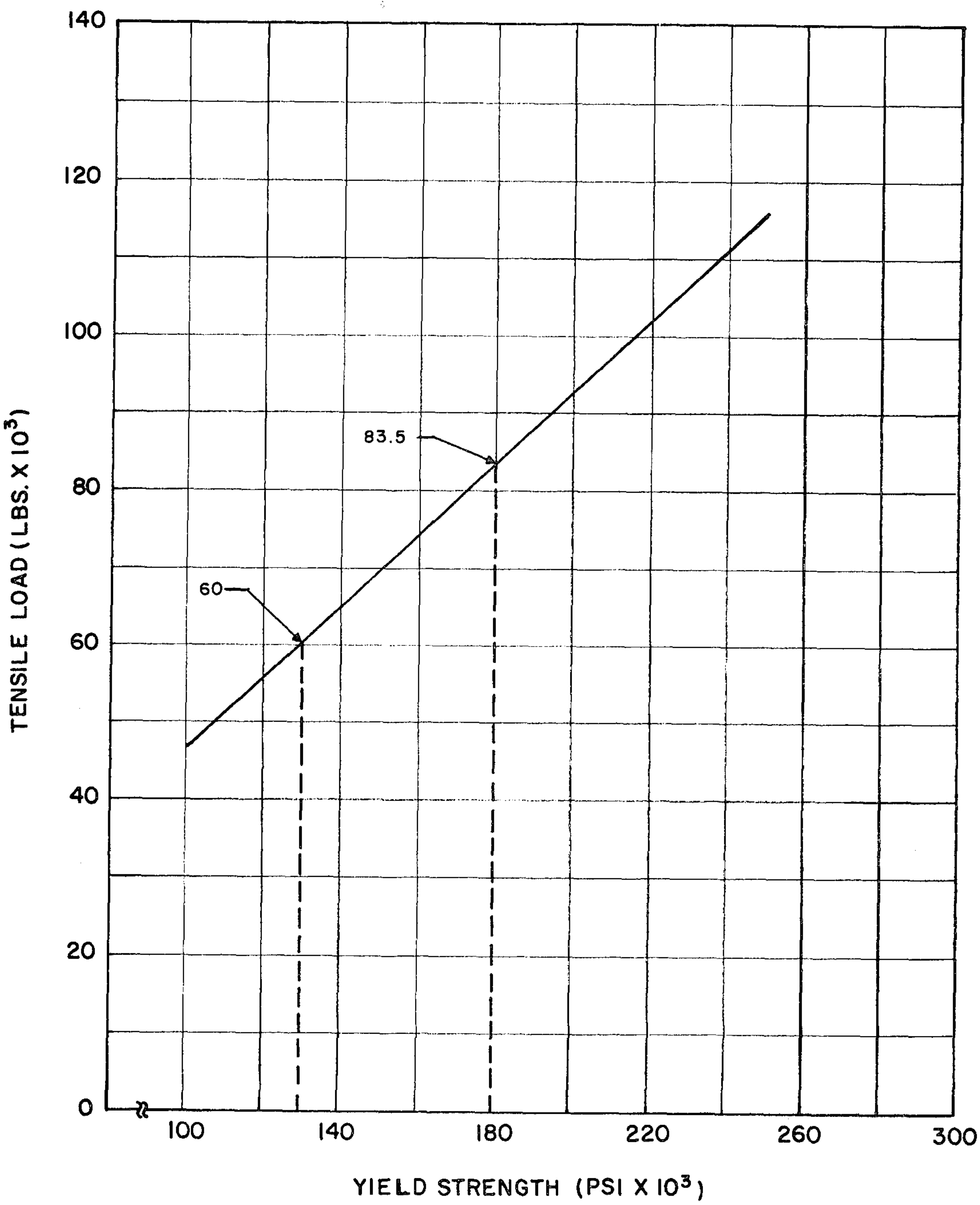

FIGURE 52

STRUCTURAL RIG DETAILS

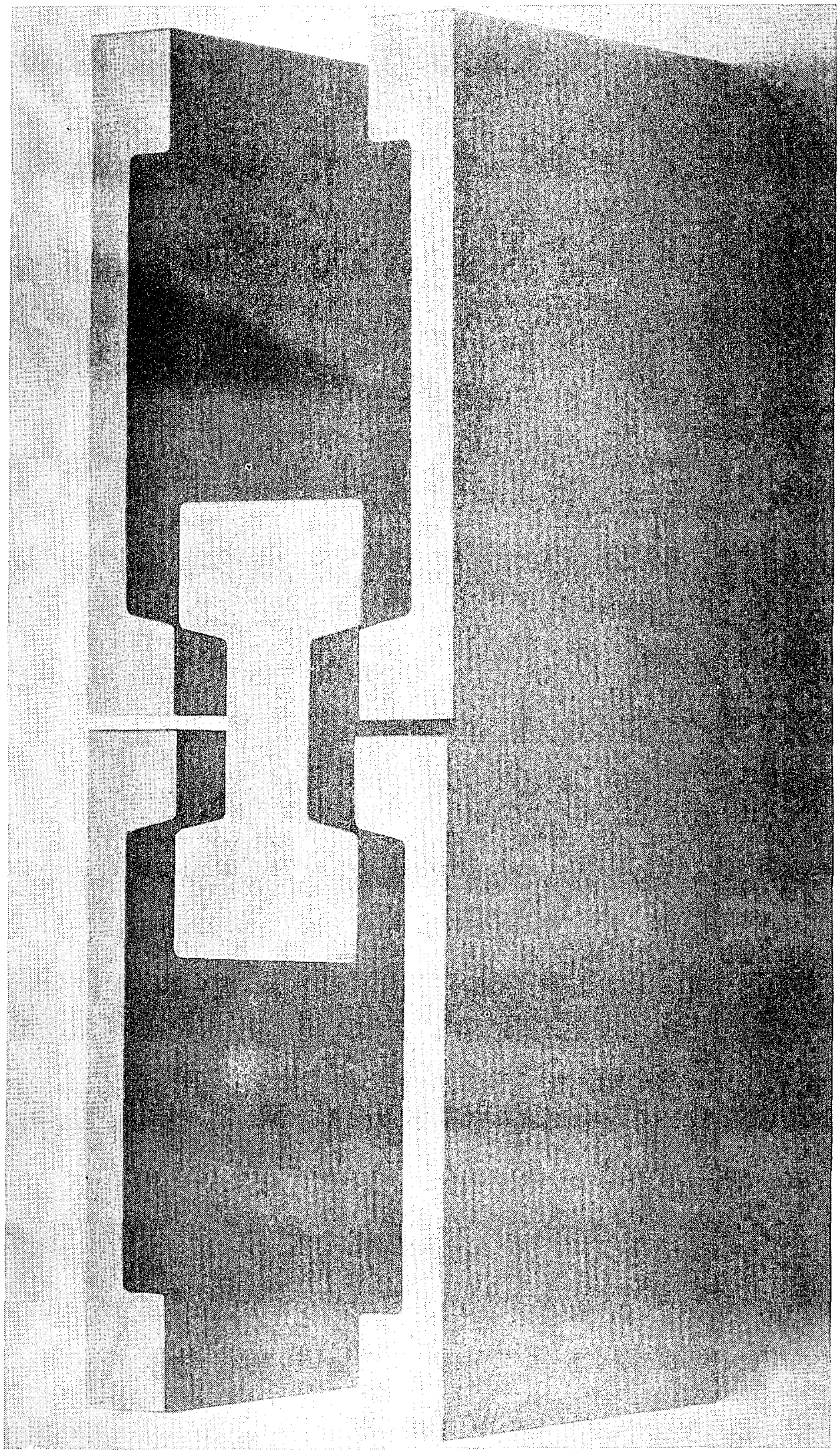

FIGURE 53

ASSEMBLY

TAPE WRAP INTERFERENCE TEST RIG

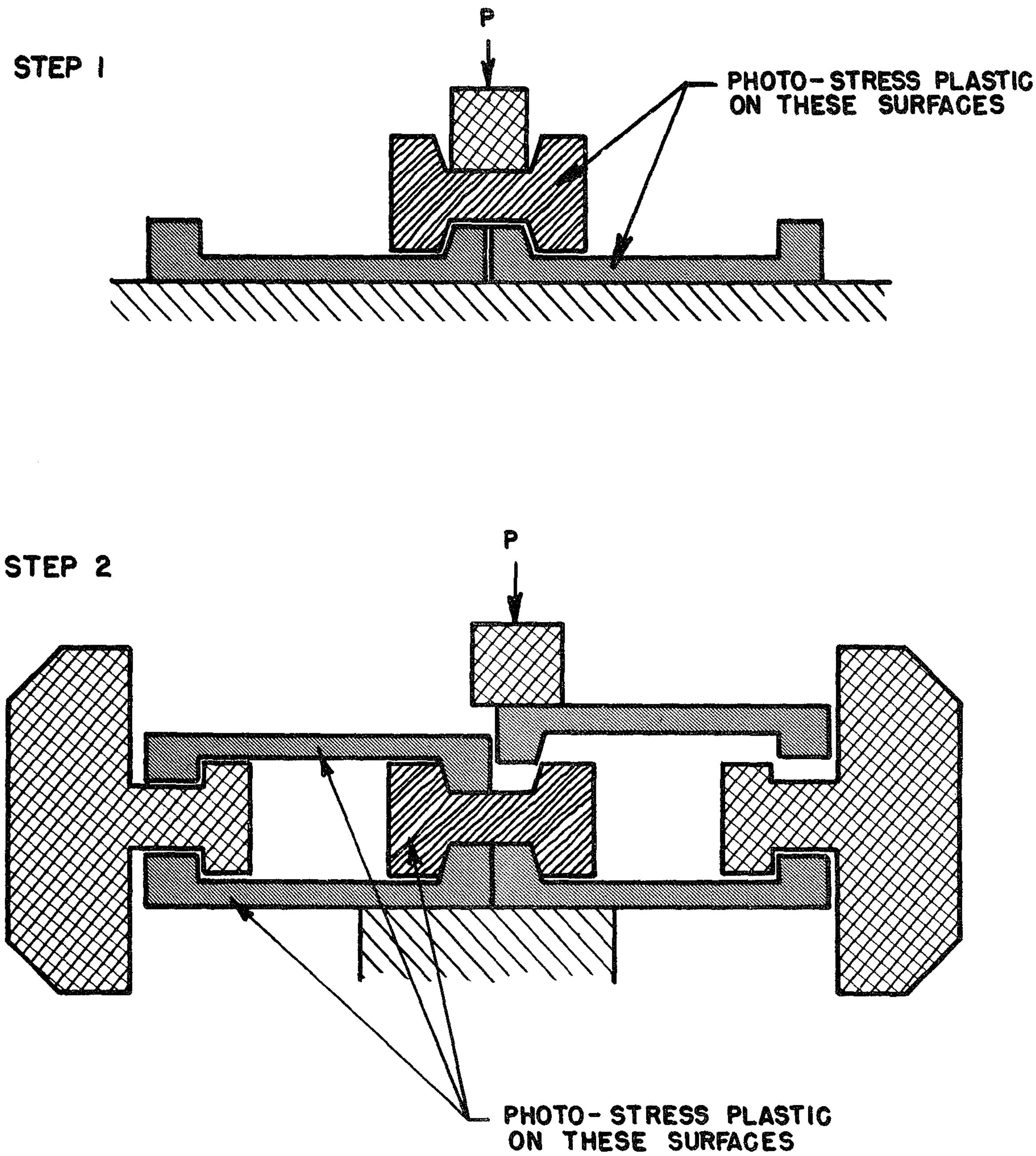

FIGURE 54

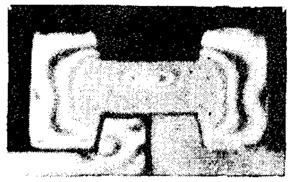

Interference Test Rig No. 1 - Photo-Stress Pattern

FIGURE 55

TAPE WRAP INTERFERENCE TEST RIG NO. I

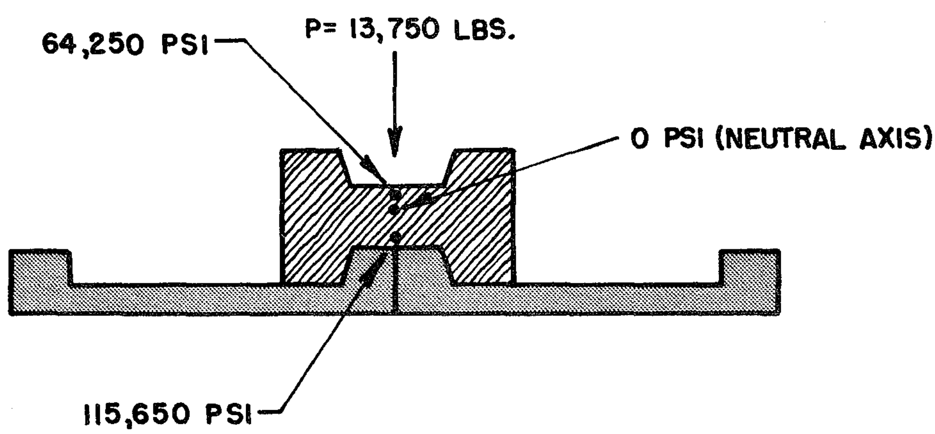

PHOTO-STRESS VALUES IN I-BEAM FOLLOWING ASSEMBLY
STEP NO. I

FIGURE 56

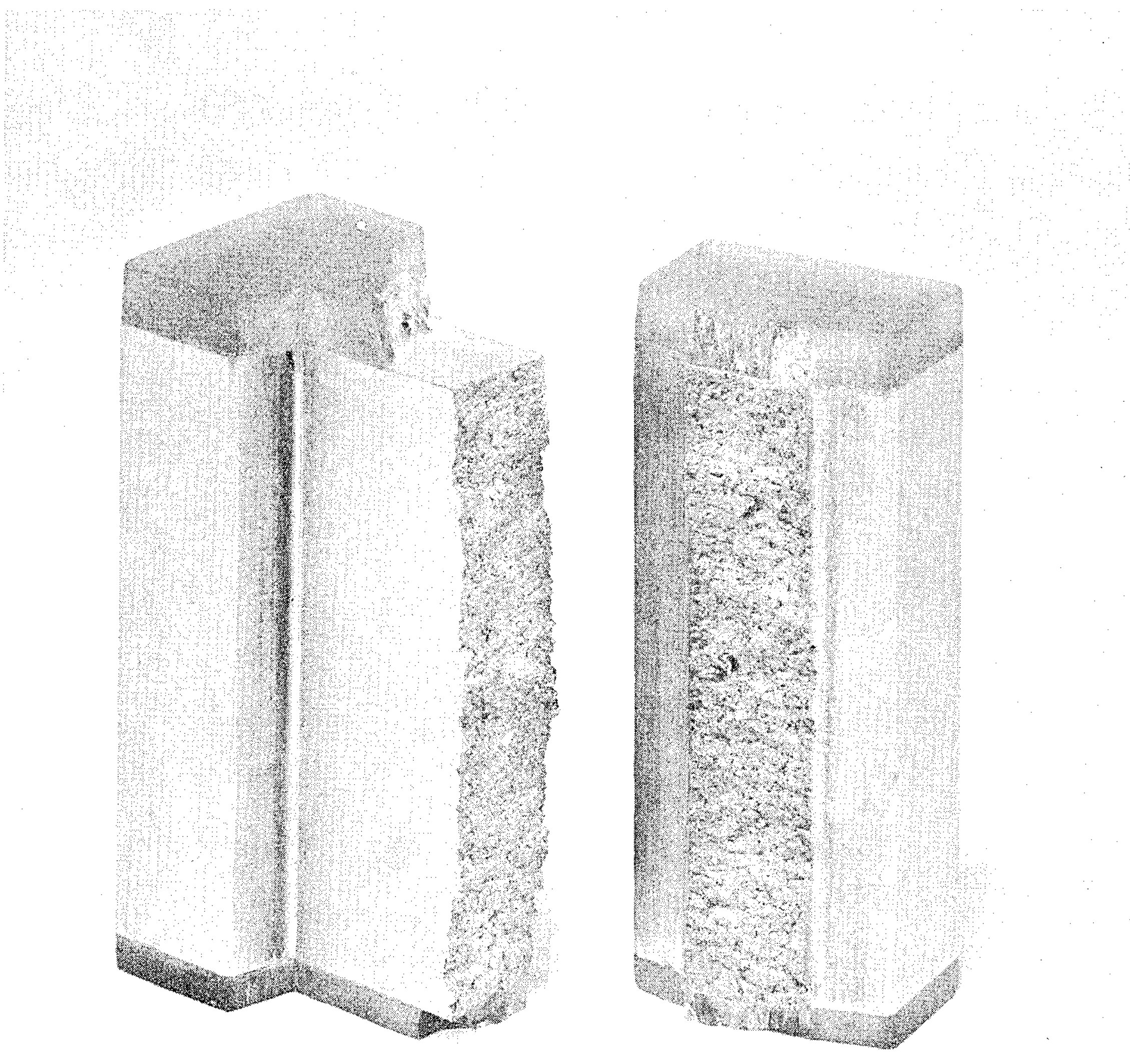

Interference Rig No. 1 - Failure of I-Beam

FIGURE 57

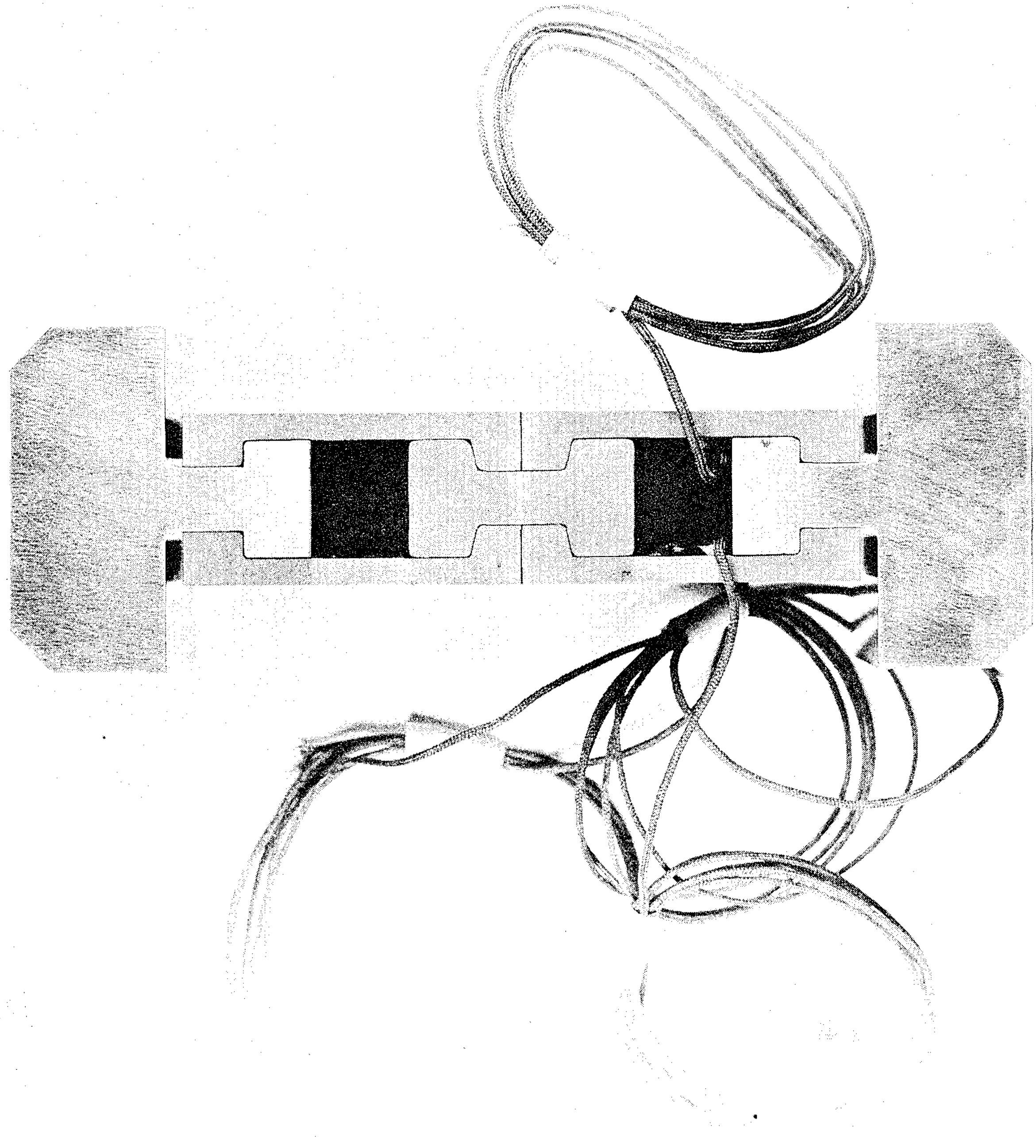

Wire Wrap Interference Test Rig No. 2 Assembled

FIGURE 58

TAPE WRAP INTERFERENCE TEST RIG NO. 2
12° ANGLE - .012" INTERFERENCE FIT
ANNEALED MATERIAL

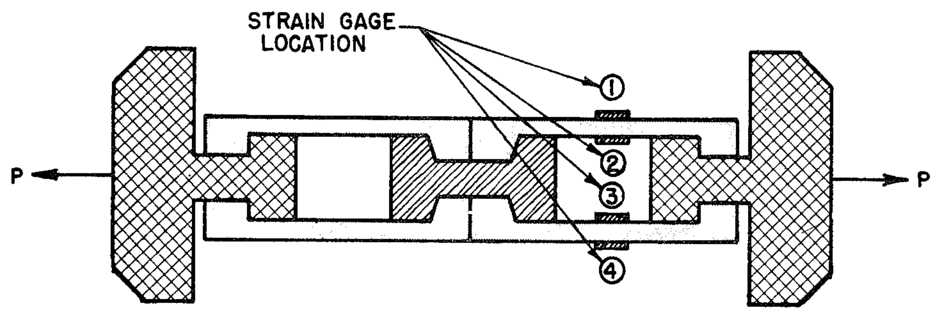

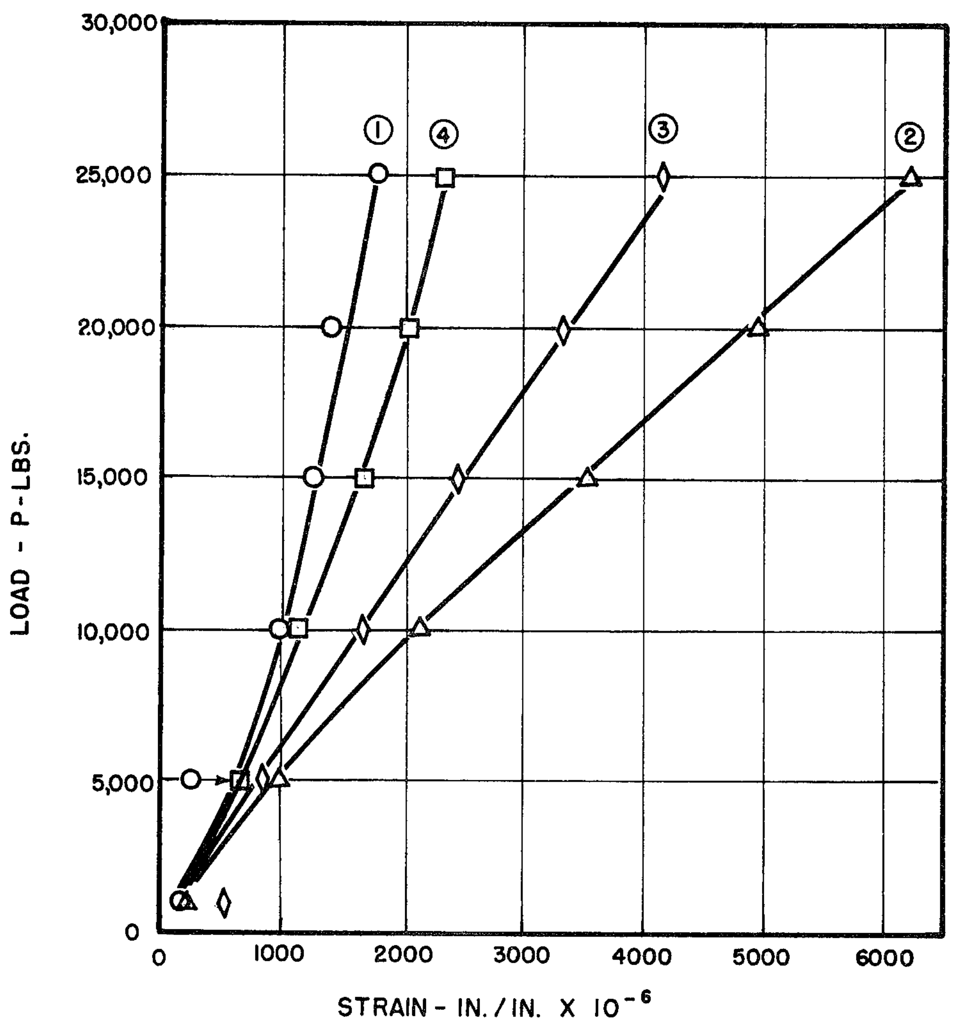

FIGURE 59

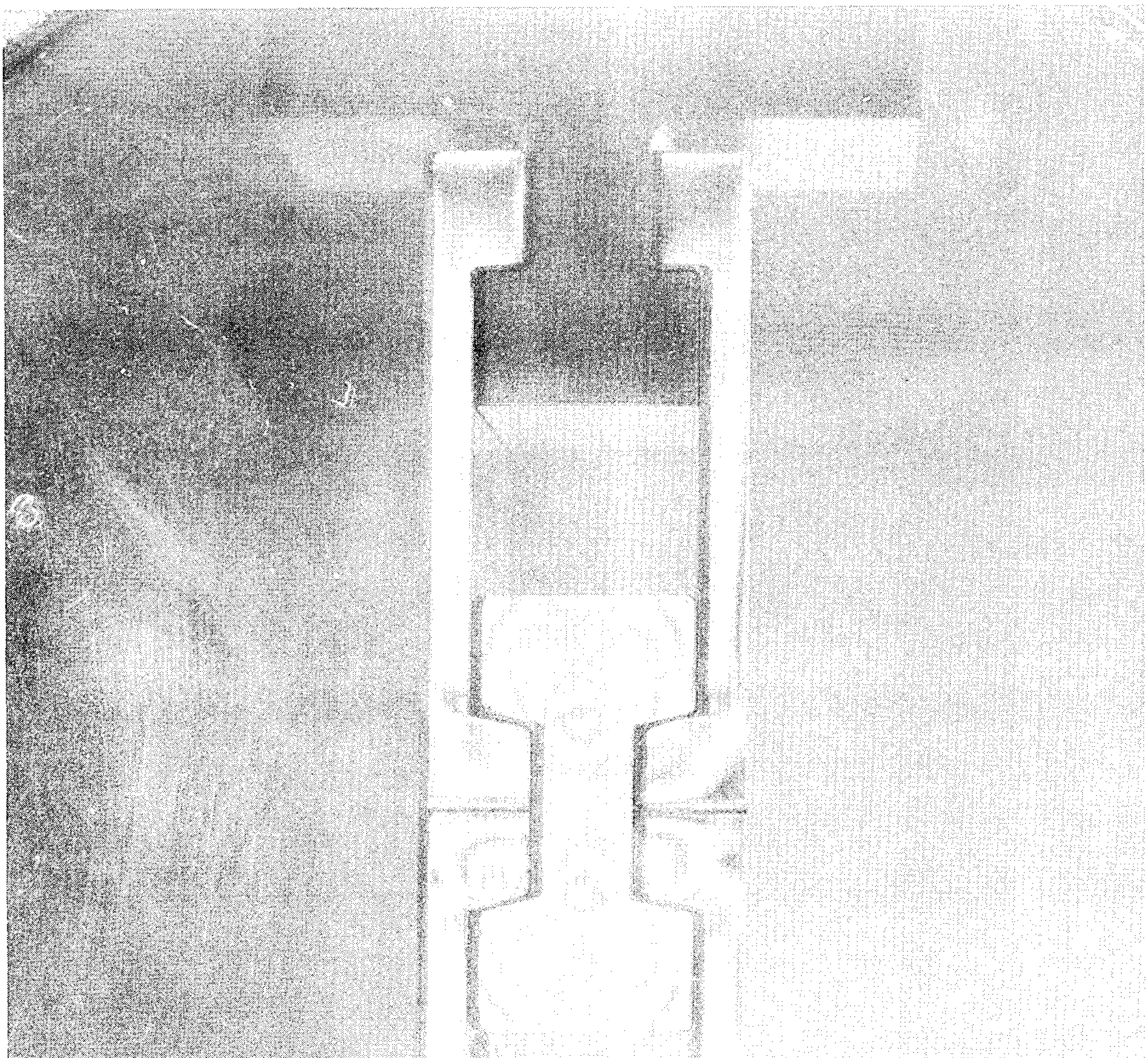

TEST RIG NO. 3 ASSEMBLY

FIGURE 60

TAPE WRAP INTERFERENCE RIG. NO. 3
PHOTO-STRESS VALUES AFTER ASSEMBLY

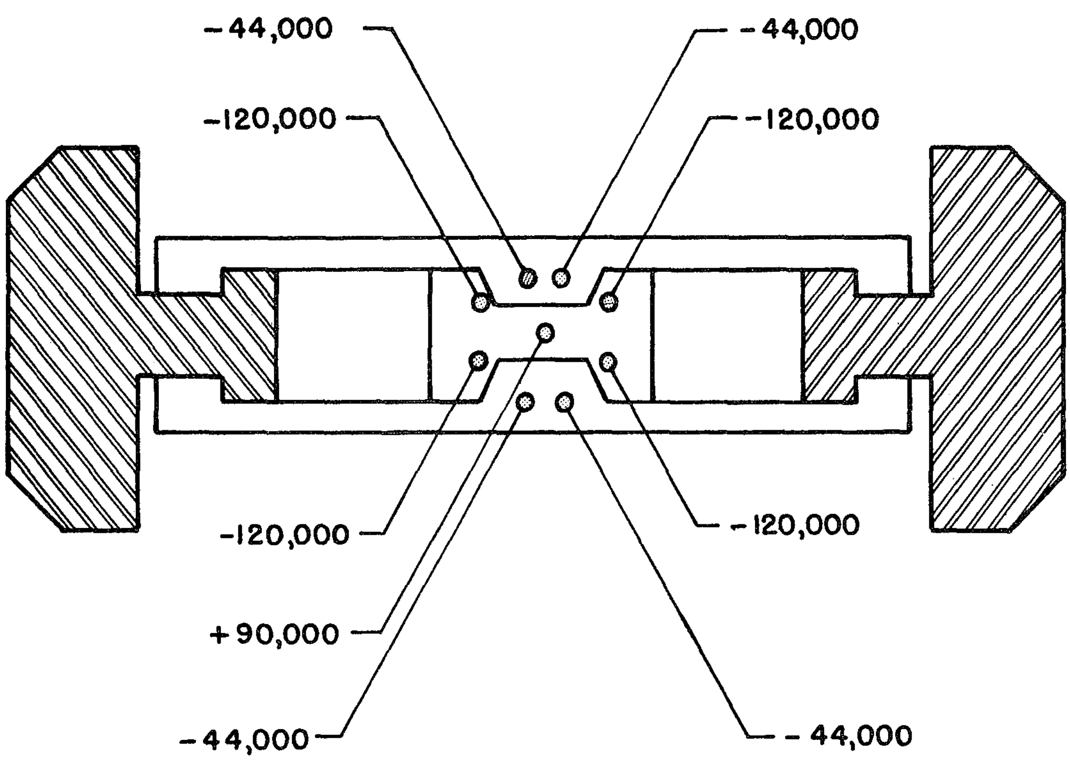

NOTE: STRESS VALUES ARE IN P. S. I.
+ DENOTES TENSION
— DENOTES COMPRESSION

FIGURE 61

TAPE WRAP INTERFERENCE TEST RIG NO. 3

12° INTERFACE ANGLE – .012" INTERFERENCE FIT

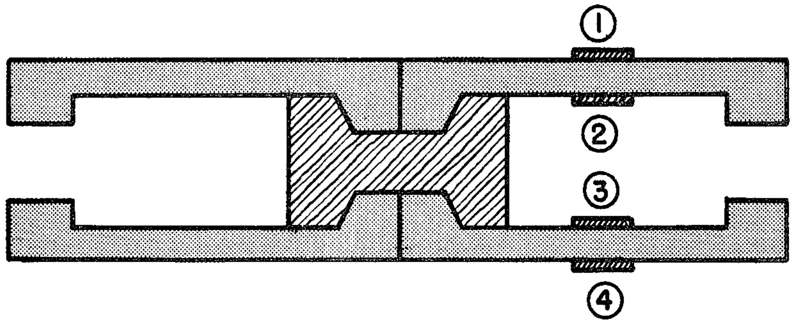

RESULTS: I BEAM BROKE AT 16,200 LBS

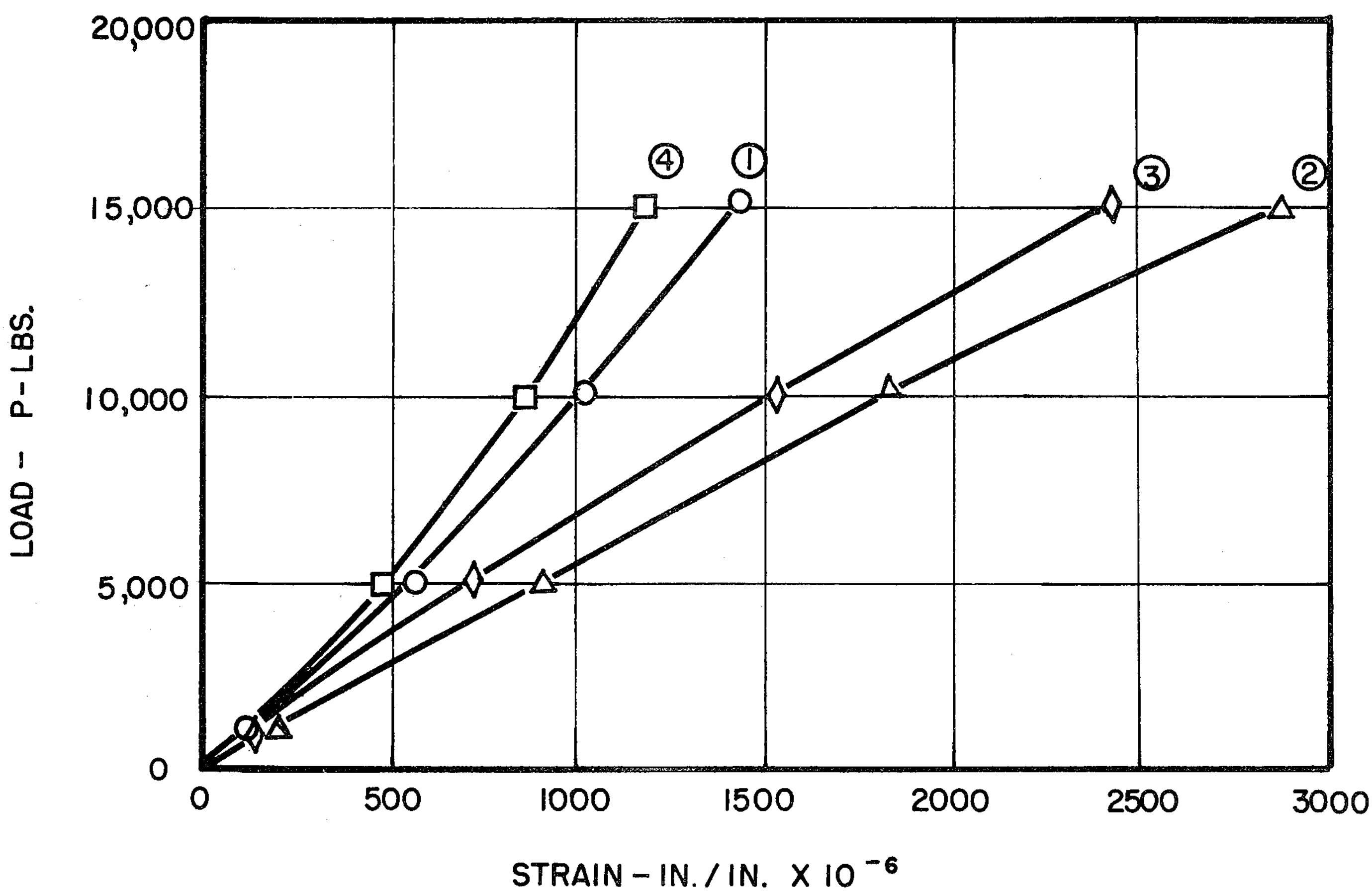

FIGURE 62

TAPE WRAP INTERFERENCE TEST RIG NO. 6

9° INTERFACE ANGLE

.012" INTERFERENCE FIT WITH MACHINED LIP

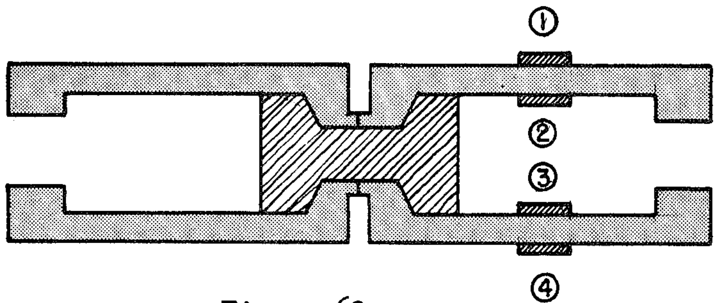

Figure 63

RESULTS: I BEAM BROKE AT 7600 LBS.

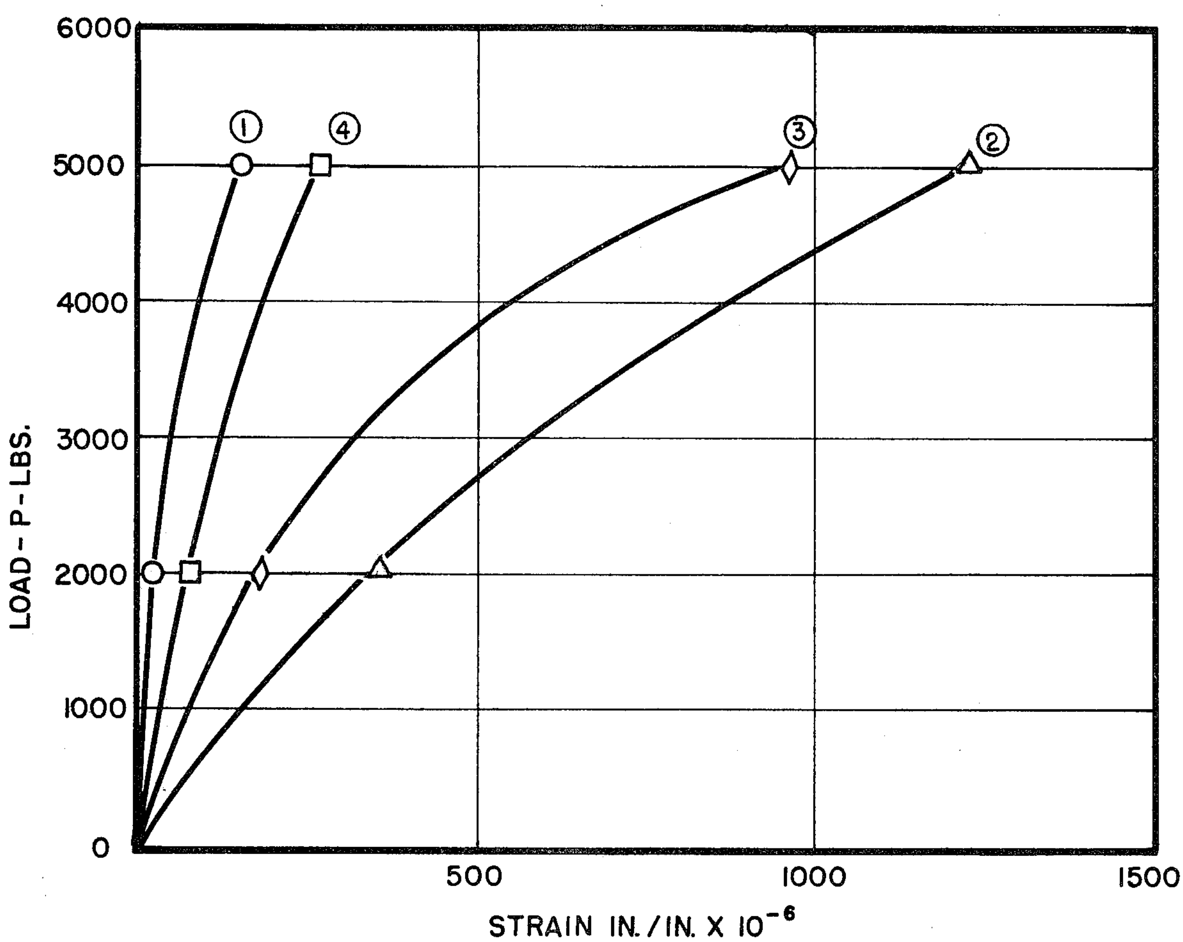

FIGURE 64

TAPE WRAP INTERFERENCE TEST RIG NO. 7

9° INTERFACE ANGLE
.012" INTERFERENCE FIT WITH .040" BRASS SHIM

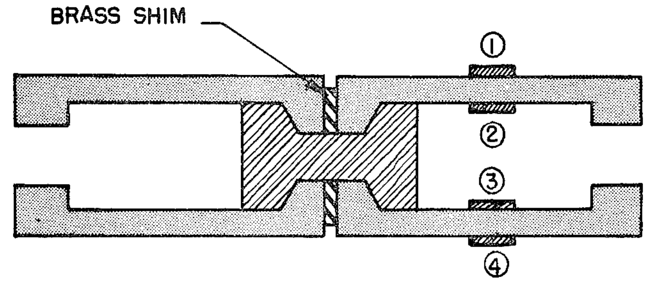

RESULTS: BOTH CHANNELS BROKE AT 21,000 LBS.

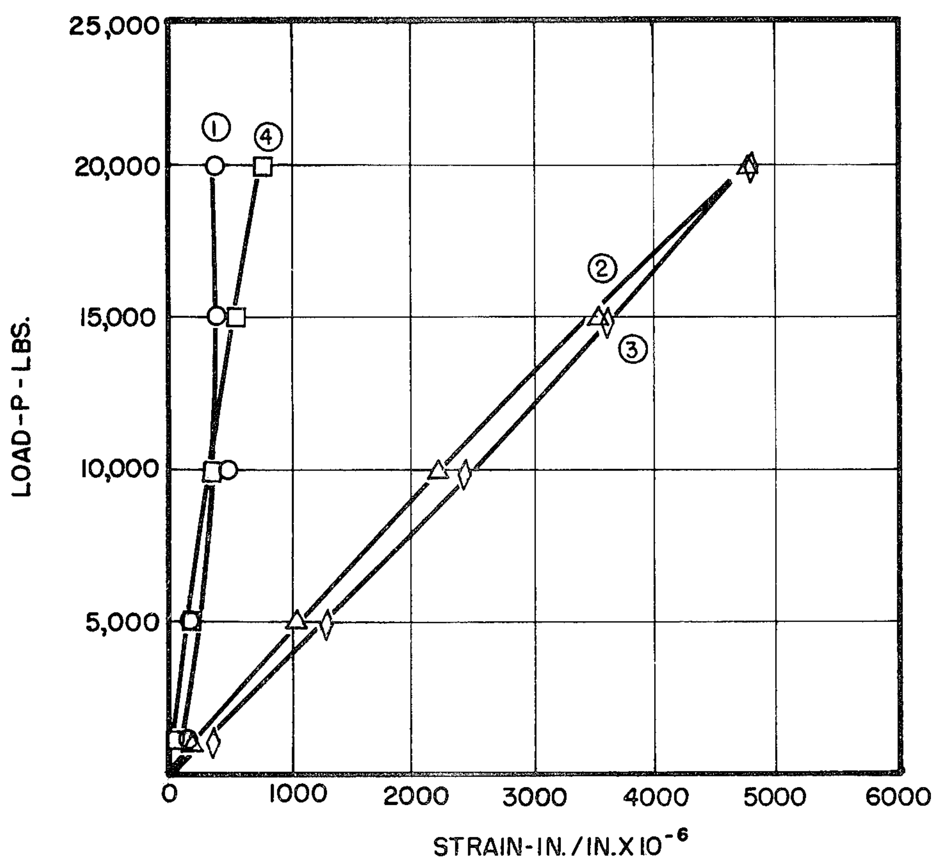

FIGURE 65

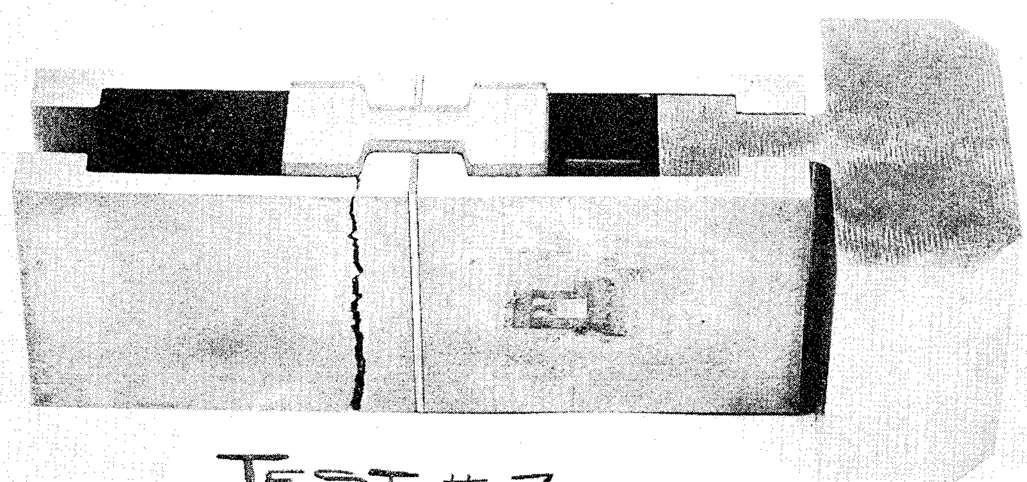

TEST # 7

9° – 0.012" interference
fit with 0.040" brass
Shim.

FIGURE 66

TAPE WRAP INTERFERENCE TEST RIG NO. 8

12° INTERFACE ANGLE

.012" INTERFERENCE FIT WITH .040" BRASS SHIM

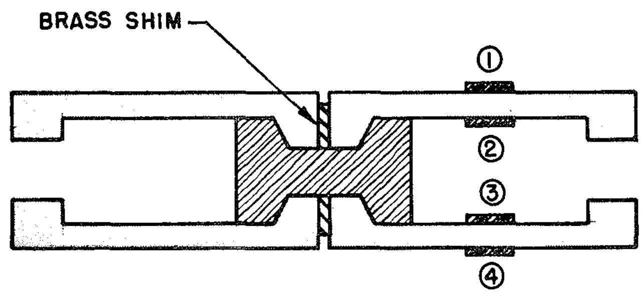

RESULT: BOTH CHANNELS BROKE AT 21,000 LBS.

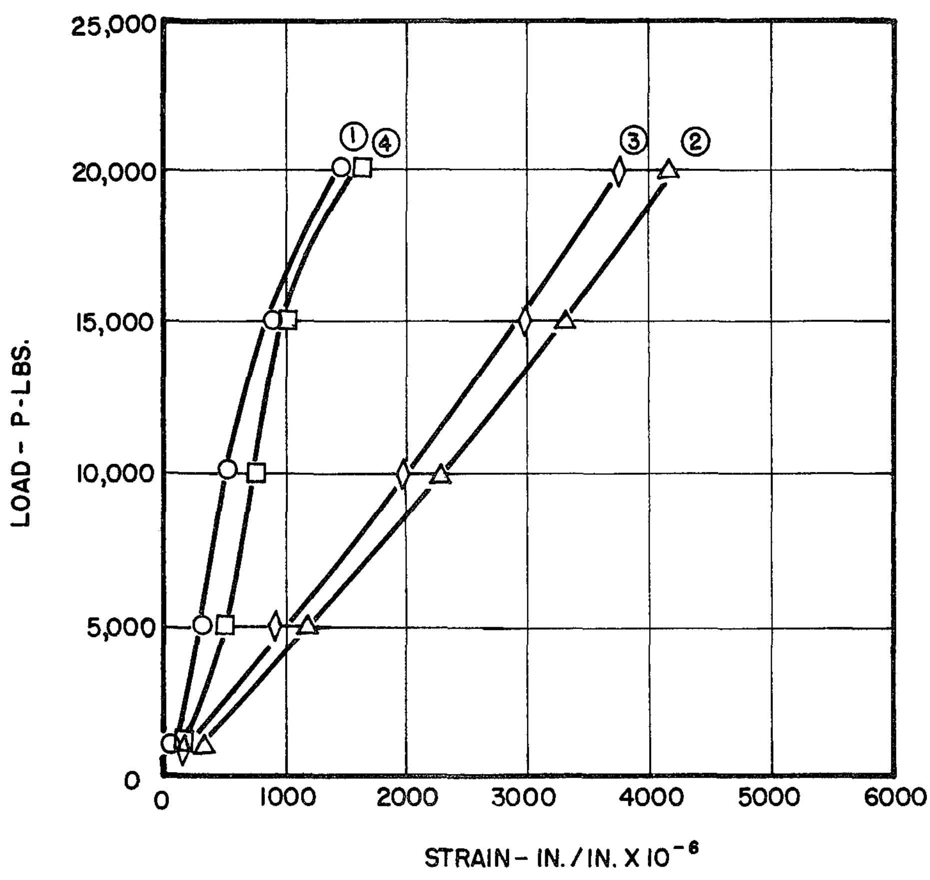

FIGURE 67

FREE BODY DIAGRAM

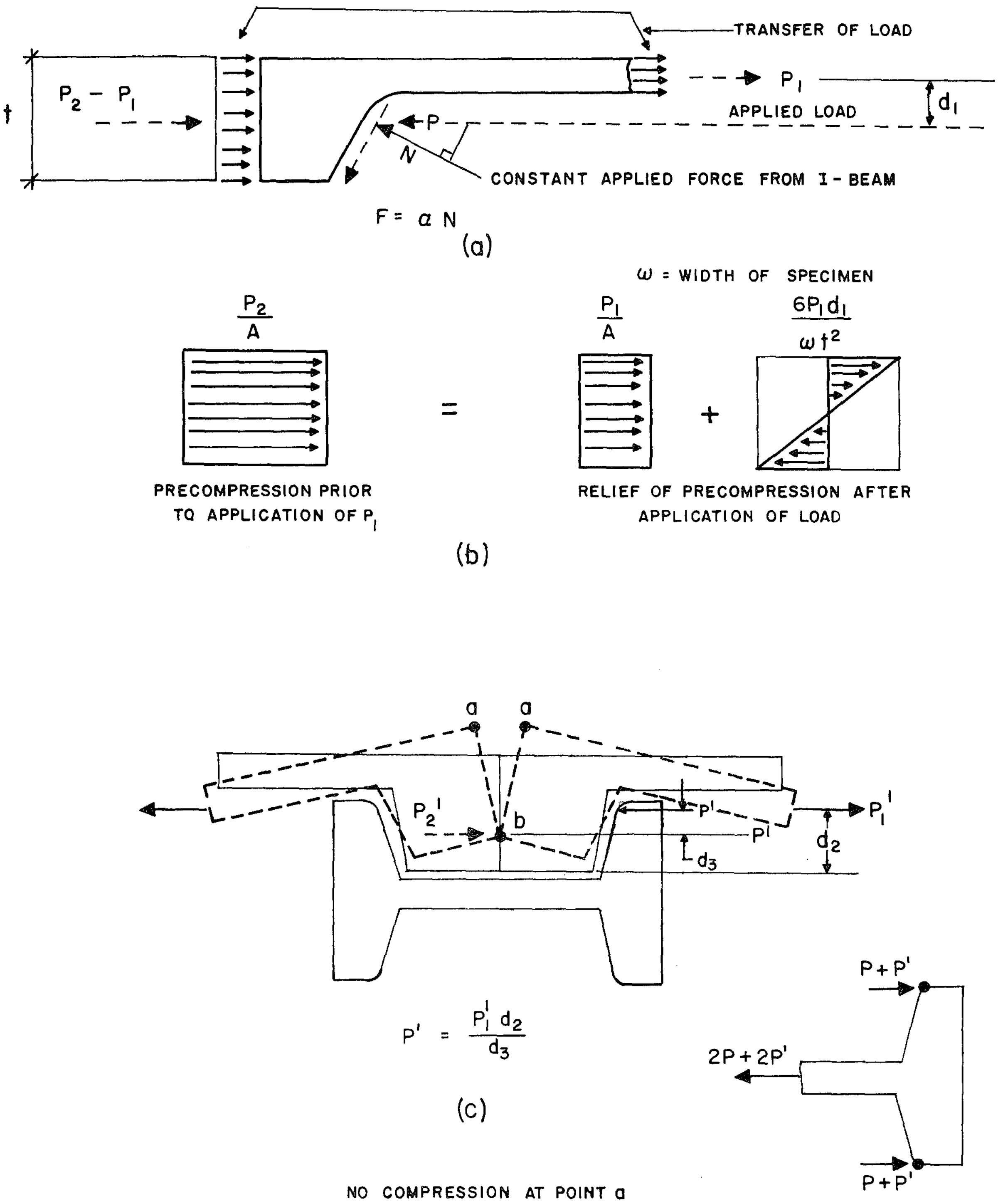

FIGURE 68

T-HEAD STRESS CONCENTRATION FACTOR

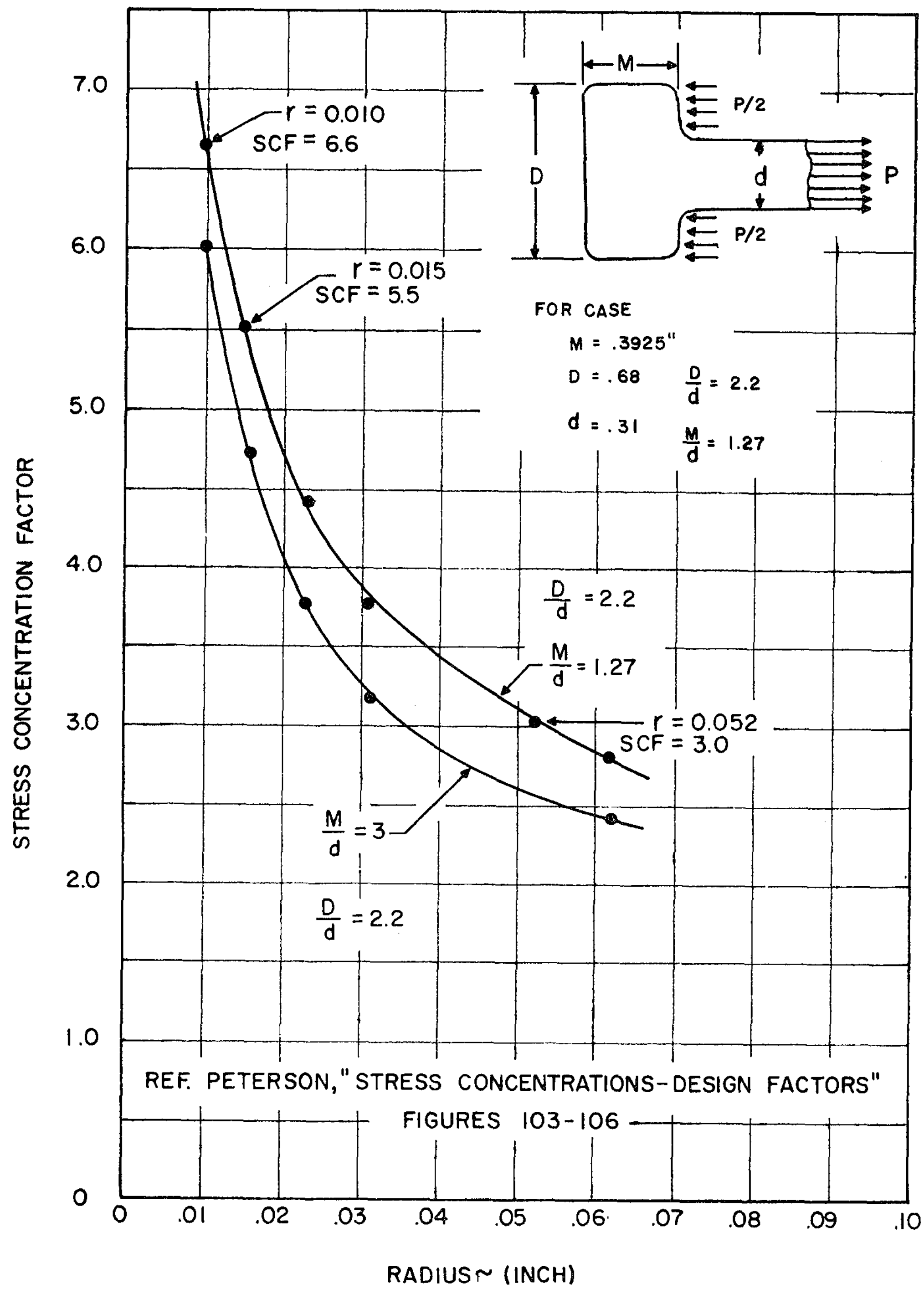

FIGURE 69

10 X TAPE - WRAP SPECIMEN

LENGTH OF SPECIMEN = 1.50"

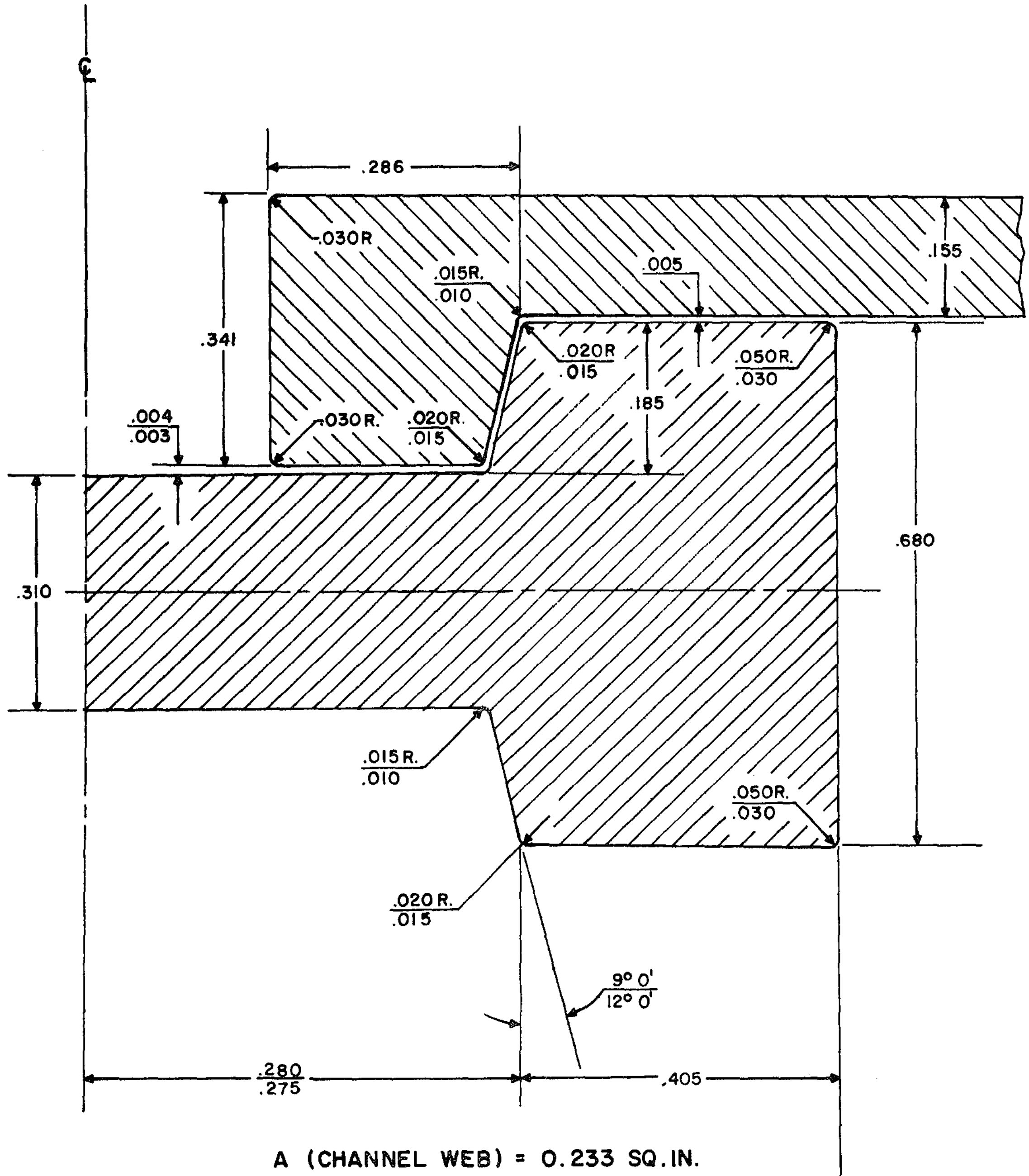

A (CHANNEL WEB) = 0.233 SQ.IN.
A (I- SHANK) = 0.465 SQ.IN.

FIGURE 70

WEIGHT COMPARISON OF TAPE WRAPPED AND CONVENTIONAL MOTOR CASINGS

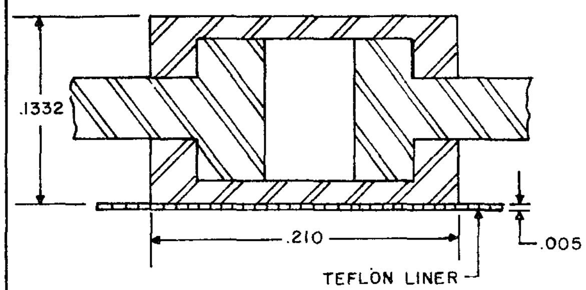	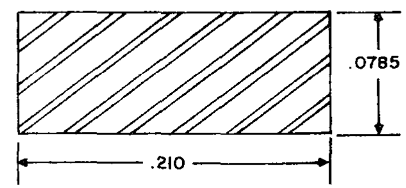	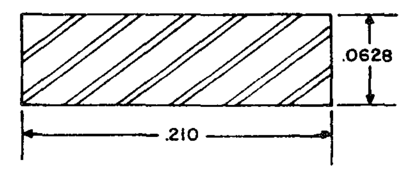
TITANIUM AT 250,000 PSI Y.S.	LADISH D6 AT 200,000 PSI Y.S.	18% NICKEL AT 250,000 PSI Y.S.
CHANNEL (2) = .001618 LBS DUMBELL (1) = .001763 LINER = .000072 TOTAL = .003453 LBS.	SHELL WEIGHT = .004665 LBS.	SHELL WEIGHT = .003811 LBS.
TITANIUM AT 180,000 PSI Y.S.		
TOTAL = .004796 LBS.		

(A) TI Y.S. = 250,000 PSI

(1) WEIGHT SAVING OVER CYLINDRICAL SECTION OF LADISH D6 MOTOR = 26%

(2) WEIGHT SAVING OVER CYLINDRICAL SECTION OF 18% NICKEL MOTOR = 9.4%

(B) TI Y.S. = 180,000 PSI

(1) WEIGHT SAVING OVER CYLINDRICAL SECTION OF LADISH D6 OR 18% NICKEL MOTOR = NONE

FIGURE 71

TABLE 1

Change in Tape Dimensions Due to
Curvature of 6 Inch Diameter Vessel

Detail	Δd (in)	Δb (in)
Phase 1 Channel	$+3.05 \times 10^{-4}$	-0.25×10^{-4}
Phase 1 I-beam	$\pm 0.49 \times 10^{-4}$	$\pm 0.61 \times 10^{-4}$
Phase 2 Channel	$+3.60 \times 10^{-4}$	-0.34×10^{-4}
Phase 2 I-beam	$\pm 0.45 \times 10^{-4}$	$\pm 0.94 \times 10^{-4}$

TABLE 2

SUMMARY OF TEST RIGS - WIRE WRAP MOTOR

Test Rig No.	Description of Rig Surface angle-Interference	Load During Assy. (lbs)	Load at Failure (lbs)	Location of Fracture	Remarks
1	12° - .012 in.	11,000	-	Web & flange intersection of I-beam	Failed during assembly of 2nd channel layer
2	12° - .012 in. (Annealed) (Y.S. = 130,000 psi)	-	30,000	None	Channels disengaged from I-beam
3	12° - .012 in.	24,000	16,200	Web & flange intersection of I-beam	Failed in Pull Test
4	9° - .012 in.	40,000	-	Web & flange intersection of I-beam	Failed during assembly
5	12° - .040 in.	37,000	-	Web & flange intersection of I-beam	Failed during assembly
6	9° - .012 in. (Machined Lip)		7,200	Web & flange intersection of I-beam	Failed in Pull Test
7	9° - .012 in. (0.040 Brass Shim)	45,000	21,000	Web & flange intersection of channel	Failed in Pull Test
8	12° - .012 in. (.040 Brass Shim)	37,000	21,000	Web & flange intersection of channel	Failed in Pull Test

NOTE: All Ti material heat treated to 180,000 psi Y.S. unless otherwise noted.

SUMMARY

COMPATIBILITY EQUATIONS AT ELASTIC CENTER

HELICAL COIL OF ONE TURN

Defl.	REDUNDANT MOMENTS AND FORCES					
	M_{xo}	M_{yo}	M_{zo}	X_o	Y_o	Z_o
$\theta_x =$	$+1$	0	0	0	0	0
$\theta_y =$	0	K_2+K_3	0	0	0	0
$\theta_z =$	0	0	K_2+K_3	0	0	0
$\delta_x =$	0	0	0	$+1$	$+\tan\psi$	0
$\delta_y =$	0	0	0	$2K_2\tan\psi$	$K_4+(K_2K_5+K_3K_6)\tan^2\psi$	$\pi(K_3-K_2)\tan^2\psi$
$\delta_z =$	0	0	0	0	$\pi(K_3-K_2)\tan^2\psi$	$K_4+(K_2K_5+K_3K_6)\tan^2\psi$

$K_2 = \frac{1}{JG}$ $\quad K_6 = \frac{8\pi^2}{6}+\frac{1}{2}$

$K_3 = \frac{1}{EI_r}$ $\quad K_7 = \frac{8\pi^2}{6}-\frac{1}{2}$

$K_4 = \frac{1}{EI_x}$ $\quad K_8 = \frac{8\pi^2}{6}+\frac{11}{2}$

$K_5 = \frac{8\pi^2}{6}-\frac{1}{2}$

Defl.	APPLIED LOADS			
	radial Load $P\left(\frac{lbs}{in}\right)$	Shear flow $q\left(\frac{lbs}{in}\right)$	axial Load $\omega\left(\frac{lbs}{in}\right)$	circumferential Torque $\tau\left(\frac{in\text{-}lbs}{in}\right)$
$\theta_x =$	$-\frac{R^2}{\cos\psi}$	$+\pi R^2$	$+\pi R^2\tan\psi$	$+\pi R^2\tan\psi$
$\theta_y =$	$+\frac{R^2}{2}\frac{\tan\psi}{\cos\psi}(K_2+3K_3)$	$+\pi R^2(K_2-K_3)\tan\psi$	$+\pi R^2(K_2-K_3)\tan^2\psi$	0
$\theta_z =$	$-\pi R^2(K_2+K_3)\frac{\tan\psi}{\cos\psi}$	$+\frac{R^2}{2}(9K_2+K_3)\tan\psi$	$+\frac{R^2}{2}\left[6K_2+2K_3-(3K_2+K_3)\tan^2\psi\right]$	$R(-K_2+K_3)$
$\delta_x =$	$-2R\frac{\tan\psi}{\cos\psi}$	$+\pi R\tan\psi$	$+\pi R$	0
$\delta_y =$	$-\frac{R}{\cos\psi}\left[K_4+K_7(K_2+K_3)\tan^2\psi\right]$	$+\pi R(7K_2+K_3)\tan^2\psi$	$-\pi R\tan\psi\left[2K_2\tan^2\psi-(5K_2+K_3)\right]$	$-\pi(K_2-K_3)\tan\psi$
$\delta_z =$	$-2\pi RK_3\frac{\tan^2\psi}{\cos\psi}$	$+R\left[(K_3K_5-K_2K_8)\tan^2\psi-3K_4\right]$	$+\frac{R}{2}\left[(2K_7\tan^2\psi-9)K_2+(2K_7\tan^2\psi-3)K_3 -6K_4\right]\tan\psi$	$+\frac{\tan\psi}{2}(K_2-3K_3-4K_4)$

TABLE 3

DISTRIBUTION LIST

ORDEH-0-M(30-069-ORD-3101)	No. of Copies
Office of the Director of Defense Research and Engineering ATTN: Mr. J. C. Barrett Room 3D-1067, The Pentagon Washington 25, D. C.	1
Advanced Research Project Agency ATTN: Dr. G. Mock The Pentagon Washington 25, D. C.	1
Defense Metals Information Center Battelle Memorial Institute Columbus, Ohio	1
Solid Propellant Information Agency Applied Physics Laboratory The Johns Hopkins University Silver Spring, Maryland	3
Office Chief of Ordnance ATTN: ORDTB-Materials Department of the Army Washington 25, D. C.	1
Commanding General Aberdeen Proving Ground ATTN: Dr. C. Pickett, C&CL Aberdeen Proving Ground, Maryland	1
Commanding General Ordnance Tank-Automotive Command ATTN: Mr. S. Sobak, ORDMC-1F-2 Detroit 9, Michigan	1
Commanding General Ordnance Weapons Command ATTN: Mr. B. Gerke, ORDOW-IA Rock Island, Illinois	1

	No. of Copies
Commanding General	
U. S. Army Ballistic Missile Agency	
ATTN: Dr. G. H. Reisig	1
Mr. W. B. Thomas, ORDAB-RPEM	1
Documentation of Technical Information Branch	2
ORDAB-IEE	1
Redstone Arsenal, Alabama	
Commanding General	
U. S. Army Rocket and Guided Missile Agency	
ATTN: Mr. Robert Fink, ORDXR-RGA	3
Mr. W. K. Thomas, ORDXR-IQE	1
Mr. A. L. Price, ORDXR-IXD	1
Mr. N. M. Shapiro, ORDXR-RR	2
Technical Library	4
E. Fohrell, ORDXR-RFE	1
Redstone Arsenal, Alabama	
Commanding Officer	
Frankford Arsenal	
ATTN: Dr. H. Gisser, ORDBA-1330	1
Mr. H. Markus, ORDBA-1320	1
Philadelphia 37, Pa.	
Commanding Officer	
Ordnance Materials Research Office	
Watertown Arsenal	
ATTN: RPD	1
Watertown 72, Mass.	
Commanding Officer	
Picatinny Arsenal	
ATTN: Mr. J. J. Scavuzzo, Plastics & Packaging Lab.	3
Mr. D. Stein, ORDHB-DE3	1
Dover, New Jersey	
Commanding Officer	
PLASTEC	
Picatinny Arsenal	
Dover, New Jersey	1
Commanding Officer	
Rock Island Arsenal	
ATTN: Materials Section, Laboratory	
Rock Island, Illinois	1

	No. of Copies
Commanding Officer Springfield Armory ATTN: Mr. R. Korytoski, Research Mat'ls. Lab. Springfield 1, Mass.	1
Commanding Officer Watertown Arsenal ATTN: ORDBE-LX Watertown 72, Mass.	3
Commanding Officer Watervliet Arsenal ATTN: Mr. F. Dashnaw, ORDBF-RR Watervliet, New York	1
Headquarters U. S. Army Signal R&D Laboratory ATTN: Mr. H. M. Kedesky, SIGRA/SL-XE Fort Monmouth, N. J.	1
Commander Army Research Office Arlington Hall Station Arlington 12, Virginia	1
Chief of Research and Development U. S. Army Research & Development Liaison Group ATTN: Dr. B. Stein APO 757, New York, N. Y.	1
Chief, Bureau of Naval Weapons Department of the Navy ATTN: RMMP Room 2225, Munitions Building Washington 25, D. C.	1
Department of the Navy Office of Naval Research ATTN: Code 423 Washington 25, D. C.	1
Department of the Navy Special Projects Office ATTN: SP 271 Washington 25, D. C.	1

	No. of Copies
Commander U. S. Naval Ordnance Laboratory ATTN: Code WM White Oak, Silver Spring, Maryland	1
Commander U. S. Naval Ordnance Test Station ATTN: Technical Liorary Branch China Lake, California	1
Commander U. S. Naval Research Laboratory ATTN: Mr. J. E. Strawley Anacostia Station Washington 25, D. C.	1
U. S. Air Force Directorate of R&D ATTN: Lt. Col. J. B. Shipp, Jr. Room 4D-313, The Pentagon Washington 25, D. C.	1
Wright Air Development Division ATTN: M. Zoeller, ASRCEE-1 Wright-Patterson Air Force Base, Ohio	2
ARDC Flight Test Center ATTN: Solid Systems Division, FTRSC Edwards Air Force Base, California	5
AMC Aeronautical Systems Center ATTN: Mfg. & Mat'ls. Technology Div., LMBMO Wright Patterson Air Force Base, Ohio	2
Commander Armed Services Technical Information Agency ATTN: TIPDR Arlington Hall Station Arlington 12, Virginia	10
National Aeronautics & Space Administration ATTN: Mr. R. V. Rhode	1
Mr. G. C. Deutsch Washington, D. C.	1

	No. of Copies
Dr. W. Lucas George C. Marshall Space Flight Center National Aeronautics & Space Administration ATTN: M-86M-M Huntsville, Alabama	1
Dr. L. Jaffe Jet Propulsion Laboratory California Institute of Technology 4800 Oak Grove Drive Pasadena, California	1
Mr. William A. Wilson George C. Marshall Space Flight Center ATTN: M-F&AE-M Huntsville, Alabama	1
Aerojet-General Corporation ATTN: Librarian Post Office Box 1168 Sacramento, California	1
Aerojet-General Corporation ATTN: Librarian Mr. C. A. Fournier Post Office Box 296 Azusa, California	 1 1
Allison Division General Motors Corporation ATTN: Mr. D. K. Hanink Indianapolis 6, Indiana	1
ARDE-Portland, Inc. ATTN: Mr. R. Alper 100 Century Road Paramus, N. J.	1
Atlantic Research Corporation ATTN: Mr. E. A. Olcott Shirley Highway and Edsall Road Alexandria, Virginia	1
Hercules Powder Company Allegheny Ballistics Laboratory ATTN: Dr. R. Steinberger Post Office Box 210 Cumberland, Maryland	1

	No. of Copies
Hughes Aircraft Company ATTN: Librarian Culver City, California	1
Library, Rohm & Haas Company Redstone Research Division Redstone Arsenal, Alabama	1
Tapco Group ATTN: Mr. W. J. Piper 23555 Euclid Avenue Cleveland 17, Ohio	1
Library, Thiokol Chemical Corp. Redstone Division Redstone Arsenal, Alabama	1
Chief, Bureau of Naval Weapons Department of the Navy ATTN: Mr. P. Goodwin Washington 25, D. C.	1
Headquarters Aeronautical Systems Division ATTN: Dr. Tamborski, ASRCNP Wright-Patterson Air Force Base, Ohio	1
Wright Air Development Division ATTN: Mr. G. Peterson, ASRCNC-1 Wright-Patterson Air Force Base, Ohio	1
Allegheny Ludlum Steel Corporation Research Center ATTN: Mr. R. A. Lula Brackenridge, Pennsylvania	1
Alloyd Electronics Corporation ATTN: Dr. S. S. White 35 Cambridge Parkway Cambridge, Mass.	1
Armco Steel Corporation General Offices ATTN: Mr. J. Barnett Middletown, Ohio	1

	No. of Copies
Battelle Memorial Institute	
ATTN: Mr. R. Monroe	1
Mr. G. Faulkner	1
505 King Avenue	
Columbus 1, Ohio	
The Boeing Company	
Aero Space Division	
P. O. Box 3707	
Seattle 24, Washington	1
Berg-Warner Corporation	
Ingersoll Kalamazoo Division	
ATTN: Mr. L. E. Hershey	
1810 N. Pitcher Street	
Kalamazoo, Michigan	1
The Budd Company	
Defense Division	
ATTN: Mr. R. C. Dethloff	1
Mr. Ohman	1
Philadelphia 32, Pennsylvania	
Climax Molybdenum Company	
ATTN: Mr. R. R. Freeman	
1270 Avenue of the Americas	
New York 20, New York	1
Douglas Aircraft Company, Inc.	
Santa Monica Division	
ATTN: Mr. J. L. Waisman	
Santa Monica, California	1
E. I. Dupont DeNemovrsk Company	
ATTN: Mr. C. P. Williams	
Eastern Laboratory	
Gibbstown, New Jersey	1
General Electric Company	
Rocket Engine Section	
Flight Propulsion Laboratory Department	
Cincinnati 15, Ohio	1
Jones and Laughlin Steel Corporation	
ATTN: Mr. N. Steinbrenner	
45 South Montgomery Avenue	
Youngstown 1, Ohio	1

	No. of Copies
Arthur D. Little, Inc. ATTN: Dr. R. Davis Acorn Park Cambridge 40, Mass.	1
Lyon, Inc. ATTN: Mr. W. Martin 13881 W. Chicago Boulevard Detroit, Michigan	1
Manufacturing Laboratories ATTN: Dr. P. Fopiano Dr. V. Radcliffe 21-35 Erie Street Cambridge 42, Mass.	1 1
Minneapolis-Honeywell Regulator Company 1230 Soldiers Field Road Boston 35, Mass.	1
Norris-Thermador Corporation ATTN: Mr. L. Shiller 5215 South Boyle Avenue Los Angeles 58, California	1
The Perkin-Elmer Corporation ATTN: Mr. M. L. Sachs Main Avenue Norwalk, Connecticut	1
Pratt & Whitney Aircraft ATTN: Mr. F. A. Crosby East Hartford, Connecticut	1
Reactive Metals Corporation ATTN: Mr. M. Lundstrom Niles, Ohio	1
Republic Steel Corporation Research Center ATTN: Mr. M. P. Manger Independence, Ohio	1
Rohm & Haas Company Redstone Arsenal Research Division ATTN: Library Huntsville, Alabama	1

	No. of Copies
Space Technology Laboratories, Inc. ATTN: Technical Information Center Document Procurement Post Office Box 95001 Los Angeles 45, California	1
Thiokol Chemical Corporation Utah Division Brigham City, Utah	1
Titanium Metals Corporation ATTN: Mr. G. Erbin 233 Broadway New York, New York	1
Universal-Cyclops Steel Corp. Stewart Street Bridgeville, Pennsylvania	1
U. S. Borax Research Corp. ATTN: Mr. R. J. Brotherton 412 Crescent Way Anaheim, California	1
United States Rubber Company Research Center ATTN: Dr. E. J. Joss Wayne, N. J.	1
Massachusetts Institute of Technology ATTN: Prof. W. A. Backofen Prof. M. C. Flemings Cambridge, Massachusetts	 1 1
Mellon Institute ATTN: Dr. H. L. Anthony Mr. C. J. Owen 4400 Fifth Avenue Pittsburgh 13, Pa.	 1 1
Michigan State University ATTN: Mr. R. N. Hammer Department of Chemistry East Lansing, Michigan	1

Wright Aeronautical Serial Report No. MP.00-249

No. of Copies

Ohio State University Research Foundation ATTN: Dr. R. McMaster Columbus, Ohio	1